Summer 2015

# Curved spiral antennas for underwater biological applications

Ruben A. Llamas
*University of Iowa*

# CURVED SPIRAL ANTENNAS FOR UNDERWATER BIOLOGICAL APPLICATIONS

by

Ruben Llamas

A thesis submitted in partial fulfillment
of the requirements for the Doctor of
Philosophy degree in Electrical and Computer Engineering
in the Graduate College of
The University of Iowa

May 2015

Thesis Supervisor: Professor Anton Kruger

Graduate College
The University of Iowa
Iowa City, Iowa

CERTIFICATE OF APPROVAL

_____

PH.D. THESIS

_____

This is to certify that the Ph.D. thesis of

Ruben Llamas

has been approved by the Examining Committee
for the thesis requirement for the Doctor of Philosophy
degree in Electrical and Computer Engineering at the May 2015 graduation.

Thesis Committee: _____
Anton Kruger, Thesis Supervisor

_____
Craig L. Just

_____
David R. Andersen

_____
Vincent G. J. Rodgers

_____
Fatima Toor

To my mother, Gladys Maria Morales Cupajita.

In all things insist, persist and never desist

Ruben Augusto Llamas Morales

# ACKNOWLEDGMENTS

My deepest gratitude to my advisor, Professor Anton Kruger, for his time, support and guidance on my research work, without his input and extensive knowledge this thesis would not be possible. Professor Kruger has supported me not only on my thesis work, but also academically and emotionally throughout my Ph.D. journey. I also thank my committee members Dr. Craig L. Just, Dr. David R. Andersen, Dr. Vincent G. J. Rodgers, and Dr. Fatima Toor for their valuable guidance.

I would like to extend my profound gratitude to Dr. James J. Niemeier for his mentorship and contribution to innumerable experiments and discussions on the different research projects that we worked on together. The IIHR Hydroscience and Engineering Laboratories staff, my fellow students and undergraduate research assistants for their help. Hannah Taylor for her help with initial prototypes of testing radio boards. Robert B. Hart (Gabriel) for his time as diver in the underwater experiments at the University of Iowa Aquatic Center diving pool. Jeffrey T. Schnell, high school intern, for his assistance with some of the initial experiments (Summer 2013) and 3-D modeling of *cybermussel*'s backpack (Summer 2014). Matthew J. Janechek for his wonderful help in the 3-D curved spiral antenna modeling and 3-D printing of the antenna housing fixture. Michael J. Salino-Hugg for his assistance during the last stage of the research in testing the radio-antenna system assemblage and underwater antenna measurements at the Wind Tunnel Annex Laboratory facilities water tank. Kathryn Temple for her assistance on the mussel shell material characterization related measurements. I express my gratitude to the following IIHR's shop staff for their collaboration in numerous tasks: Brandon Barquist, Christian Borgwardt, Nicholas T. Thornburg, Timothy J. Houser, among others.

I thank everyone in the University of Iowa Electrical and Computer Department (ECE), and special thanks to Catherine H. Kern for her tireless support and motivation throughout my entire time in Iowa City, The University of Iowa and my Ph.D. Studies. Professor Jon Kuhl for his support and guidance.

I acknowledge the U.S. Department of Education, the University of Iowa College of Engineering, and the University of Iowa Electrical and Computer Engineering Department for their financial support from Graduate Assistance in Areas of National Need (GAANN) fellowship.

Thank you to the Director of the University of Iowa Aquatic center, Phillip L. Julson, for allowing me to use their Diving pool for my underwater antenna experiments.

I express my gratitude Dr. Tonya L. Peeples, Associate Dean for Diversity and Outreach, for her support and guidance during my time at the University of Iowa.

I was involved in many activities outside the classrooms and the lab, where I met amazing people and promoted STEM (Science, Technology, Engineering, and Mathematics) fields and Hispanic culture. I would like to thank Multi-Ethnic Engineering and Sciences Association (MESA) and the Ethnic Inclusion Effort for Iowa Engineering ($eI^2$) for giving me the great opportunity to mentor and tutor High School students in the Iowa City district. I was also active in and an executive board member of The University of Iowa Society of Hispanic Professional Engineers (SHPE) student chapter, *Gracias* SHPE *Familia*.

I would like to express my thanks to all my friends in Iowa and in the College of Engineering. A special word of thanks goes to Henry E. Baidoo-Williams for his friendship and all our countless discussion and group studies during our Ph.D. times. Felipe Nicolau Manterola for all his support during my time in Iowa. Kumar Vijay Mishra for his support and encouragement and for being a great lab-mate and friend these last three years of my Ph.D. Carlos Arturo Peroza

Meza (*mi compadre costeño de Iowa*) and his family for their friendship and encouragement in these last two years.

And to the most important supporters, my family, *MUCHAS GRACIAS!!* I extend my greatest gratitude from the bottom of my heart to my mother. She is always there for me to help me endure the most difficult times and get out victorious. I also want to express tremendously thank you to Evelin Y. Vides, my fiancé, soon to be my wife (we are getting married the day after my graduation) for her patience and support during my graduate studies. To my sisters and brothers, especially to my sister Geine Austin for her support in helping me to come to the U.S., as well in my initial months in U.S. helping me with the English, and during my entire life. I also include my brother-in-law and *compadre*, John Charles Austin, whom spent hours teaching me English in my-early-days in U.S., and was always willing to proofread writing assignments and manuscripts. I want to express my gratitude to my brother and *compadre*, Climaco Alberto Llamas, whom spent a lot of nights supporting me and helping me improve my programming skills.

I close this section thanking all the people whom in one way or another have contributed to this great achievement from my childhood up to this point. Specially my family, friends and teachers during all these years, and for believing in me. *Sí, Se Puede!!! Gracias Infinitas!!! Getsemanicense por Siempre!!!*

# ABSTRACT

We developed curved spiral antennas for use in underwater (freshwater) communications. Specifically, these antennas will be integrated in so-called *mussel backpacks*. Backpacks are compact electronics that incorporate sensors and a small radio that operate around 300 MHz. Researchers attach these backpacks in their freshwater mussel related research. The antennas must be small, lightweight, and form-fit the mussel. Additionally, since the mussel orientation is unknown, the antennas must have broad radiation patterns. Further, the electromagnetic environment changes significantly as the mussels burrow into the river bottom. Broadband antennas, such a spiral antennas, will perform better in this instance. While spiral antennas are well established, there has been little work on their performance in freshwater. Additionally, there has been some work on curved spiral antennas, but this work focused on curving in one dimension, namely curving around a cylinder. In this thesis we develop spiral antennas that curve in two dimensions in order to conform the contour of a mussel's shell.

Our research has three components, namely (a) an investigation of the relevant theoretical underpinning of spiral antennas, (b) extensive computer simulations using state-of-the art computational electromagnetics (CEM) simulation software, and (c) experimental validation. The experimental validation was performed in a large tank in a laboratory setting. We also validated some designs in a pool (~300,000 liters of water and ~410 squared-meter dive pool) with the aid of a certified diver.

To use CEM software and perform successful antenna-related experiments require careful attention to many details. The mathematical description of radiation from an antenna, antenna input impedance and so on, is inherently complex. Engineers often make simplifying assumptions such as assuming no reflections, or an isotropic propagation environment, or operation in the antenna

far field, and so on. This makes experiments on antennas challenging since it often quite difficult to replicate the simplifying assumptions in an experimental setting.

Still, with careful consideration of the important factors and careful experimental design it is possible to perform successful experiments. For example, antenna measurements are often performed in anechoic chambers. For our research we used a large swimming pool to mimic an underwater anechoic chamber. Our CEM simulations and experimental results are in most cases congruent. We are confident that we can design formfitting, compact (spiral) antennas that one could deploy on mussels. This will greatly enhance the mussel backpacks that are used by researchers at the University of Iowa.

# PUBLIC ABSTRACT

Researchers at the University of Iowa are developing so-called mussel *backpacks.* These backpacks contain sensors, a microcontroller, and a small radio to transmit data from the sensors to an on-shore receiver, or to other backpacks in the vicinity. Backpacks are attached to freshwater mussels that can then be deployed in their natural habitat or in a laboratory-based habitat. Typical sensors measure mussel heartrate and mussel gape (the rhythmic opening and closing of their valves). The backpacks will aid several ongoing freshwater mussel research efforts. The underwater radio propagation environment is complex and reliable data transmission requires a specialized antenna. It is the antenna design that is the focus of this thesis.

We identified spiral antennas as suitable for this application. They are broadband and compact. Conventional spiral antennas are flat. In this thesis we explore curved spiral antennas. Curving is required so that the antenna snuggly fit the mussel shell, so as to not impede its motion. We have developed procedure to design curved spiral antennas. The design starts from the well-known flat spiral antenna, and then we project it onto the mussel shell. This projection disturbs the intrinsic properties of the flat spiral antenna. In the second step, we apply a correction.

Our investigation has three components, namely a study of the existing spiral antennas, computer simulations, and finally an experimental verification. The experimental verification was performing in a large tank in a laboratory as well as a large diving pool. Our results indicate that our spiral antennas will work well in the mussel backpack application. We have developed the engineering CAD model for the antenna housing using 3D-printed techniques.

# TABLE OF CONTENTS

LIST OF FIGURES ..... XII

LIST OF TABLES ..... XVI

CHAPTER I. INTRODUCTION ..... 1

Motivation, Scope of the Thesis ..... 1
Antenna Requirements and Conceptual Solution ..... 5
Challenges ..... 8
Approach I Used ..... 9
Thesis Roadmap ..... 9

CHAPTER II. LITERATURE REVIEW ..... 11

Underwater Antennas ..... 11
Underwater-Freshwater Radio Propagation ..... 20
Spiral Antennas ..... 24
Summary ..... 34

CHAPTER III. SUMMARY OF RELEVANT EM THEORY RELATED TO THESIS 36

Maxwell's Equations ..... 36
Properties of Dielectric Materials ..... 39
Classification of medium based on its loss tangent ..... 40
EM Properties of Propagation in Water ..... 41
Computing Antenna Radiating Fields ..... 46
EM Properties of Mussel Shell, River Water, and Sand at River Bottom ..... 53
Relative Permittivity of the Freshwater Mussel Shell ..... 53

CHAPTER IV. EXPERIMENTAL AND SIMULATED PROTOCOLS ..... 63

Preliminaries ..... 63
Antenna-Radio Testing System ..... 65
Dipole Antenna Air Measurements ..... 65
Underwater Antenna Measurements ..... 69
Underwater Experiments in Tank located in Laboratory Facilities ..... 69
Range Measurements ..... 69
Elevation and Azimuthal Measurements ..... 69
Antenna Input Impedance Measurements ..... 71
Underwater Experiments in Diving Pool Located in the University of Iowa Aquatic Center ..... 73
Dipole Antenna Simulations ..... 78

CHAPTER V. SPIRAL ANTENNAS ..... 80

Flat Archimedean Spiral Antennas ..... 80
Theoretical Analysis ..... 80
Description of the flat Archimedean Spiral Antenna ..... 83
Flat Archimedean Spiral Antenna Practical Design ..... 84

CHAPTER VI. CURVED SPIRAL ANTENNAS AND CORRECTION PROCEDURE87

Curved Spiral Antennas-Brief Summary.....87
Two-Step Curved Spiral Antennas Correction Procedure.....88
Step One: Corrected Curved Spiral Cross-sections Elements.....88
Step Two: Corrected Curved Spiral Elements.....91

CHAPTER VII. SPIRAL ANTENNAS SIMULATIONS .....96

Projected Spiral Mounted in Mussel Simulation.....97
Discussion.....98

CHAPTER VIII. RESULTS AND DISCUSSION.....101

Range Measurements.....101
Elevation and Azimuth .....103
$S11$ Measurements.....104

CONCLUSIONS.....107

REFERENCES .....112

# LIST OF FIGURES

Figure 1. 'Big picture': Freshwater mussels in their natural ecosystem forming an underwater wireless biological sensor network. Mussels are equipped with backpacks, which houses radios and antennas, are nodes in the network. Mussels' backpacks also contain sensors to monitor their behavior such as gape and other environmental factors. Then, data is transferred via cellular modems to remote servers to be studied [1, 2].2

Figure 2. Cybermussel and mussel's backpack. The antenna is piece of wire forming a quarter-wavelength antenna, and is a placeholder for a more sophisticated and appropriate antenna. .....3

Figure 3. Mussel bed illustrating an underwater wireless sensor network (UWSN) and their communication links .....4

Figure 4. Mussels placed in the actual environment showing the unpredictability of their motion and the multi-medium habitat where the antennas will operate. .....4

Figure 5. As these examples illustrate, broadband antennas have complex structures with many radiating elements. Yagi-like antennas is inappropriate for the mussel application, while flat and curved spiral antennas are suitable. .....7

Figure 6. Submarine with loop antenna in place, where the submarine hull is used as part of the antenna system [26]. .....12

Figure 7. Proposed idea by the Project Sanguine of the US Navy [39]. .....14

Figure 8. Propagation of a radio wave over a water surface [45]. .....15

Figure 9. Mechanical structure used by Siegel and King to perform their experiment of submerged antennas in the Atlantic Ocean. It consists of polyfoam raft supporting antennas and electronic systems [47] .....19

Figure 10. Coaxial line section used by Hafez, Chudobiak, and Wight [50] to study properties of freshwater over wide range of frequencies using a VNA and measuring s-parameters. .....21

Figure 11. Detail of the apparatus used Glenn Smith [51] in 1984 to develop a procedure to analyze antennas for directive transmission into half-space. .....22

Figure 12. Dyson's original planar equiangular spiral antenna [55]. Left: drawing of the antenna. Right: Actual antenna prototype, focused on showing the center feed point configuration. .....25

Figure 13. Dyson's [56]conical spiral antenna (unidirectional nonplanar equiangular spiral antenna). Left: etched antenna fed with coax RG141/U bonded to the arms. Right: Embedded RG8/U coax cable to form the arms that was supported by polystyrene ribs. .....26

Figure 14. Kaiser's original circular and rectangular Archimedean spiral antennas drawing [17]. .....27

Figure 15. Curtis' [57] spiral antenna. Left: Curtis semicircles approximation of Archimedean spiral antenna. Right: Curtis' built prototype for semicircles Archimedean spiral antenna.....27

Figure 16. Left: Curved Archimedean spiral antenna printed on a layered cylinder [63]. Right: Curved squared spiral antenna above a conducting cylinder [64].....30

Figure 17. Radiation pattern as a function of cylinder length, H. (a) $H = 0.3\lambda 0$. (b) $H = 1.0\lambda 0$. (c) $H = 2.7\lambda 0$. (d) $H = 5.0\lambda 0$. Solid line and dotted line are theoretical results. Solid and emptied dots represent experimental results [64].....31

Figure 18. Radiation pattern as a function of cylinder length, r. (a) $r = 0.05\lambda 0$, (b) $r = 0.5\lambda 0$, (c) $r = 0.8\lambda 0$, (d) $r = \infty$ (Reference antenna). Solid line and dotted line are theoretical results. Solid and emptied dots represent experimental results. [64].....32

Figure 19. Curl antenna and Curl antenna array [67, 68]. .....33

Figure 20. Ratio $\sigma\omega\epsilon$ as a function of frequency for some common media showing that one can consider freshwater as lossy dielectric at 315 MHz [71]. .....42

Figure 21. Computing antenna radiated field block diagram [78].....46

Figure 22. Geometrical arrangement of a Hertzian Dipole and its associated fields [79].47

Figure 23. Antenna near-field and far-field patterns are shown for an antenna [80].....48

Figure 24. The image depicts the radiated regions on the antenna under test vicinity with their respective approximate boundaries [19].....50

Figure 25. Half-wave dipole antenna field zones are depicted with their boundaries and dominant terms at different distances from the antenna. Taking into account freshwater medium properties, the half-wave dipole antenna length is ~5 cm. .....52

Figure 26. Mussel shell capacitor created to study the electrical properties of the material. The precision LCR is shown with our own built fur terminal sensing or Kelvin connection.....53

Figure 27. Mussel shell parallel plate capacitor soldered directly to BNC connector.....55

Figure 28. VNA with mussel shell parallel plate capacitor .....55

Figure 29. LCR vs VNA Measurements of Dielectric Constant from Parallel Plate Capacitor .....56

Figure 30. Measured dielectric constant of parallel plate capacitor over antenna operating frequencies.....56

Figure 31. Coaxial transmission line with pulverized mussel shell insulator.....57

Figure 32. Inner conductor and pulverized mussel shell insulator of the coaxial Tx. line 57

Figure 33. Dielectric constant from coaxial transmission line .....58

Figure 34. Water conductivity measurement experiment. .....59

Figure 35. Mussel shells samples.....61

Figure 36. UI State Hygienic Laboratory shells elemental composition analysis results..62

Figure 37. Experimental setup used for air measurements at Reynolds park at Iowa City, IA. .....63

Figure 38. The antenna-radio system used in the underwater and air experiments. .....66

Figure 39. Dipole antennas range measurements in air using an Agilent Handled Spectrum Analyzer N9340B. The measurements were collected by increments of $\lambda water4$.67

Figure 40. Half-wave dipole antennas measurements in air. Azimuth measurements (red) matched well with ideal (blue). Far-field elevation measurements is difficult since this would require the measurement probe to be at least 5 m aloft of the antenna. Consequently, we performed elevation measurements in the near field. .....68

Figure 41. Experimental setup for evaluating range measurements of underwater antennas. The tank is filled with Iowa City tap water and the stepper motor precisely controls the distance between the transmitter and the receiving antennas. The stepper was computer-controlled. .....70

Figure 42. Experimental setup for azimuth and elevation measurements. .....70

Figure 43. Experimental setup to measure antenna input reflection coefficient ($S11$) in saturated sand. .....71

Figure 44. Experimental setup to measure antenna input reflection coefficient ($S11$) in freshwater.....72

Figure 45. Illustrating the underwater experimental setup used at diving pool. .....73

Figure 46. Inside The University of Iowa Aquatic Center – diving pool photographs showing the actual setup and the certified divers. .....74

Figure 47. Exploratory plan of the location and graphical results of the signal strength of the measurements underwater with power of $-10$ dBm. After this initial study, we chose to limit our measurement to around $\sim 9\lambda$. .....75

Figure 48. Board design specifically for the antenna testing without all the sensor and components that are included in the cybermussel backpack. .....76

Figure 49. Any type of underwater work with electronic devices such as radios mounted in a circuit board requires significant effort to properly waterproof the equipment. ....76

Figure 50. Underwater range dipole antennas measurements. The measurements were collected by increments of $\lambda water4$. .....77

Figure 51. Dipole antenna elevation and azimuth measurements in freshwater. The measurements were collected by rotation increments of $22.5o$ .....77

Figure 52. Dipole antenna in freshwater numerical analysis using FEKO. The range plot is shown depicting the Near and Far field regions of a naïve (simple pieces of wires) and FEKO-recommend structural design (thinner cylinder). .....78

Figure 53. Dipole antenna elevation and azimuth simulations in freshwater using FEKO CEM software tool. The measurements were calculated by rotation increments of $1o$. .....79

Figure 54. Coordinate system used by Curtis [57]. .....81

Figure 55. Left: one-arm spiral approximation using semi-circles. Right: two-arm spiral approximated using semi-circles [57]. .....83

Figure 56. Flat Archimedean spiral antenna with its design parameters. .....85

Figure 57. Cross-section cut of the flat and curved spiral showing the geometric components used in the corrected curved spiral antenna elements. .....88

Figure 58. Cross-section calculating showing flat spiral elements, projected spiral elements and calculated corrected curved spiral elements.....91

Figure 59. Illustration of parameters for finding spiral elements over the 3D contour. ....92

Figure 60. Mussel Model depicting materials and dimensions.....96

Figure 61. 3D model of the geometry and mesh for the simulation. The shells are modeled as a paraboloid with a radius of 5 cm and a focal depth of 2.5 cm. The radiation patterns were calculated in spherical coordinates in increments of radius $\boldsymbol{r}$ by 10 cm, angle $\theta$ by 5°, angle $\phi$ by 5° with a total of 83,731 field points. .....97

Figure 62. Normalized power and normalized $S11$ simulation results for a projected spiral antenna mounted on a mussel. .....100

Figure 63. Range measurements in freshwater for dipole, flat spiral and projected spiral antennas. .....102

Figure 64. Simulated and measured range for a flat spiral antenna. .....102

Figure 65. Elevation measurements for a flat (blue) and projected (red) spiral antennas in freshwater.....103

Figure 66. Azimuth measurements for a flat (blue) and projected (red) spiral antennas in freshwater. Points are measured values and lines are the theoretical values. .....104

Figure 67. Normalized $S11$ magnitude for a flat-, projected-, and curved spiral antenna.105

Figure 68. The projected surface in this simulation is 2.5 times than that of the surface for Figure 61. This result demonstrates that as the projected spiral antenna surface radius increases, its $S11$ behavior approaches that of the flat spiral. .....105

Figure 69. Normalized S11 simulated with FEKO and measured in freshwater as is illustrated in Figure 37 using a VNA. The measured and calculated results are consistent. .....106

# LIST OF TABLES

Table 1.Water conductivity experiment results. .....60

Table 2. Mussel shell samples dimensions .....61

Table 3. Flat Archimedean spiral antenna specifications .....86

Table 4. Poynting vector parameters calculation in water .....97

# CHAPTER I. INTRODUCTION

## Motivation, Scope of the Thesis

Researchers at the University of Iowa have been exploring the use of freshwater mussels as biological sensors [1-6]. Fertilizer runoff from Midwestern farms impact the river environment and eventually end up in the Gulf of Mexico, where the nutrients contribute to the creation of so-called *dead zones* [7]. Through their feeding and excreting the mussels impact the river ecosystem. The mussels are filter feeders [8] and ingest algae and phytoplankton. By studying mussel gape (the rhythmic opening and closing of their valve), researchers aim to correlate mussel gape and feeding, and ultimately estimating the nutrient load. Mussels also impact the river environment. They excrete ammonium ($NH_4^+$) in the benthic zone where bacteria and other organisms transform the ammonium back to nitrogen gas [9-11]. They are considered an indicator or *sentinel species* [12-15] in that their health is an indication of the overall health of their river environment.

Freshwater mussels—typically Pocketbook (*lampsilis cardium*)—are equipped with *backpacks* that house sensors and small radios that operate at 315 MHz [16]. The backpack includes temperature, heartbeat, and Hall Effect sensors (see Figure 2). The latter, along with a small magnet, is used for sensing mussel gape. The radios relay the sensed data via underwater wireless links (shown in Figure 1) to an onshore receiver. There are many facets to the vision depicted in the figure: sensor design, physical design of the backpack, and wireless sensor network (WSN) design. The underwater RF environment is complex and requires careful consideration of many issues, including antenna design. The latter is the focus of this thesis.

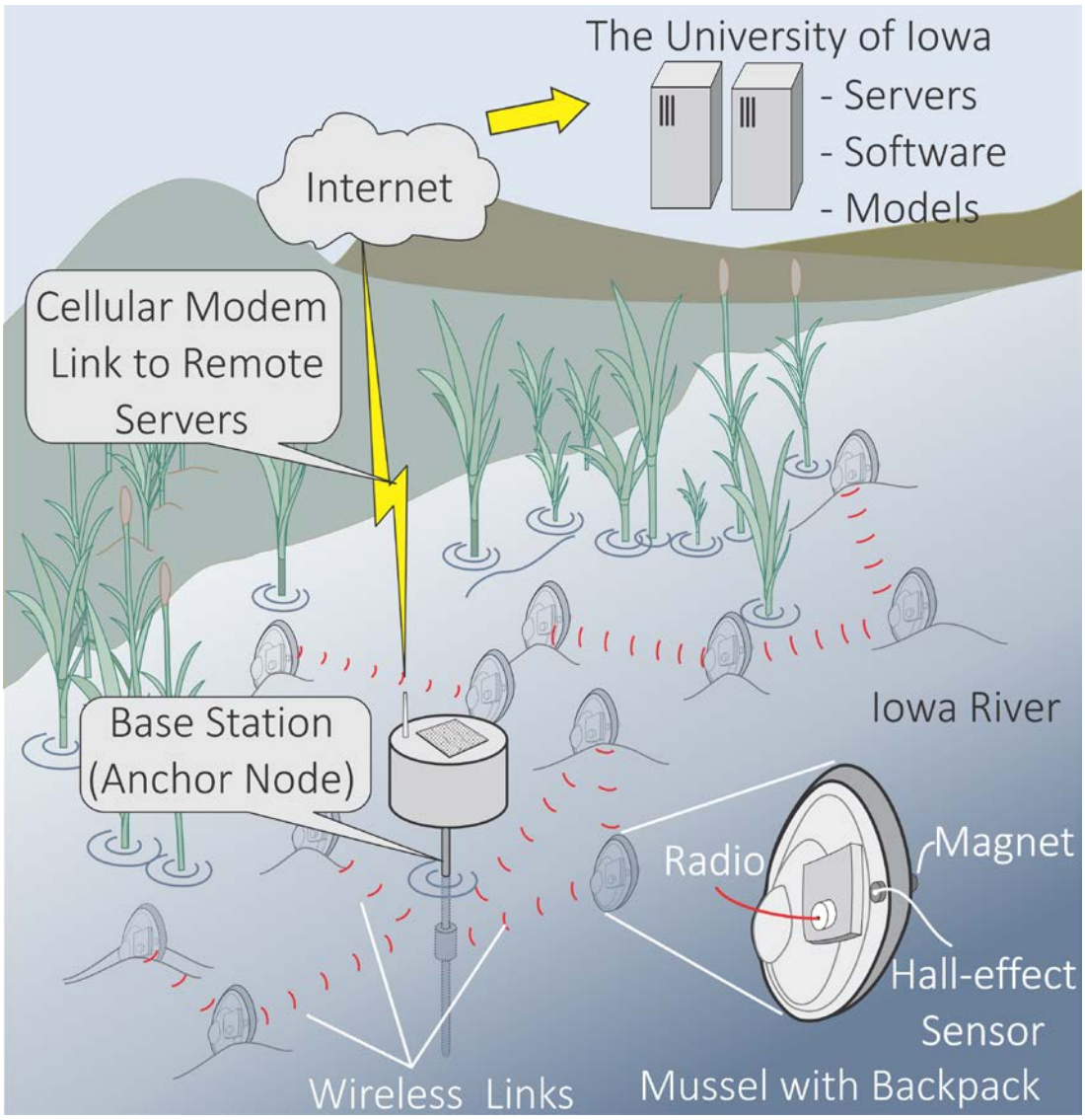


Figure 1. 'Big picture': Freshwater mussels in their natural ecosystem forming an underwater wireless biological sensor network. Mussels are equipped with backpacks, which houses radios and antennas, are nodes in the network. Mussels' backpacks also contain sensors to monitor their behavior such as gape and other environmental factors. Then, data is transferred via cellular modems to remote servers to be studied [1, 2].

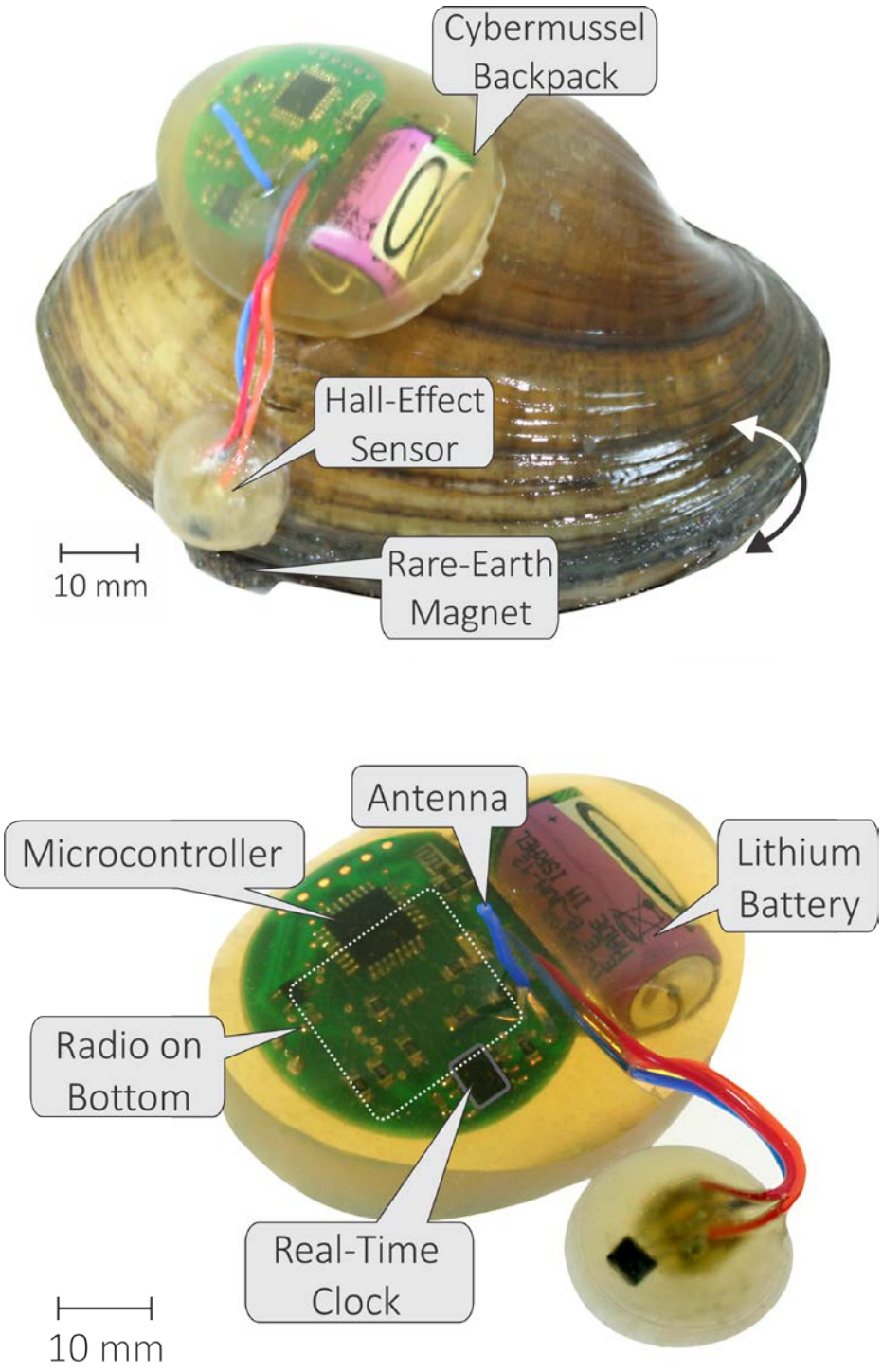


Figure 2. Cybermussel and mussel's backpack. The antenna is piece of wire forming a quarter-wavelength antenna, and is a placeholder for a more sophisticated and appropriate antenna.

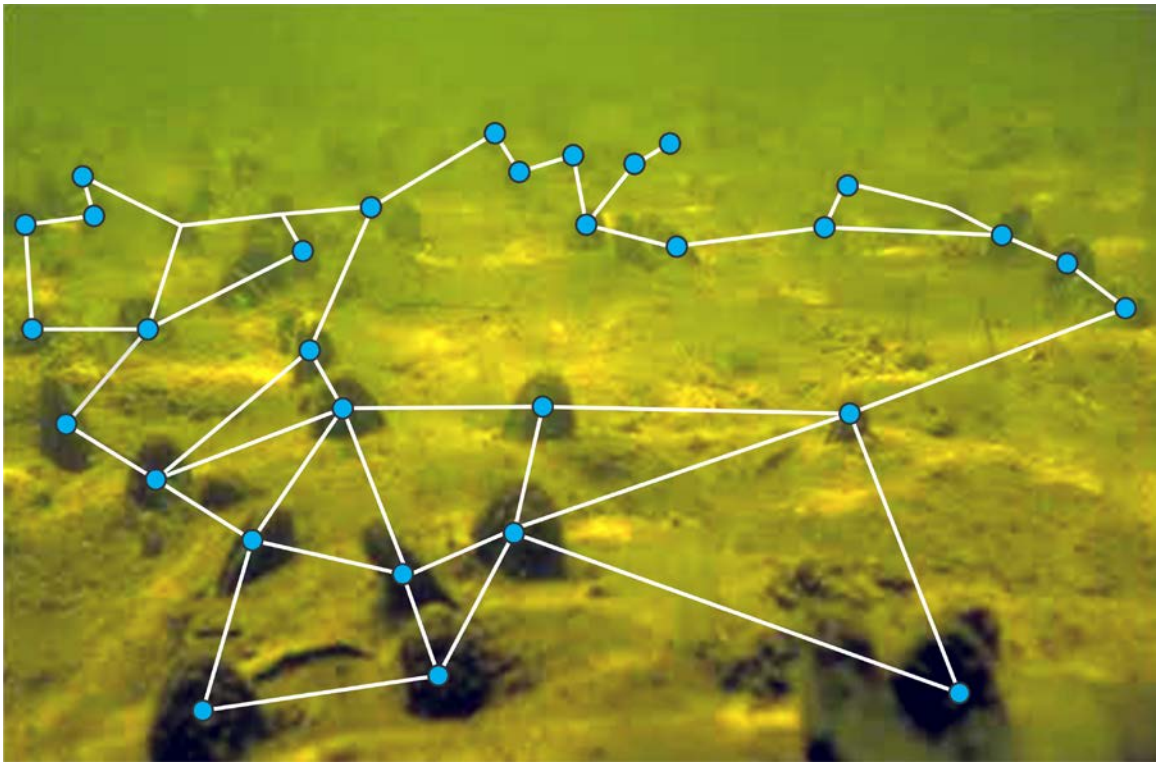

Figure 3. Mussel bed illustrating an underwater wireless sensor network (UWSN) and their communication links

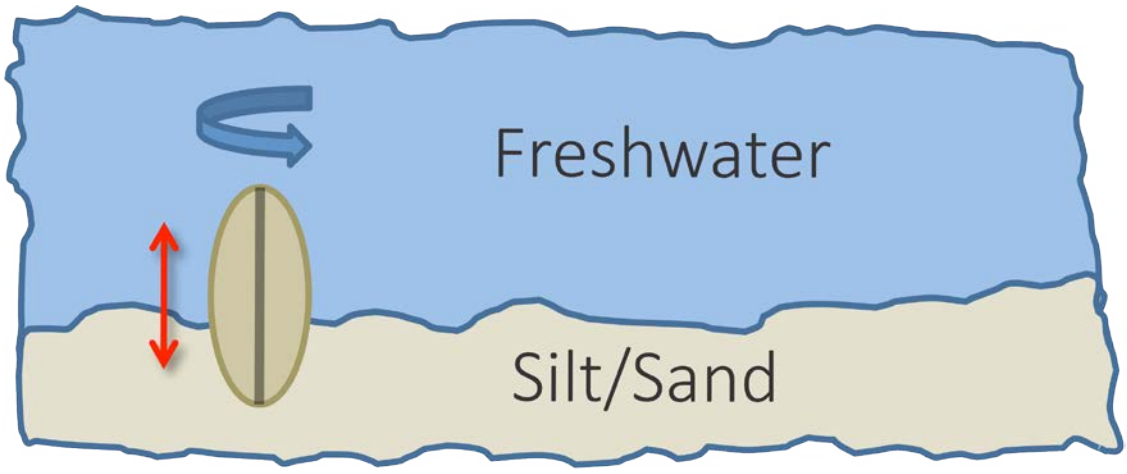


Figure 4. Mussels placed in the actual environment showing the unpredictability of their motion and the multi-medium habitat where the antennas will operate.

## Antenna Requirements and Conceptual Solution

The physical requirements for the mussel application dictate that the antennas be small, lightweight, and not impede their hosts' motion. The Pocketbook mussel dimensions are roughly 8 cm × 12.5 cm. A backpack and hence antenna should fit the contour of the mussel's shell. Mussel movement and antenna orientation is unpredictable as shown on Figure 4, so non-directional antennas are desirable. Further, mussels burrow into the silt at the river bed, and these change an antenna's electromagnetic environment significantly. This is because an antenna may be partially in sand/slit or completely in/out of the sand/slit at the river bed, and the dielectric properties of water and a water/sand mixture are different. Different mediums have different electromagnetic properties, and thus have different wavelength—about 10 cm in water and 17 cm in saturated sand at 315 MHz—radiation resistance, and input impedance. If we take an antenna designed for free-space and place it into water or silt, it is effectively a new antenna and behaves differently.

The input impedance of an antenna changes if the antenna is moved between different mediums. These changes affect radiation efficiency as well as the antenna's input impedance. Changes in input impedance can lead to severe impedance mismatch with the radios, which may cause the radios to cease functioning. Even if the impedance mismatch does not cause the radios to malfunction, impedance mismatch is problematic. Radios are designed to see a certain antenna input impedance. When the antenna and radio are well-matched (impedance-wise) maximum power is radiated allowing for longer communication links and/or extended battery life for the mussel backpacks.

The need for constant input impedance implies the need for a broadband antenna [17]. There are several types of broadband antennas such as biconical, helical, log periodic,

sleeve, and spiral. Broadband antennas are divided into two main categories based on their geometry: *circular* or *linear* [18]. The antenna geometry defines the active region, polarization, and the gain of the antennas. Most of the power is radiated out of the active region. Circular geometry antennas have circular polarization and their active region is located where the circumference is one wavelength. Examples of spiral antennas are shown in Figure 5 (c) and (d). Linear antennas have linear polarization, and their active region is where the extension of their elements reaches half-wavelength. Examples of linear antennas include log-periodic antennas shown in Figure 5 (a) and (b).

As explained above, for our particular application we require an antenna that is small, lightweight, fits the contour of the mussel's shell, and has relatively constant input impedance over multiple mediums. We have chosen circular geometry broadband antennas for the mussel application as they work better for our needs given the above criteria. Spiral antennas belong to a class of frequency-independent antennas, and more importantly for our application, they have relatively constant input impedance over a wide bandwidth [19]. Furthermore, (curved) spiral antennas can fit snuggly to the mussel shell contour. This is an important consideration, since biologists are concerned that protruding attachments may impede mussels' burrowing.

(a) SAS-517 Log Periodic Antenna 80 MHz – 4 GHz manufacturer by A. H. Systems Inc. [20]

(b) Model 0285 Log Periodic Antenna 2-18GHz Wideband Antenna manufacturer by Syndetic Pty. Ltd. [21]

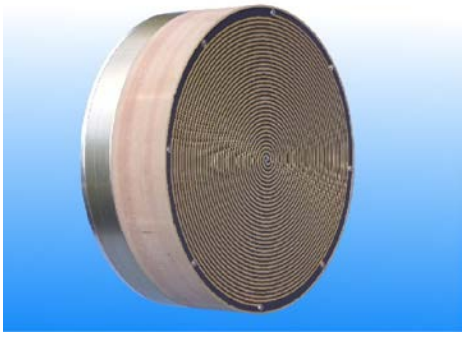

(c) QSPCP0.5-22SLH Circularly Polarized Spiral Antenna 0.5 to 22 GHz manufacturer by Q-par Angus Ltd Barons Cross Laboratories [22].

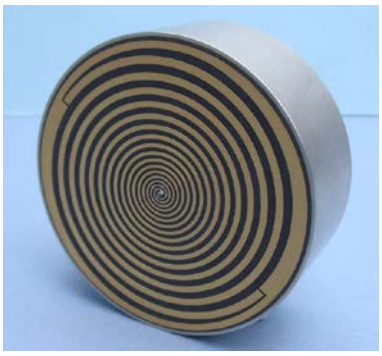

(d) QSPCP2-18SRHRA Circularly Polarized Spiral Antenna 2 to 18 GHz manufacturer by Q-par Angus Ltd Barons Cross Laboratories [22].

Figure 5. As these examples illustrate, broadband antennas have complex structures with many radiating elements. Yagi-like antennas is inappropriate for the mussel application, while flat and curved spiral antennas are suitable.

## Challenges

As is shown in the Literature Review (Chapter II), others have done research related to underwater EM propagation and antennas. However, much of this research is only partially relevant the focus of this thesis. For example, there has been underwater antenna research, but mostly for seawater and driven by military applications. Our antenna is designed for application in *freshwater*. Freshwater has a conductivity of 0.04 S/meter which is about hundred times less than the conductivity of seawater. Consequently, at the nominal 315 MHz where the mussel backpack antennas operate, freshwater behaves as a lossy dielectric [23].

Even when theory exists, the resulting equations are unwieldy and one has to resort to numerical techniques. Additionally, antenna measurements are challenging. Ideally one would use an underwater anechoic chamber similar to what is used in underwater acoustics research [24]. Our solution is to make measurements in a diving pool and a large water tank. Still, the logistics of such measurements are considerable. Therefore, it makes sense to rely on computer Computational Electromagnetics (CEM) software tools. Fortunately, modern CEM software tools are very mature and by some accounts [25] have replaced mathematical analysis and experimental work as the main design and analysis tool for antennas. However, to utilize CEM software tools, one must understand the tool capabilities and limitations. Further, these tools have many input parameters that must be carefully considered in order to obtain valid results.

## Approach I Used

I started with a well-known case—dipole in air—and made measurements and simulations and made sure the results are congruent. This gave me confidence that I am using the simulation software properly and that experimental protocols are valid. Next, I performed measurements and simulations on a dipole in water and show that results are congruent. Then, I performed extensive simulation on spiral antennas, and experimentally validated a small number of test cases.

## Thesis Roadmap

Chapter II, *Literature Review*, is a review of the current literature related to this thesis, namely underwater EM propagation, some material on broadband antennas, and spiral antennas.

Chapter III, *Summary of Relevant EM Theory Related to Thesis*, starts with Maxwell's equations. Using these, we show that freshwater behaves as a lossy dielectric at the nominal backpack radio frequency. The chapter also contains a summary of relevant underwater/freshwater radio propagation issues.

Chapter IV, *Simulation and Experimental Protocols*, documents simulation and experimental results for a dipole in air and some results for a dipole in water. As explained above, the purpose of performing these simulation and measurements is to establish the proper simulation- and experimental protocols.

Chapter V, *Spiral Antennas*, reviews the theory of planar (flat) spiral antennas, and describes a procedure for flat spiral antenna design.

Chapter VI, *Curved Spiral Antennas and Correction Procedure*, starts with a brief summary of existing curved spiral antennas. I then develop a two-step technique for designing curved spiral antennas.

In Chapter VII, *Spiral Antennas Simulations*, contains spiral antennas simulation using FEKO. 3D geometry models and numerical results are presented.

In Chapter VIII, *Results and Discussion*, theoretical, simulated and experimental results are analyzed for dipole-, flat spiral, projected spiral and curved spiral antennas. We present results for range, elevation, azimuth, and $S_{11}$ measurements.

# CHAPTER II. LITERATURE REVIEW

## Underwater Antennas

The vast majority of prior work related to underwater antennas was done in seawater, with the normal impetus military applications. The earliest papers that documented underwater antenna experiments were published in 1919 and 1920, shortly after World War I, when submarine communications stimulated the study of submerged antennas. Willoughby and Lowell [26] conducted experiments with the objective of developing an apparatus for the detection of submarines, and in the process they found that radio signals could be received by means of loop antennas in water. Successful communication was achieved between two submarines running at full speed and entirely underwater at about 20 km (12 miles) apart with a wavelength of 952 m. Loop antennas, which incorporated the hull of the submarine as part of the antenna system, were used, as shown in Figure 6 [26-28]. U.S. Navy Lieutenant-Commander Taylor carried out underground and underwater antenna experiments. The underwater experiments were conducted using long antenna wires of up to 153 m at a Navy Station in Washington and a submarine base [27].

Even though many experiments were done before and during World War II regarding fully submerged submarine-to-submarine communication in sea water, Ronald K. Moore was the first to work out the Electromagnetic (EM) theory of submerged antennas in 1951 in his doctorate thesis at Cornell University [29]. In the subsequent postwar research boom, many studies on antennas in lossy and/or conducting medium were conducted by Wait [30-33], Anderson [34], Moore [35], and Kraichman [36].

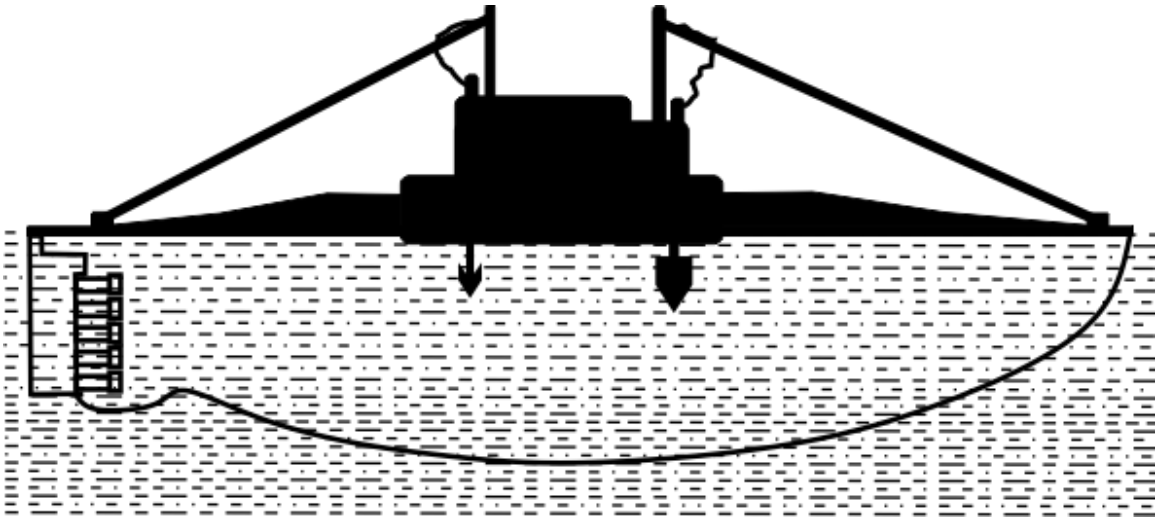

Figure 6. Submarine with loop antenna in place, where the submarine hull is used as part of the antenna system [26].

Wait [30-33] studied magnetic dipole (or small current-carrying loop), finite wire, insulated loop, and Hertzian dipole (or electric dipole) antennas in a conducting medium. The last case, the Hertzian dipole, was investigated in seawater by situating the antenna perpendicular to the surface of the water, and just above the surface. He concluded that the field attenuated at least 20 dB with respect of the field on the surface for a distance of 30 m into the water using an operating frequency of 30 kHz.

Anderson [34] illustrated by calculations using seawater as medium and a magnetic dipole as a source, the energy density spectra of the transient electromagnetic fields for various distances from the source using seawater as a medium and a magnetic dipole as a source. He concluded from his experiments that the power propagation downward into the water is proportionally as $1/r^2$ and $1/r^3$ for the electric and magnetic fields, respectively.

Moore [35] analyzed antennas in air as well as in a conducting medium and noticed great differences in antenna gain and radiation pattern between the two mediums. He investigated biconical, loop, and two forms of straight wire antennas. He concluded that the dissipation of energy in the medium affected the gain and radiation pattern.

Kraichman [36] undertook experimental work using dipoles and loops as electromagnetic sources in a specially built pool facility. To simulate seawater, the pool was filled with a concentrated sodium chloride solution.

With increasing technological advances during and after World War II, submerged submarine communications through seawater gained importance. In the 1950s nuclear power sources became available and removed the need to recharge batteries on submarines. Therefore, submarines could stay submerged for extended periods. This introduced the need for improved communication between submarines deep underwater and stations on land. Furthermore, the U.S. Navy needed a robust communication system that neither revealed submarines' locations nor reduced their motion velocity or maneuverability. The most significant challenge was to communicate with submarines at sea 100 m underwater.

In 1959, the U.S. Navy started the secret Sanguine Project (Figure 7) to develop communication systems for submerged nuclear submarines and submarine stations. The project was made public in 1971 [37]. The project's main goal was to facilitate one-way radio communications with submarines at depth anywhere in the world [38]. Here, extremely low frequency (ELF), the frequency band 30 Hz to 3kHz, was chosen since the lower a wave's frequency, the less of its energy is absorbed by seawater.

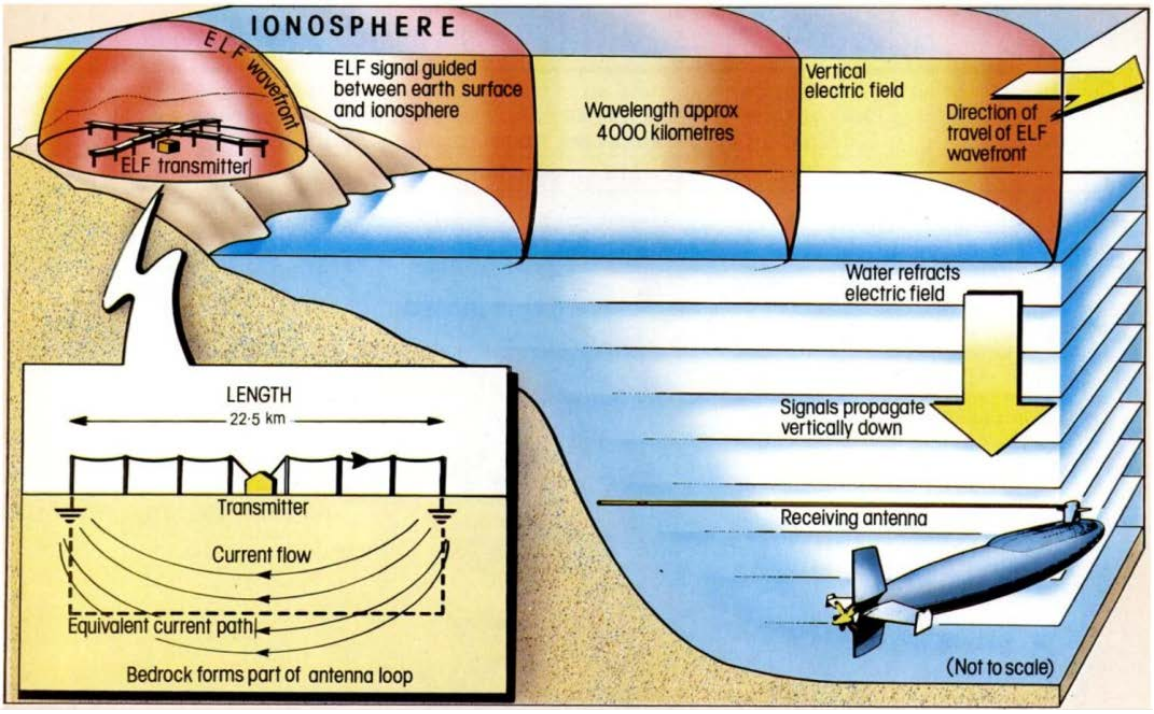


Figure 7. Proposed idea by the Project Sanguine of the US Navy [39].

In 1963, an experiment between a radio station located at North Carolina and a nuclear submarine at 3,200 km range using an antenna located near keel depth was conducted using ELF (30–300 Hz) [40]. The Sanguine ELF operating frequency of 300 Hz implies that a half-wave dipole antenna would be 1,000 km long. This is clearly impractical, and the designers had to settle for antennas that were very small compared to the ELF wavelength. Different configurations were proposed for the both surface and underwater station antennas. Some the surface antennas considered were helicopter-suspended wires and mountain loops [41]. For the underwater antennas, a buoyant-cable antenna of 610 m was attached to the submarine [42].

Challenges to submarine antenna design included not only complications common to antennas in general, but a variety of unique environmental conditions such as wide temperature variations, hydrostatic pressures, salt deposits, exposure to sunlight, and icing

conditions. After World War II, the Navy Research Laboratory developed an omnidirectional crossed-loop antenna mounted on a retractable mast for submarines [43]. The investigation of air-to-undersea communication gained importance for military applications such as helicopter-to-submarine communication. One suggested solution consists of a vertical electrical dipole in air with a horizontal electric dipole in sea at 10 to 100 kHz based on field-strength considerations. This study showed the changes in wavelengths with respect to the medium of propagation at different frequencies [44].

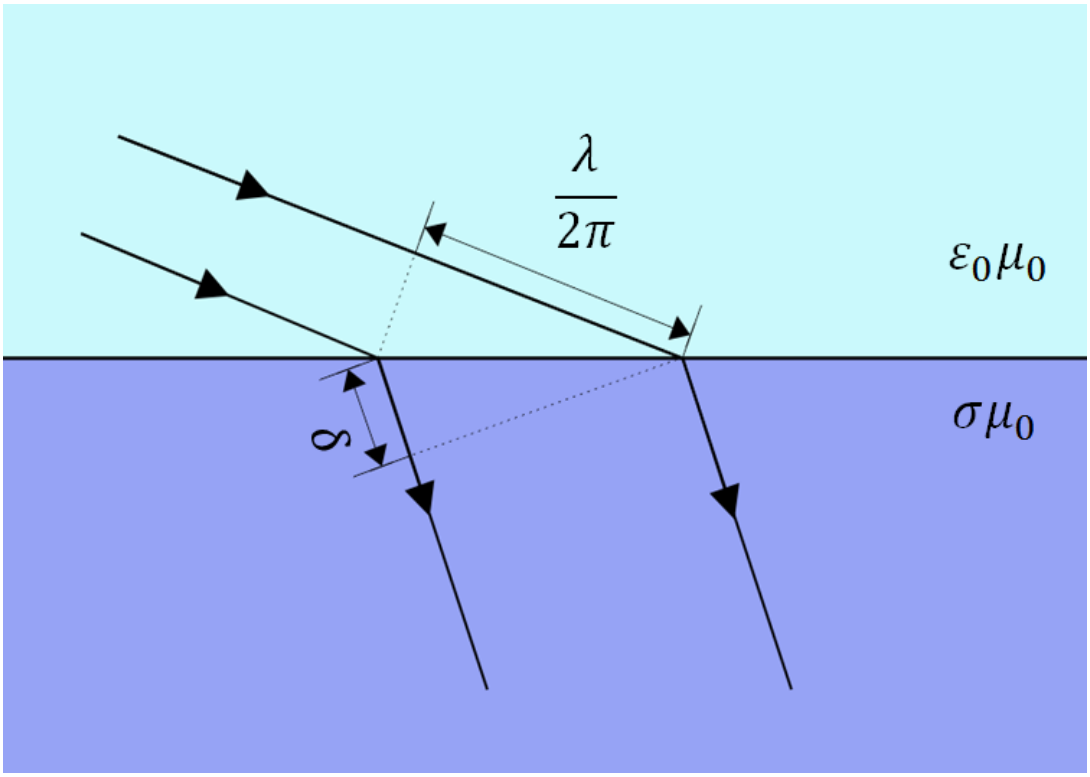


Figure 8. Propagation of a radio wave over a water surface [45].

In 1958, Wheeler investigated performance of Very Low Frequency (VLF) antennas located under the surface of seawater and mounted on a submarine. The sketch in

Figure 8 is used by Wheeler to explain the propagation of a radio wave over a water surface. The direction of propagation is tilted downward, and a fraction of the power is directed into the water. Thus, the vertical propagation downward in the water is accomplished by horizontal crossed electric and magnetic fields. The following values were used: seawater conductivity of 4 S/meter, a frequency of 15 kHz and skin depth of 2 m or 4.3 dB/meter. Wheeler calculated skin depth using the formula in Equation 1, where $\delta$ is skin depth, $\omega$ is radian frequency, $\mu_O$ is permeability, $\sigma$ is conductivity in water, and $\lambda$ is wavelength in air [45].

$$\delta = \sqrt{\frac{2}{w\mu_O\sigma}} = \frac{1}{2\pi}\sqrt{\frac{\lambda}{30\sigma}} \qquad \text{Equation 1}$$

A cornerstone of underwater communication at sea was Richard K. Moore's publication in 1967 [46], where he did a broad examination of the topic. By this time, undersea communication had become vital, not only for submarines, but also oceanography. Moore concluded that due to depth attenuation and atmospheric noise within the sea, the communication with men in the moon would be easier than with a 100 km submerged depth submarine. Electromagnetic properties of seawater and its mathematical formulations were presented as follows. Consider a plane wave traveling in the sea, with electric field *E* given by

$$E = E_o e^{j\omega t - \gamma x} \qquad \text{Equation 2}$$

where γ, the propagation constant, describes the properties of the medium:

$$\gamma = \sqrt{j\omega\mu(\sigma + j\omega\varepsilon)} = \alpha + j\beta = \frac{1}{\delta} + j\beta \qquad \text{Equation 3}$$

In the specific case where a high enough frequency is used such that the displacement current greatly exceeds conduction current, the frequency-independent value of α becomes

$$\alpha = \frac{1}{\delta} = \frac{\sigma}{2}\sqrt{\frac{\mu}{\varepsilon}} \qquad \text{Equation 4}$$

For example, $\sigma = 4\ \mathrm{S/m}$ and $\epsilon = 81\epsilon_o$ results in an $\alpha = 84\ \mathrm{nepers/m}$. Therefore, $\delta = 0.0119\ \mathrm{m}$, and this kind of penetration at these high frequencies is unacceptable. For this reason, Moore justified the use of low frequencies for communication under the sea. Thus, at low frequencies, where displacement current may be neglected, the propagation constant is approximately

$$\gamma = \sqrt{\mathrm{j}\omega\mu\sigma} = \sqrt{\frac{\omega\mu\sigma}{2}}(1 + \mathrm{j}) = \alpha + \mathrm{j}\alpha = \frac{1}{\delta} + \mathrm{j}\frac{1}{\delta} = \beta + \mathrm{j}\beta \qquad \text{Equation 5}$$

where,

| | |
|---|---|
| $\gamma$ | propagation constant, |
| $\omega$ | radian frequency [rad/s], |
| $\mu$ | permeability (magnetivity) [H/m], |
| $\varepsilon$ | permittivity [F/m], |
| $\sigma$ | conductivity [S/m], |
| $\delta$ | skin depth, Napier depth, or radian length in water [m], |

$\alpha$ attenuation constant, parameter or coefficient [Nepers/m],

$\beta$ phase constant, parameter or coefficient [rad/m].

In this work, surface-to-submarine, submarine-to-surface, and submarine-to-submarine propagation had been considered for further analysis. Submarine-to-submarine propagation implies the combination of the other two cases to create the communication link owing to the extremely high attenuation for direct waves between two submerged stations. As mentioned before, Moore concluded that depth attenuation and atmospheric noise limits the communication ranges. Ranges in tens of kilometers are possible with bandwidths restricted to order of 1 Hz, using trailing-wire antennas, and transmit powers of tens of kilowatts, for antennas submerged within 5 m of the surface of the water [39].

Siegel and King [47] performed experiments between antennas submerged in the Atlantic Ocean using the setup shown in Figure 9. They measured electric field strength, antenna current distribution, and antenna input impedance and they compared their measurements with theoretical predictions and obtained good agreement. They used short dipoles at 100 kHz and 14 MHz submerged at 0.15 m [47]. They measured electric field strength at $-10.9$ dB/m and $-128$ dB/m for 100 kHz and 14 MHz respectively.

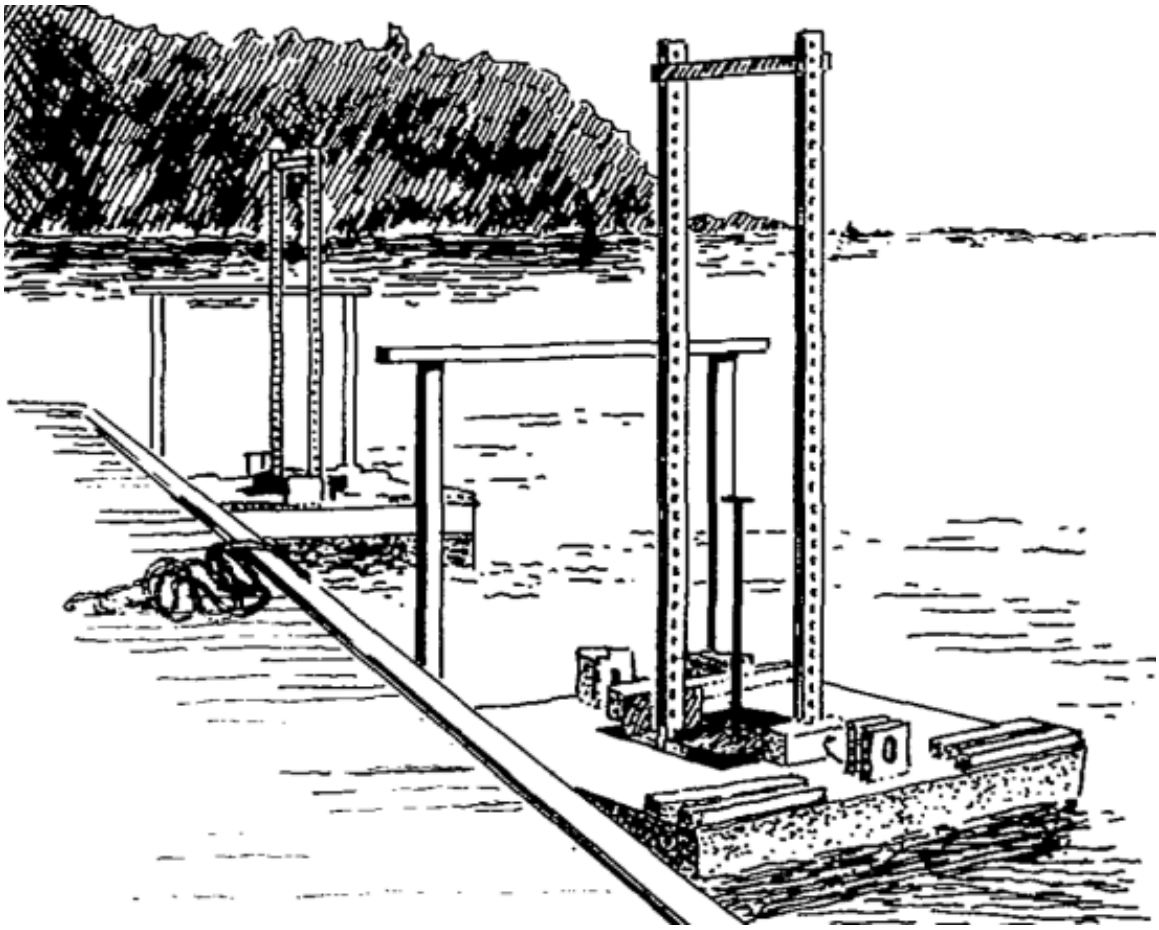

Figure 9. Mechanical structure used by Siegel and King to perform their experiment of submerged antennas in the Atlantic Ocean. It consists of polyfoam raft supporting antennas and electronic systems [47].

**Underwater-Freshwater Radio Propagation**

Freshwater research has been done mainly by experimentation in different lakes at different depths, though there were attempts at calculating radiation patterns for an antenna in half-space. In 1960, Saran and Held [48] performed experiments measuring field strength of monopoles and loop antennas at different depths in a lake up to 304.8 m (1,000 ft). They used a transmission frequency of 18.6 kHz and measured the lake conductivity as 2.66 mS/m. Their experimental and theoretical results demonstrated that for different antennas the field strength attenuates exponentially with depth in freshwater.

In 1976, Shen, King, and Sorbello [49] measured field patterns of submerged antennas in the Mystic Lake in Massachusetts at 144 MHz. The lake water had a relative permittivity of 81 and conductivity of 60 mS/m. They used a traveling wave antenna for the transmitter, which was constructed using a 0.32 cm diameter brass wire insulated by an air-filled Plexiglas tube. The arms of the antenna were the length of one wavelength in air, namely 2.08 m. The transmitter antenna was placed 17.5 cm below the surface of the water. They had two receiver antennas, one inside the lake, which was a bare dipole antenna with length of half-wavelength in water, 11.6 cm. The other receiver antenna used for measuring the field strength outside the water, was a dipole antenna of approximately quarter-wavelength at its operating frequency in air. Therefore, the experiment was set such that they had two dipoles, one in air and another that went deep into the water (~50 m), and the third antenna, which is the antenna under test, was the traveling wave antenna that was barely into the water, and fastened below to their floating structure. They computed theoretical data for the electric field pattern and measured the electric field pattern with the setup described. Their computed and measured electric field pattern shapes are similar.

They concluded that an insulated travelling-wave antenna is suitable for subsurface communication in a lake water at 144 MHz. They conclude that 144 MHz water behaves like a dielectric.

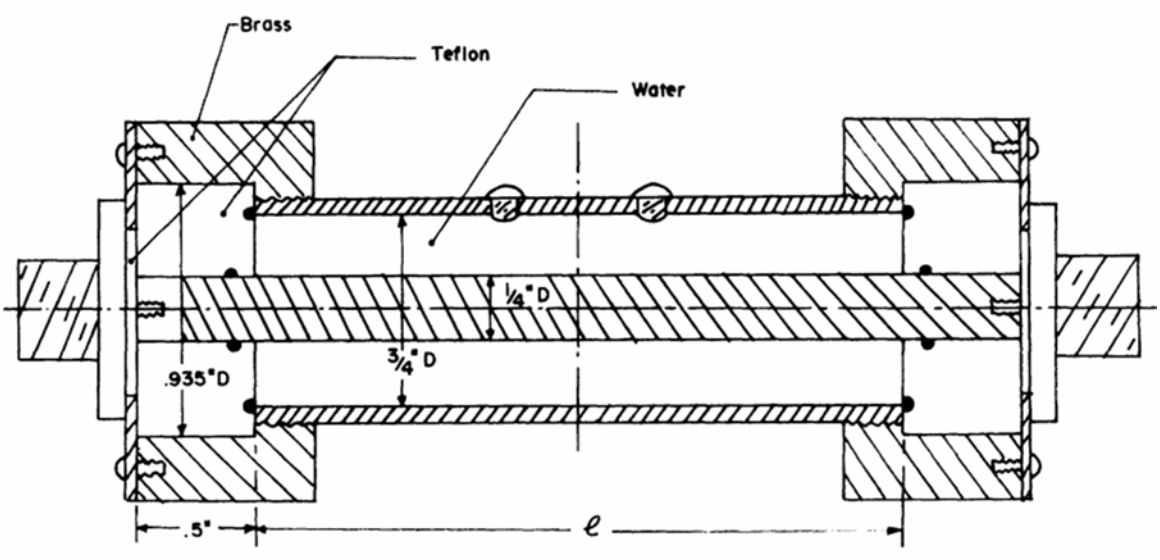


Figure 10. Coaxial line section used by Hafez, Chudobiak, and Wight [50] to study properties of freshwater over wide range of frequencies using a VNA and measuring s-parameters.

In 1979, Hafez, Chudobiak, and Wight [50] investigated the attenuation in freshwater, using a coaxial line apparatus (shown in Figure 10), to verify the feasibility of developing a VHF radar system capable of sensing the depth of shallow freshwater (<10 m) for remote sensing applications. They used a VNA to measure s-parameters between frequencies ranges of 33 and 363 MHz. They concluded that it is possible to develop an airborne VHF radar system capable of sensing the depth and/or detecting large objects in shallow freshwater since the attenuation rates were about 2.5 dB/m at 100 MHz and 100 mS/m of frequency and conductivity, respectively.

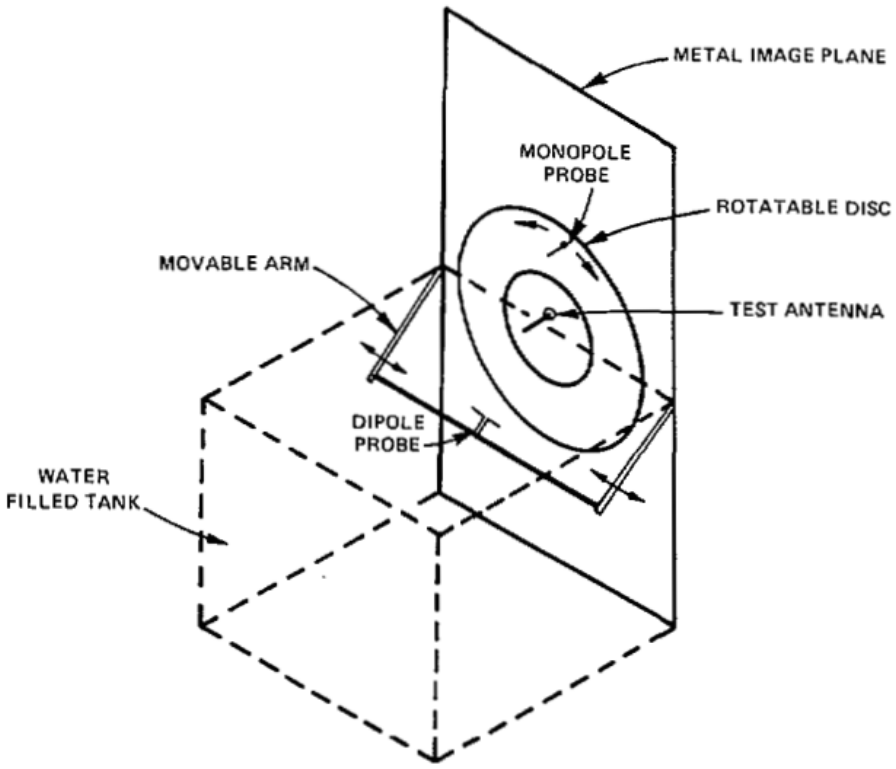


Figure 11. Detail of the apparatus used Glenn Smith [51] in 1984 to develop a procedure to analyze antennas for directive transmission into half-space.

Glenn Smith [51] developed a procedure to analyze for directive transmission into half-space. The antennas' half-space directive properties are pattern function, gain and directivity. Half-space refers to the case where antennas are placed in adjacent mediums, air (region 1) and water (region 2) in this instance. Theoretical results were presented for infinitesimal electric and magnetic horizontal dipole antennas in a dielectric half-space. The directive transmission was into the adjacent dielectric half-space, where $\varepsilon_2/\varepsilon_1 > 1$. Smith's apparatus, shown in Figure 11, was used to measured field patterns at different distances. He compared theoretical and experimental results for dipole and loop antennas

in half-space, and these showed good agreement. He concluded that the directivity increases with ratio of height and $\lambda_o$.

A newer application, 2012, for antenna in freshwater and also related to freshwater mussel was presented by Fischer, Neebling and Quist [52]. They developed and tested a boat-mounted RFID (radio frequency identification) antenna for monitoring freshwater mussels. They used commercially available low-frequency half-duplex RFID readers. It is not clear which one of the RFID frequencies they used. They achieved detection up to 1.8 m distances in vertical orientation into the freshwater.

**Spiral Antennas**

Spiral antennas are a class of broadband antennas, which exhibit characteristics such as circular polarization, radiation pattern and input impedance that are largely independent of frequency over wide range of frequencies [53], and they are compact. They have been studied for almost 60 years.

In 1955, Edwin M. Turner [54] submitted a patent of his invention that he called a *spiral slot antenna,* thus becoming the pioneer of spiral antennas. His spiral antenna was designed for high-speed aircraft, and to cover VHF and UHF frequency bands. Several publications related to spiral antennas appeared in the subsequences years. In 1959, Dyson's presented two publications on his work on planar [55] and nonplanar equiangular spiral antennas [56]. Dyson verified the characteristics of the planar (Figure 12) balanced equiangular spiral antennas (Figure 13).

Dyson investigation determined that the antenna bandwidth is only limited by the precision of the construction of the feed point and the selected arm length. In other words, the outer radius determines the lowest frequency. The lowest frequency of the bandwidth of the spiral antennas occurs when the circumference of the spiral is equal to one wavelength. Dyson's second contribution was inventing unidirectional nonplanar equiangular spiral antennas, which was achieved by wrapping the arms on a conical surface.

Kaiser, in 1960 [17], pioneered with the Archimedean two-wire spiral antenna. He intuitively explained the radiation of the square and circular Archimedean spirals, shown in Figure 14. Kaiser also presented different antenna configurations such as single spiral,

spiral doublet, spiral double array, spiral in a trough, and spiral trough array. In the same year, Curtis [57] calculated the radiation pattern of the Archimedean spiral by approximating the spiral with a series of semicircles (Left on Figure 15). He calculated the radiation field of a single semicircle and then generalized for the entire spiral, added the second arm rotated and translated to form a symmetrical and balanced spiral. Curtis presented step-by-step clear calculations for the radiation field of the Archimedean spiral antenna. He also presented experimental validation (Right on Figure 15), concluding that the pattern breaks into two lobes when the arm is greater that half-wavelength.

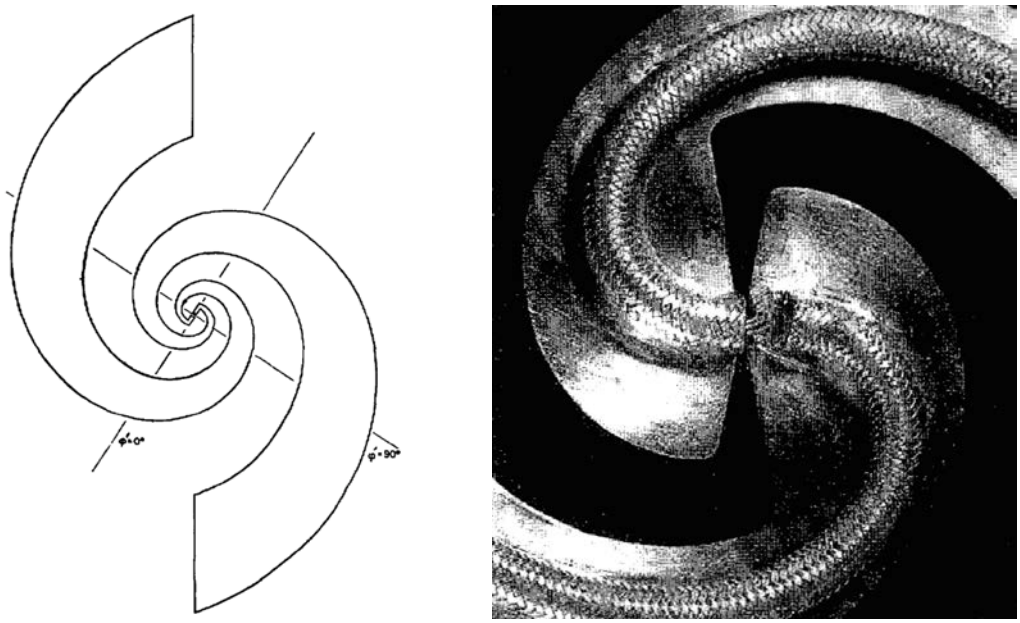

Figure 12. Dyson's original planar equiangular spiral antenna [55]. Left: drawing of the antenna. Right: Actual antenna prototype, focused on showing the center feed point configuration.

Bawer and Wolfe [58] presented a complete study on spiral antennas, considering various parameters such as cavity diameter, cavity depth, conductor loading, spiral rate of

growth in a logarithmic fashion, and square and Archimedean shapes. One particular result on the study was a comparison of round and square spirals, showing their differences in measured gains. The authors explained that their difference was that since their radiation occurs when the circumference of the spiral is one-wavelength for the round one and when width is equal to quarter-wavelength for the square one. However, the width of square spiral was 75% of the diameter of the round antennas.

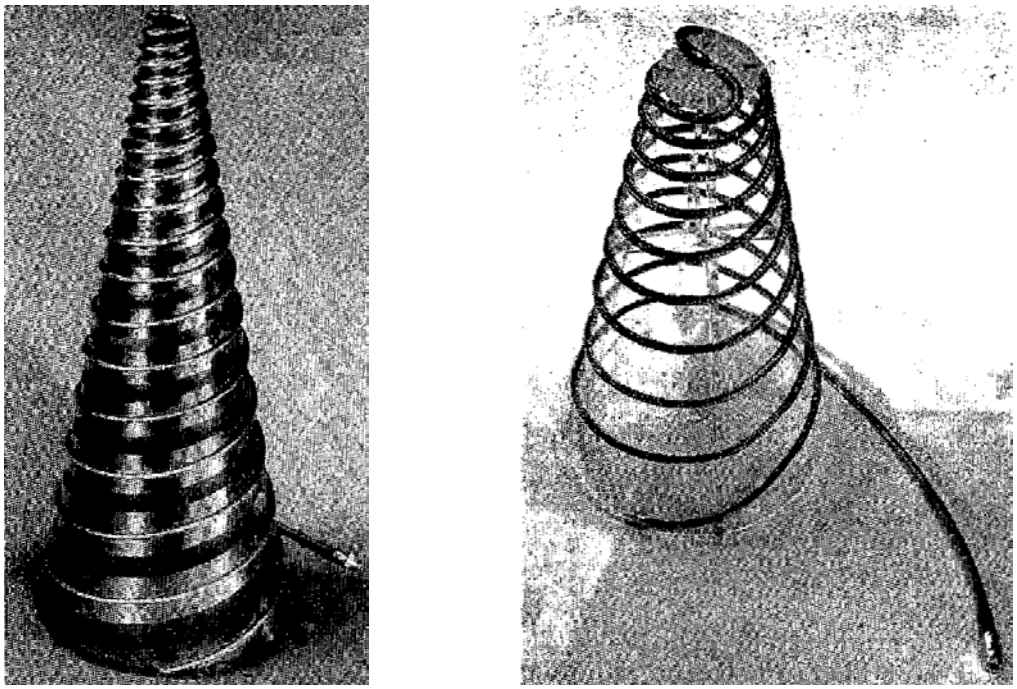

Figure 13. Dyson's [56]conical spiral antenna (unidirectional nonplanar equiangular spiral antenna). Left: etched antenna fed with coax RG141/U bonded to the arms. Right: Embedded RG8/U coax cable to form the arms that was supported by polystyrene ribs.

The diameter dimension of the round spiral antennas is proportional to the wavelength. The use of this kind of antennas at low frequencies was not viable with the better-known spiral configurations (Archimedean and equiangular). Hence, Morgan [59]

presented a solution for this problem by forming a zigzagged arm squared spiral antennas. It was designed to operate from 500 MHz to 4 GHz.

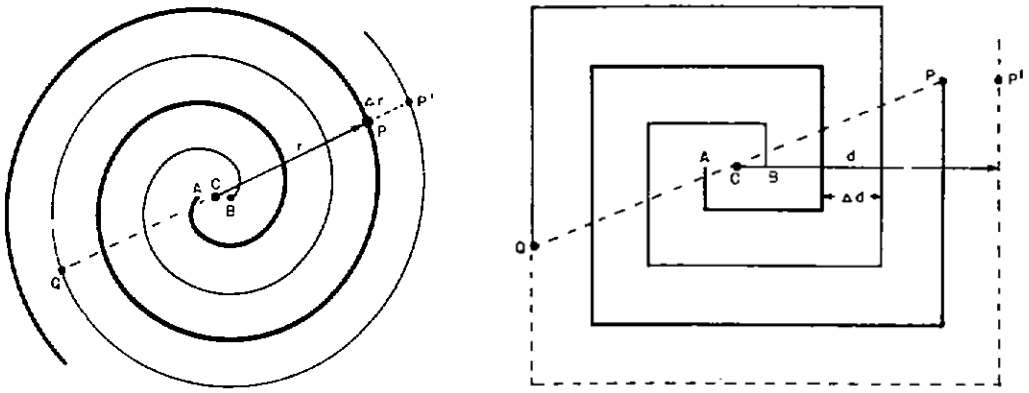


Figure 14. Kaiser's original circular and rectangular Archimedean spiral antennas drawing [17].

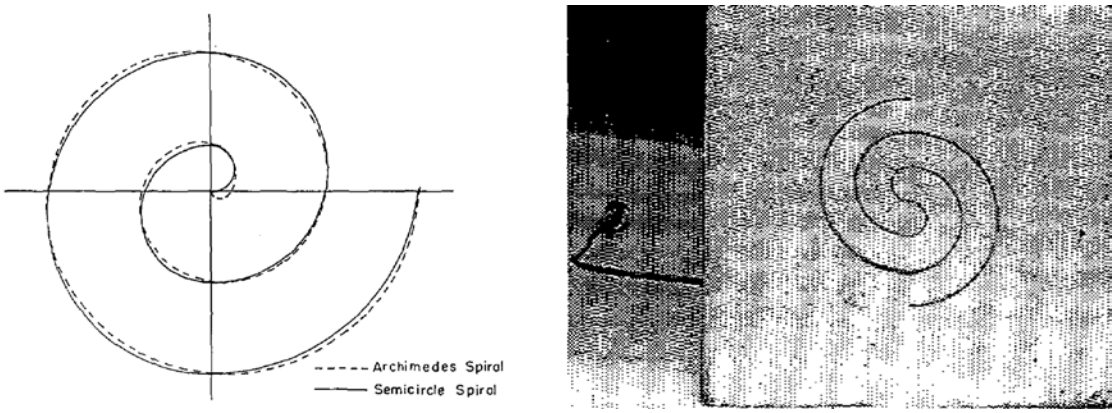


Figure 15. Curtis' [57] spiral antenna. Left: Curtis semicircles approximation of Archimedean spiral antenna. Right: Curtis' built prototype for semicircles Archimedean spiral antenna.

The first frequency-independent antenna was discovered by Dyson while he was working on his Ph.D. at The University of Illinois [60]. Dyson tried great number of equiangular spiral antenna pattern measurements until he achieved the frequency-independent characteristics and defined the measurements technique. Rumsey [53] stated

that if it is possible to specify the antenna shape entirely by angles, it would be independent of frequency. These antennas are such that their radiation pattern and input impedance is practically independent over a certain range of frequencies. Rumsey initially gave biconical antennas as an example. However this concept is general to other kinds of antennas as well as spiral antennas. Duhamel and Isbell [61] set the log-periodicity standard for broadband antennas. The authors presented a new approach to the design of broadband antennas, which consisted of designing the antenna structure such that the antenna characteristics are periodic with regard to the logarithm of the frequency.

Tang [62] presented polygonal spiral antennas. The author verified experimentally that polygonal spiral antennas were frequency-independent and had similar performance as the log-spiral antennas. Inserting periodic discontinuities into the conical structures creates the polygonal spiral antenna, which preserves the frequency independent-properties.

Spiral antenna studies have been limited to planar geometries, and they are normally flat, but some have investigated curved spirals with round and square Archimedean configurations [63, 64]. In [63] the authors simulated a curved spiral antenna which was printed on a dielectric layered cylinder with a conducting cylinder core of various radii shown in Figure 16(Left). They calculated the antenna's input impedance, gain, and axial ratio and then compared their results with CST Microwave Studio software. They used a flat spiral over a flat dielectric surface as their reference. They observed that when the radius of the cylinder was larger than some threshold the behavior of the curved spiral become comparable to that of the flat spiral. Their results showed that the curved

antennas exhibited greater variation of input impedance and gain with frequency than their flat spiral reference counterparts.

In [64] the authors simulated a curved spiral antenna above a hollow conducting cylinder of finite dimensions shown in Figure 16 (Right). They used a flat spiral antenna above a flat conductive surface as a reference. They focused their study of the curved spiral antenna changes in its radiation pattern with variation on the cylinder's radius and length. Their results showed that above some threshold cylinder length, antenna input impedance and gain is essentially constant. Furthermore, the antenna input impedance is largely independent of the cylinder radius, and the antenna gain shows a slight increase as the cylinder radius increases. The overall gain of the curved spiral antenna is lower than that of their reference flat spiral, about 2.7 dB. The radiation patterns showed marked dependence on both the cylinder height and radius. The general trend is that if the length or the radius is increased, the lobe towards the cylinder disappears as shown in Figure 17 and Figure 18.

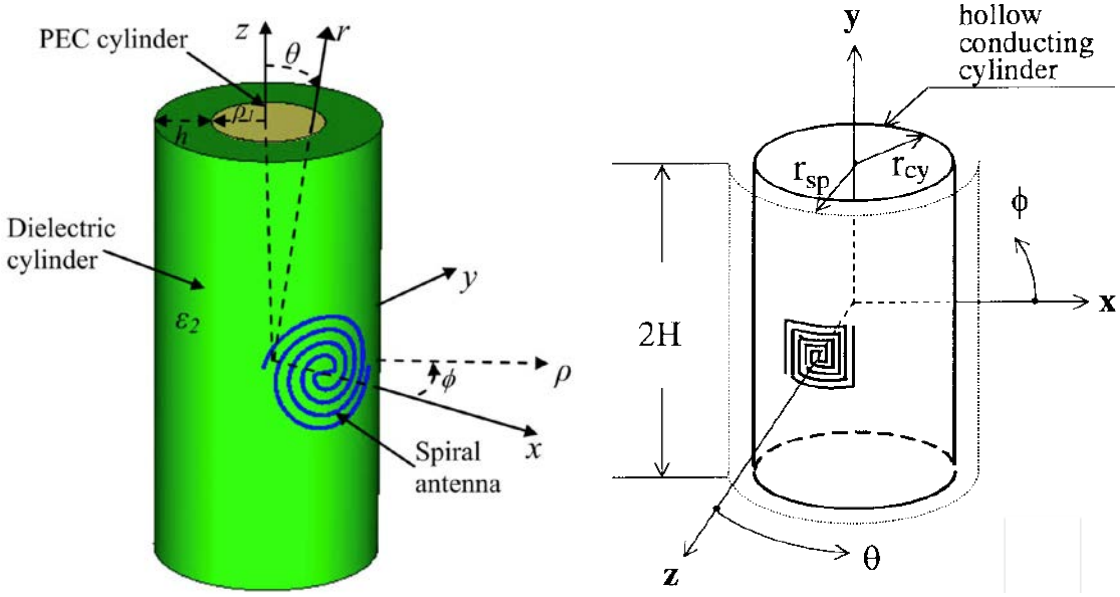


Figure 16. Left: Curved Archimedean spiral antenna printed on a layered cylinder [63]. Right: Curved squared spiral antenna above a conducting cylinder [64]

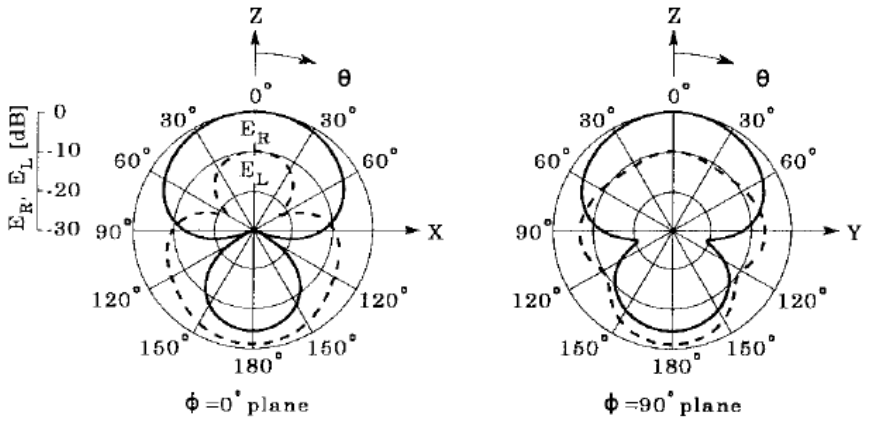


(a)

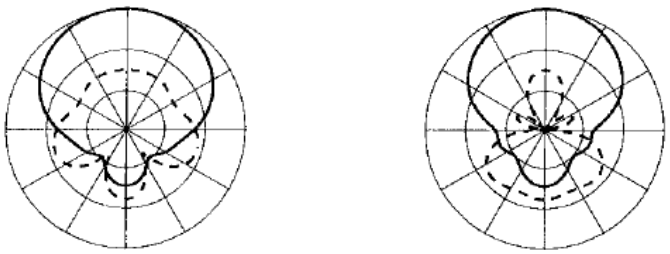

(b)

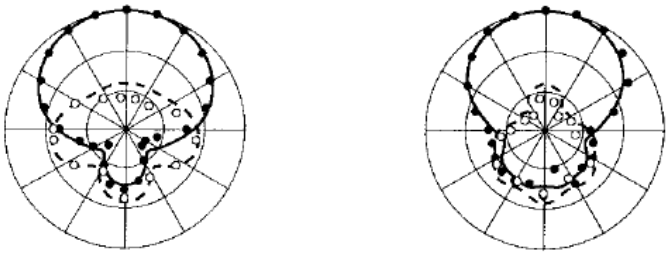

(c)

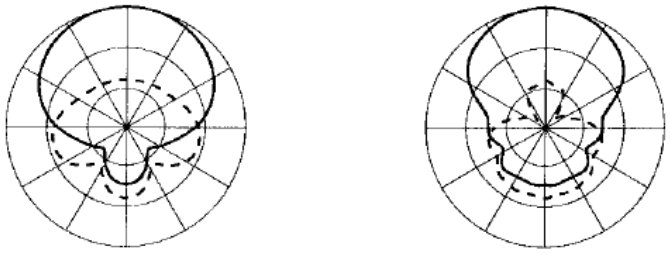

(d)

Figure 17. Radiation pattern as a function of cylinder length, H. (a) $H = 0.3\lambda_0$. (b) $H = 1.0\lambda_0$. (c) $H = 2.7\lambda_0$. (d) $H = 5.0\lambda_0$. Solid line and dotted line are theoretical results. Solid and emptied dots represent experimental results [64].

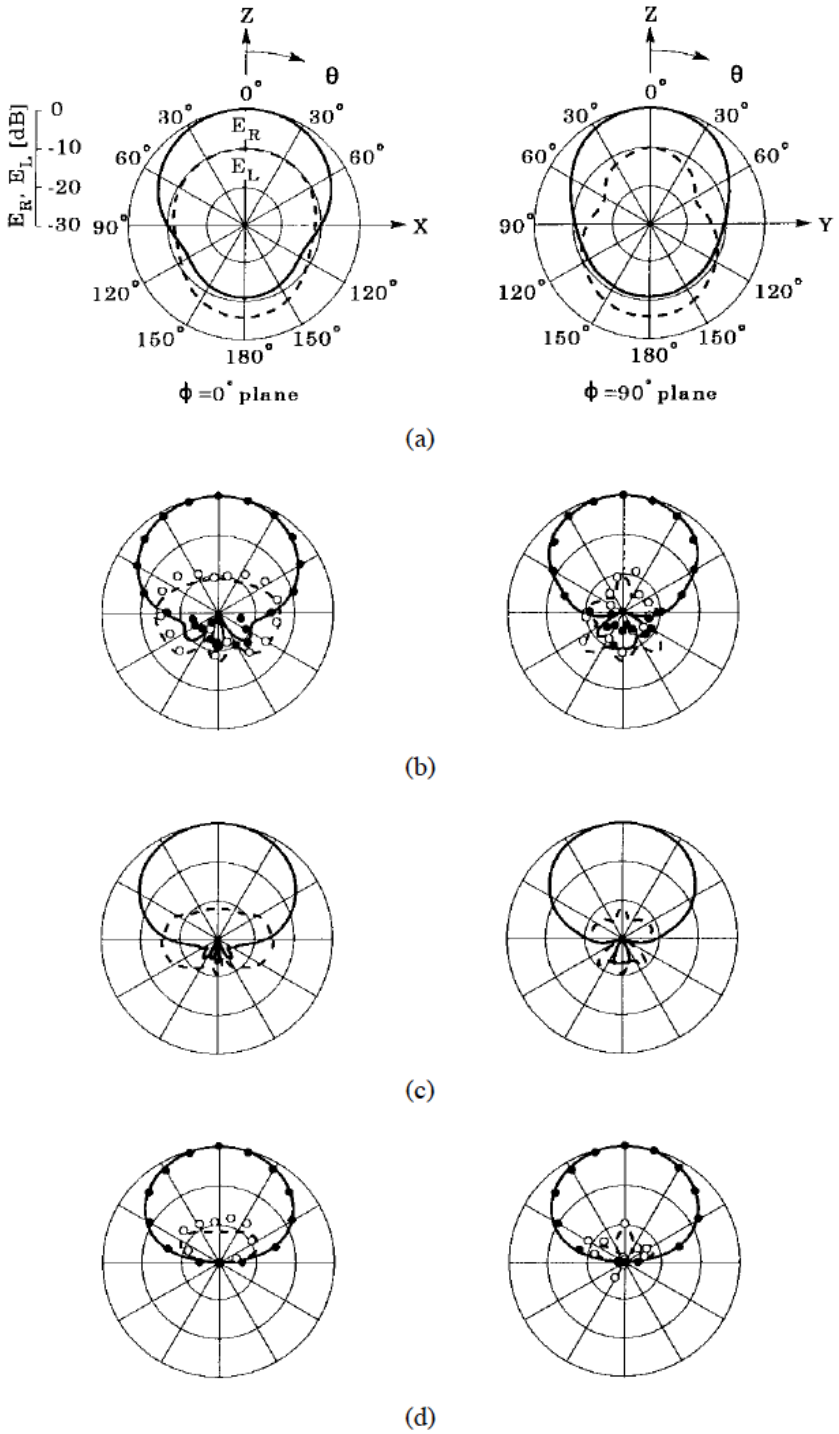


Figure 18. Radiation pattern as a function of cylinder length, r. (a) $r = 0.05\lambda_0$, (b) $r = 0.5\lambda_0$, (c) $r = 0.8\lambda_0$, (d) $r = \infty$ (Reference antenna). Solid line and dotted line are theoretical results. Solid and emptied dots represent experimental results. [64]

The authors in [65] investigated employing an array of square spiral antennas on an hollow cylinder to compensate for the loss of the back lobe and create an omnidirectional radiation pattern. They calculated the arrayed spiral antennas around a conducting cylinder. They used a 3 GHz frequency for their calculations. They analyzed variations in the radiation pattern with different numbers of elements with identical characteristics in the antenna's array. Their conclusion was that as the number of elements in the array increases, the radiation pattern becomes more omnidirectional.

Khamas [66] analyzed Archimedean spiral antennas printed on a sphere. Two configurations were considered, one above a conducting sphere and the other printed on a layered dielectric sphere. The calculations were validated against CST Microwave Studio software. He used a flat spiral antenna over a planar surface as a reference. The conclusion of this investigation was that spiral antennas conforming to a spherical surface have preserved flat spiral characteristics.

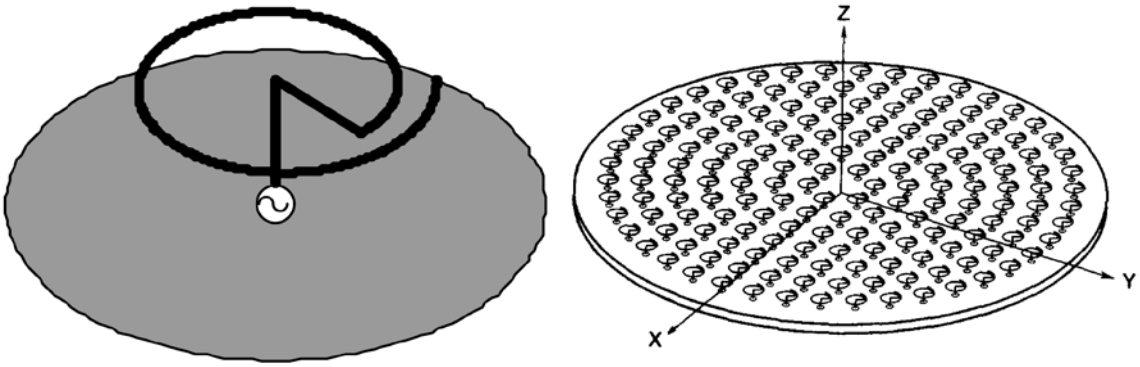


Figure 19. Curl antenna and Curl antenna array [67, 68].

Another kind of single arm spiral antenna, named a *curl antenna*—see Figure 19, was presented for the first time by Nakano and his collaborators [67, 68] as a solution to generate a circularly polarized wave (CPW) without perturbation elements. Perturbation

elements are added to a path antenna to make it resonate and generate a CPW, however perturbation elements reduce CPW size as frequency increases. Curl antennas are easy to fabricate. Curl antennas are used to form curl arrays that give high gain performance and allow them to be used as satellite receiving antennas. The curl antennas showed a gain of 8.4 dB, and a curl-antenna array consisting of 168 curl elements showed a gain of greater than 31 dB. A modification of the curl antenna was presented in [69] and consisted of staircase curl antenna with a 50% increment in the bandwidth compared with the conventional curl antenna. A curved curl antenna (single arm spiral antenna) printed with in a layered dielectric cylinder was analyzed using MoM calculations and simulations [70]. The authors used a flat curl antenna over a similarly characterized flat surface as a reference.

## Summary

In the first three chapters we researched the use of antennas for underwater communication. The motivation for this work is to enhance the communication capabilities of so-called mussel backpacks used by researchers at the University of Iowa. Most of the preceding chapter is devoted to a review of the literature related to this thesis. We concluded that while much antenna work has been done in underwater communication, most studies were done primarily in seawater. We identified spiral antennas as attractive for the mussel backpack application. Spiral antennas are compact and inherently broadband. The broadband attribute translates to constant input impedance, which is important for our particular application. While spiral antennas have been studied for several decades, some gaps in our knowledge remain. First, as far as we can establish, there are no

published work on spiral antennas in underwater applications. Second, there are very few published results related to curved (or non-flat) spiral antennas.

# CHAPTER III. SUMMARY OF RELEVANT EM THEORY RELATED TO THESIS

## Maxwell's Equations

Maxwell's equations in differential equation form are [71-75]:

$$\nabla \cdot \mathbf{D} = \rho \text{ (Gauss' Law)} \quad \text{Equation 6}$$

$$\nabla \cdot \mathbf{B} = 0 \text{ (Gauss' Law for Magnetism)} \quad \text{Equation 7}$$

$$\nabla \times \mathbf{E} = -\frac{\partial \mathbf{B}}{\partial t} \text{ (Faraday's Law)} \quad \text{Equation 8}$$

$$\nabla \times \mathbf{H} = \mathbf{J} + \frac{\partial \mathbf{D}}{\partial t} \text{ (Ampere's Law)} \quad \text{Equation 9}$$

where, **E** = electric field (V/m), **H** = magnetic field (A/m), **D** = electric flux density (C/m$^2$), **B** = magnetic flux density (T), **J** = electric current density (A/m$^2$), $\rho$ = electric charge density (C/m$^3$), and $\sigma$ = conductivity (S/m). Additional companion relations are required to complete the basic set of equations that define classical electricity and magnetism theory, namely:

$$\mathbf{D} = \varepsilon_0 \varepsilon_r \mathbf{E} \text{ (definition of permittivity)} \quad \text{Equation 10}$$

$$\mathbf{B} = \mu \mathbf{H} \text{ (definition of permeability)} \quad \text{Equation 11}$$

$$\mathbf{J} = \sigma \mathbf{E} \text{ (definition of conduction current)} \quad \text{Equation 12}$$

In this chapter we focus on the analysis of plane wave propagation in a lossy dielectric, which is appropriate for transmitting in freshwater [23] at around 300 MHz, where the mussel backpack radios operate.

Assume that all of the fields (**E** and **H**) are functions of $e^{j\omega t}$. That is, they are sinusoidal with radian frequency $\omega$. Then $\frac{\partial e^{j\omega t}}{\partial t} = j\omega e^{j\omega t}$. This illustrates that taking the partial derivative of a field quantity that is time-varying as $e^{j\omega t}$ with respect to time, is same as multiplying by $j\omega$. Consequently, Equation 6, Equation 7, Equation 8, and Equation 9 can be written as Equation 13 and Equation 14. In addition, if we assume a charge free region ($\rho = 0$), then Equation 6 becomes $\nabla \cdot \mathbf{D} = 0$.

$$\nabla \times \mathbf{E} = -j\omega\mu\mathbf{H} \qquad \text{Equation 13}$$

$$\nabla \times \mathbf{H} = (\sigma + j\omega\varepsilon)\mathbf{E} \qquad \text{Equation 14}$$

Equation 13 and Equation 14 form a pair of coupled first order differential equations that are functions in space and time. We can see that an electric field (**E**) generates a magnetic field (**H**) in Equation 13, and a magnetic field generates an electric field in Equation 14. Taking the curl of Equation 13 we obtain:

$$\nabla \times (\nabla \times \mathbf{E}) = -j\omega\mu(\nabla \times \mathbf{H}) \qquad \text{Equation 15}$$

Substituting Equation 13 into Equation 15, and using the vector identity $\nabla \times (\nabla \times \mathbf{E}) = \nabla(\nabla \cdot \mathbf{E}) - \nabla^2\mathbf{E}$, and from $\nabla \cdot \mathbf{D} = 0$ in a charge-free region the first term of the right side vector identity is zero, we obtain Equation 16. Similarly, for magnetic field we get Equation 17.

$$\nabla^2\mathbf{E} - j\omega\mu(\sigma + j\omega\varepsilon)\mathbf{E} = 0 \qquad \text{Equation 16}$$

$$\nabla^2\mathbf{H} - j\omega\mu(\sigma + j\omega\varepsilon)\mathbf{H} = 0$$ Equation 17

Now, assuming that the electric field is linearly polarized in the $x$-direction and the wave propagates only in the $z$-direction. Equation 16 and Equation 17 are referred to as the vector Helmholtz equation. Taking these considerations into account, Equation 16 becomes:

$$\frac{d^2E_x(z)}{dz^2} - j\omega\mu(\sigma + j\omega\varepsilon)E_x(\mathrm{z}) = 0$$ Equation 18

Rewriting Equation 18,

$$\frac{d^2E_x(z)}{dz^2} - \gamma^2E_x(\mathrm{z}) = 0$$ Equation 19

where $\gamma$ is the propagation constant:

$$\gamma^2 = j\omega\mu(\sigma + j\omega\varepsilon) = \alpha + j\beta$$ Equation 20

A solution to the wave equation, Equation 19, is:

$$E_x(\mathrm{z}) = E_0e^{-\gamma z} = E_0e^{-\alpha z}e^{-j\beta z}$$ Equation 21

Multiplying Equation 21 by $e^{j\omega t}$ leads to perhaps a more familiar form, and allows for better visualization.

$$E_x(\mathrm{z}) = E_0e^{-\alpha z}\cos(\omega t - \beta z)$$ Equation 22

Equation 22 represents a uniform plane wave that propagates in the forward $z$-direction.

## Properties of Dielectric Materials

The propagation constant is a complex quantity. It has real and imaginary parts as shown in Equation 20. The properties of dielectric materials are described by their complex permittivity [73], where the complex permittivity is:

$$\varepsilon = \varepsilon_0(\varepsilon' - j\varepsilon'') = \varepsilon_0\left(\varepsilon' - \frac{j\sigma}{\omega\varepsilon_0}\right) = \varepsilon_0\varepsilon'(1 - j\tan\delta) \qquad \text{Equation 23}$$

where $\varepsilon_0 = 8.854 \times 10^{-12}$ F/m is the free space permittivity, $\sigma$ = conductivity (S/m), $\tan\delta = \varepsilon''/\varepsilon'$ is the loss tangent or dissipation factor of the material, and $\delta$ is known as the dissipation angle. The dissipation factor is zero in a lossless medium. The imaginary part of the complex permittivity determines the absorption of electrical energy in the dielectric. The attenuation constant, phase constant, and, $\eta$, the complex wave impedance, are related to the medium which are [72, 73]:

$$\alpha = \frac{\omega\sqrt{\mu\varepsilon}}{\sqrt{2}}\sqrt{\left(1 + \left(\frac{\varepsilon''}{\varepsilon'}\right)^2\right)^{1/2} - 1} = \frac{\omega}{c}\sqrt{\frac{\varepsilon'}{2}}\sqrt{\sqrt{1 + \tan\delta^2} - 1} \qquad \text{Equation 24}$$

$$\beta = \frac{\omega\sqrt{\mu\varepsilon}}{\sqrt{2}}\sqrt{\left(1 + \left(\frac{\varepsilon''}{\varepsilon'}\right)^2\right)^{1/2} + 1} = \frac{\omega}{c}\sqrt{\frac{\varepsilon'}{2}}\sqrt{(1 + \tan\delta^2)^{1/2} + 1} \qquad \text{Equation 25}$$

$$\eta = \frac{\sqrt{\frac{\mu}{\varepsilon}}}{\sqrt[4]{1+\left(\frac{\varepsilon''}{\varepsilon'}\right)^2}} e^{\left[j\left(\frac{1}{2}\right)\tan^{-1}\left(\frac{\varepsilon''}{\varepsilon'}\right)\right]} \quad \text{Equation 26}$$

where *c* is the speed of light in a vacuum.

One can classify a medium as a good conductor, dielectric, or lossy dielectric. The first two cases are more familiar. As we show below at around 300 MHz, freshwater behaves as a lossy dielectric.

**Classification of medium based on its loss tangent**, $\tan\delta = \frac{\sigma}{\omega\varepsilon} = \frac{\varepsilon''}{\varepsilon'}$**:**

*For a good conductor*, $\frac{\sigma}{\omega\varepsilon} \gg 1$, we get:

$$\alpha = \sqrt{\frac{\omega\mu\sigma}{2}} \quad \text{Equation 27}$$

$$\beta = \sqrt{\frac{\omega\mu\sigma}{2}} \quad \text{Equation 28}$$

$$\eta = (1+j)\sqrt{\frac{\omega\mu}{2\sigma}} \quad \text{Equation 29}$$

*For a lossy dielectric*, $\frac{\varepsilon''}{\varepsilon'} \ll 1$, we get:

$$\alpha = \frac{\omega\sqrt{\mu\varepsilon}}{2}\left(\frac{\varepsilon''}{\varepsilon'}\right) \quad \text{Equation 30}$$

$$\beta = \omega\sqrt{\mu\varepsilon}\left[1+\frac{1}{8}\left(\frac{\varepsilon''}{\varepsilon'}\right)^2\right] \quad \text{Equation 31}$$

$$\eta = \sqrt{\frac{\mu}{\varepsilon}}\left[1 - \frac{3}{8}\left(\frac{\varepsilon''}{\varepsilon'}\right)^2 + j\frac{1}{2}\left(\frac{\varepsilon''}{\varepsilon'}\right)\right] \quad \text{Equation 32}$$

Equation 30 through Equation 32 [72] are calculated by considering only the first two terms of the binomial expansions of the square root quantities in Equation 24 through Equation 26 for a small loss tangent.

**EM Properties of Propagation in Water**

Water differs from air in having higher permittivity and different conductive properties. Figure 20 [71] clearly illustrates that seawater acts as a lossy conductive medium, and freshwater acts as a lossy dielectric medium [23] at ISM (Industrial, Scientific, and Medical) frequency band. Seawater is a poor medium for communications since it is a good conductor. Seawater communication requires low frequencies, large antennas, and high power. However, the goal of our investigation is to design a spiral antenna for the freshwater mussels' instrumentation.

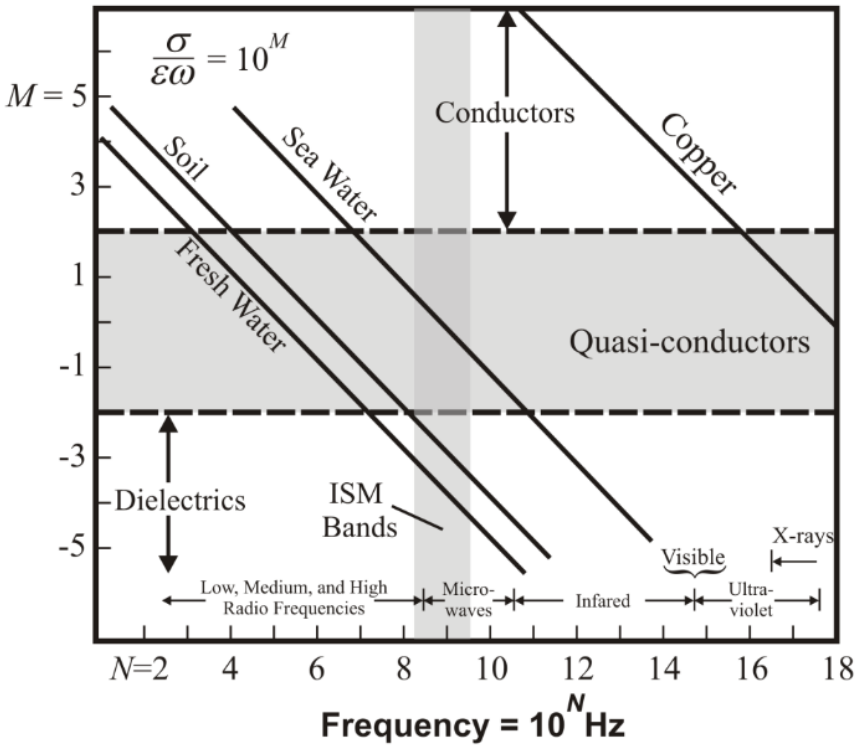


Figure 20. Ratio $\sigma/\omega\epsilon$ as a function of frequency for some common media showing that one can consider freshwater as lossy dielectric at 315 MHz [71].

Now, consider a plane wave traveling in water, with electric field $E = E_o e^{j\omega t - \gamma x}$. The medium properties are contained in the propagation constant, $\gamma = \sqrt{j\omega\mu(\sigma + j\omega\varepsilon)} = \alpha + j\beta$,

$$\alpha = \omega\sqrt{\mu\varepsilon}\sqrt{\frac{1}{2}\left(1 + \left(\frac{\sigma}{\omega\varepsilon}\right)^2 - 1\right)} \qquad \text{Equation 33}$$

$$\beta = \omega\sqrt{\mu\varepsilon}\sqrt{\frac{1}{2}\left(1 + \left(\frac{\sigma}{\omega\varepsilon}\right)^2 + 1\right)} \qquad \text{Equation 34}$$

where $\omega$ is the angular frequency, $\mu$ is the magnetic permeability, $\varepsilon$ is the electric permittivity, and $\sigma$ is the conductivity.

The attenuation, α, of EM waves at 315 MHz is high (13.6 dB/m, [23]) but one can obtain reliable links in river water up to 5 m at this frequency [2]. This is sufficient for the mussel application. One source of attenuation in water is losses due to conductivity. Seawater conductivity is about 4 S/m [46], while the measured Iowa River (freshwater) conductivity is between 0.04 and 0.06 S/m [23]. The electric permittivity is $\varepsilon = \varepsilon_o \varepsilon_r$, where $\varepsilon_o = 8.854 \times 10^{-12}$ F/m and the relative permittivity is $\varepsilon_r = \varepsilon_r' + \varepsilon_r''$ a complex quantity. At the frequency we used in our experiments, 315 MHz, the relative permittivity is $80.2 - j1.4$ at $20^oC$ [76].

The phase constant $\beta$ is larger in water than it is in air. It follows that the wavelength, $\lambda = 2\pi/\beta$, is much shorter in water than in air, and the phase velocity is slower:

$$v_p = \frac{\omega}{\beta} \qquad \text{Equation 35}$$

Another important constant for EM propagation is the intrinsic impedance η, the ratio of the transverse electric and magnetic fields, which determines power transfer.

$$\eta = \sqrt{\frac{j\omega\mu}{j\omega\varepsilon + \sigma}} \qquad \text{Equation 36}$$

Water exhibits two types of properties, depending on whether the frequency is greater or less than the transition frequency ($\omega_t = \sigma/\varepsilon$). The transition frequency is about 888 MHz in seawater and about 14 MHz in freshwater.

*Below Transition frequency, $\omega \ll \omega_t$*

This is the case for seawater, where the attenuation and propagation constants are approximately equal.

$$\alpha \cong \beta \cong \sqrt{\omega\mu\sigma/2} \quad \text{Equation 37}$$

The attenuation constant is proportional to frequency, so lower frequencies are preferred. The wavelength is shorter than it is in air. The intrinsic impedance is small and also proportional to frequency.

$$\eta \cong \sqrt{(\omega\mu)/(2\sigma)}\,(1 + \mathrm{j}) \quad \text{Equation 38}$$

*Above Transition frequency, $\omega \gg \sigma/\omega_t$*

This is case for freshwater, where the attenuation constant has reached a maximum and is now independent of frequency.

$$\alpha \cong (\sigma/2)\sqrt{\mu\epsilon} \quad \text{Equation 39}$$

The propagation constant and intrinsic impedance are approximately those of lossy dielectric.

$$\beta \cong \omega\sqrt{\mu\epsilon} \quad \text{Equation 40}$$

$$\eta \cong \sqrt{\mu/\epsilon} \quad \text{Equation 41}$$

At 315 MHz, with the relative permittivity of river water approximately 81 [77]. Therefore, the electric permittivity of water is about 9 times that of air. Further, the

wavelength, phase velocity, and intrinsic impedance in freshwater will be approximately 1/9 of that in air. Consequently, antennas' physical dimensions in freshwater are approximately 1/9 that of a comparable antenna in air [23]. This allows for antennas to be small enough to attach to larger freshwater mussels.

**Computing Antenna Radiating Fields**

An antenna's radiation pattern is a fundamental property that characterizes its performance. One approach to computing the radiation pattern is to start by combining Maxwell's equations to calculate the nonhomogeneous wave equation in E- and H- fields. However, this procedure is very tedious. The common and recommended approach is to introduce so-called *vector potentials* and use these to calculate the fields emanating from an antenna. Vector potentials are mathematical tools that aid us in the solution of the problem. The procedure is described and depicted in many antenna- and EM theory texts, for example Balanis' text on antenna theory [78]. This is illustrated in Figure 21. Path 1 involves only one step from sources to fields by an integration step. Path 2 starts with the sources and uses the intermediate vector potentials. Even though this second path involves an extra step, it turns out that this simplifies the mathematics considerably.

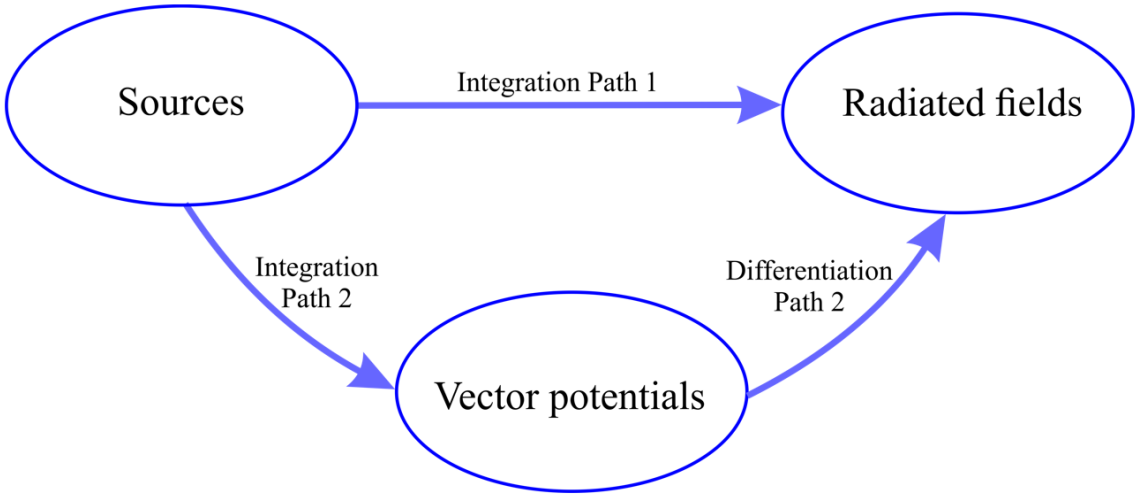


Figure 21. Computing antenna radiated field block diagram [78]

Consider the oscillating dipole called a Hertzian dipole in Figure 22.

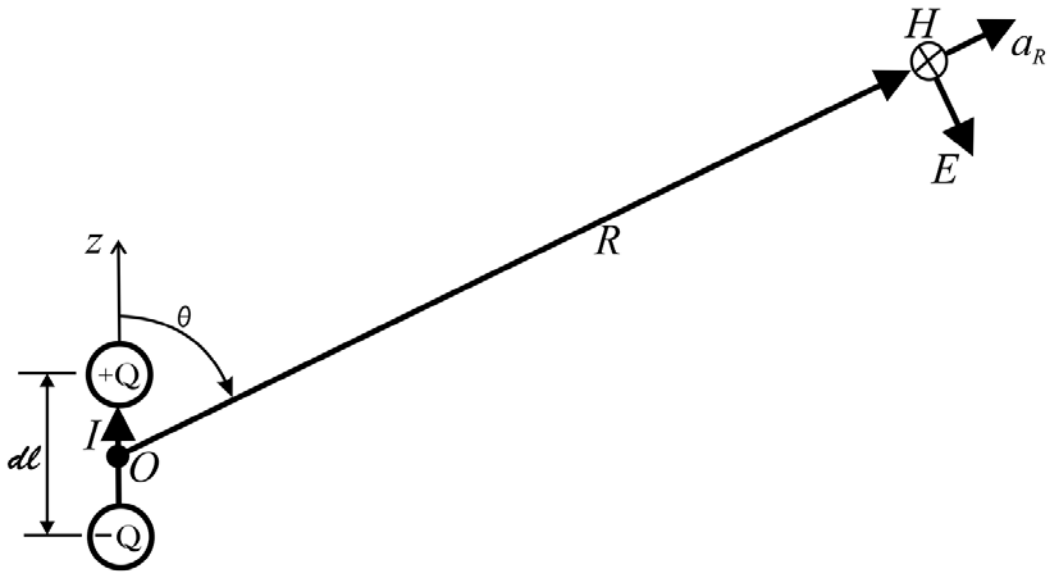


Figure 22. Geometrical arrangement of a Hertzian Dipole and its associated fields [79].

Following are the steps expressed in the block diagram in Figure 21. First, we determine **A** (vector potential) from **J** (source) using Equation 42. Second, we find **H** from **A** using Equation 43, and then find **E** from **H** using Equation 44.

$$\mathbf{A} = \frac{\mu}{4\pi}\int \frac{\mathbf{J}e^{-jkR}}{R}dl \qquad \text{Equation 42}$$

$$\mathbf{H} = \frac{1}{\mu}\nabla \times \mathbf{A} \qquad \text{Equation 43}$$

$$\mathbf{E} = \frac{1}{j\omega\varepsilon}\nabla \times \mathbf{H} \qquad \text{Equation 44}$$

Then, the phasor form of the vector potential from Equation 42 is as follows:

$$\mathbf{A} = \hat{\boldsymbol{a}}_z \frac{\mu_0 I dl}{4\pi}\left(\frac{e^{-j\beta R}}{R}\right) \quad \text{Equation 45}$$

$$\hat{\boldsymbol{a}}_z = \hat{\boldsymbol{a}}_R \cos\theta - \hat{\boldsymbol{a}}_\theta \sin\theta \quad \text{Equation 46}$$

Further, the vector potential's spherical components are: $\mathbf{A} = \hat{\boldsymbol{a}}_R \mathrm{A}_R + \hat{\boldsymbol{a}}_\theta \mathrm{A}_\theta + \hat{\boldsymbol{a}}_\phi \mathrm{A}_\phi$ to obtain,

$$\mathrm{A}_R = \mathrm{A}_z \cos\theta = \frac{\mu_0 I dl}{4\pi}\left(\frac{e^{-j\beta R}}{R}\right)\cos\theta \quad \text{Equation 47}$$

$$\mathrm{A}_\theta = -\mathrm{A}_z \sin\theta = -\frac{\mu_0 I dl}{4\pi}\left(\frac{e^{-j\beta R}}{R}\right)\sin\theta \quad \text{Equation 48}$$

$$\mathrm{A}_\phi = 0 \quad \text{Equation 49}$$

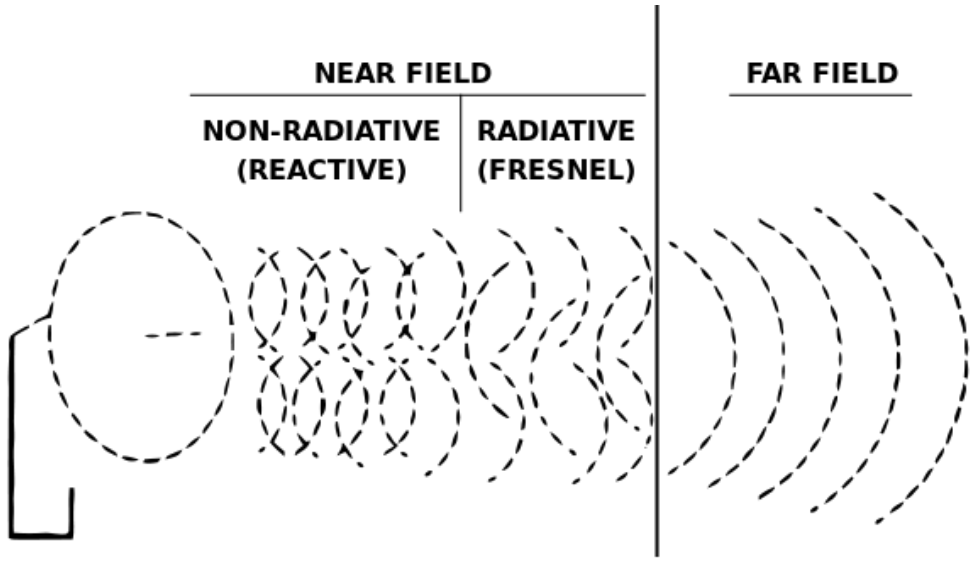


Figure 23. Antenna near-field and far-field patterns are shown for an antenna [80].

Using the symmetry of the geometrical arrangement shown in Figure 22, there are no variations in $\phi$ as implied by Equation 49. Further, we obtain the magnetic field intensity:

$$\begin{aligned}\mathbf{H} = \frac{1}{\mu_0}\nabla \times \mathbf{A} &= \hat{\boldsymbol{a}}_\theta \frac{1}{\mu_0 R}\left[\frac{\partial}{\partial R}(R\mathrm{A}_\theta) - \frac{\partial \mathrm{A}_R}{\partial \theta}\right] \\ &= -\hat{\boldsymbol{a}}_\theta \frac{Idl}{4\pi}\beta^2 \sin\theta \left[\frac{1}{j\beta R}\right. \\ &\left. + \frac{1}{(j\beta R)^2}\right] e^{-j\beta R}\end{aligned} \qquad \text{Equation 50}$$

Following the procedure the electric field intensity is obtained as follows,

$$\begin{aligned}\mathbf{E} = \frac{1}{j\omega\varepsilon_0}\nabla \times \mathbf{H} \\ = \frac{1}{j\omega\varepsilon_0}\left[\hat{\boldsymbol{a}}_R \frac{1}{R\sin\theta}\frac{\partial\left(H_\phi \sin\theta\right)}{\partial\theta}\right. \\ \left. - \hat{\boldsymbol{a}}_\theta \frac{1}{R}\frac{\partial}{\partial R}\left(RH_\phi\right)\right]\end{aligned} \qquad \text{Equation 51}$$

To obtain,

$$\mathrm{E}_R = -\frac{Idl}{4\pi}\eta_0\beta^2 2\cos\theta\left[\frac{1}{(j\beta R)^2} + \frac{1}{(j\beta R)^3}\right] e^{-j\beta R} \qquad \text{Equation 52}$$

$$\mathrm{E}_\theta = -\frac{Idl}{4\pi}\eta_0\beta^2 \sin\theta\left[\frac{1}{j\beta R} + \frac{1}{(j\beta R)^2} + \frac{1}{(j\beta R)^3}\right] e^{-j\beta R} \qquad \text{Equation 53}$$

$$\mathrm{E}_\phi = 0 \qquad \text{Equation 54}$$

The set of equations that were derived represent the electromagnetic field of the surroundings of the antenna under test. The set of equations are complex. It would be beneficial to analyze their behavior according to the far- and near-field regions.

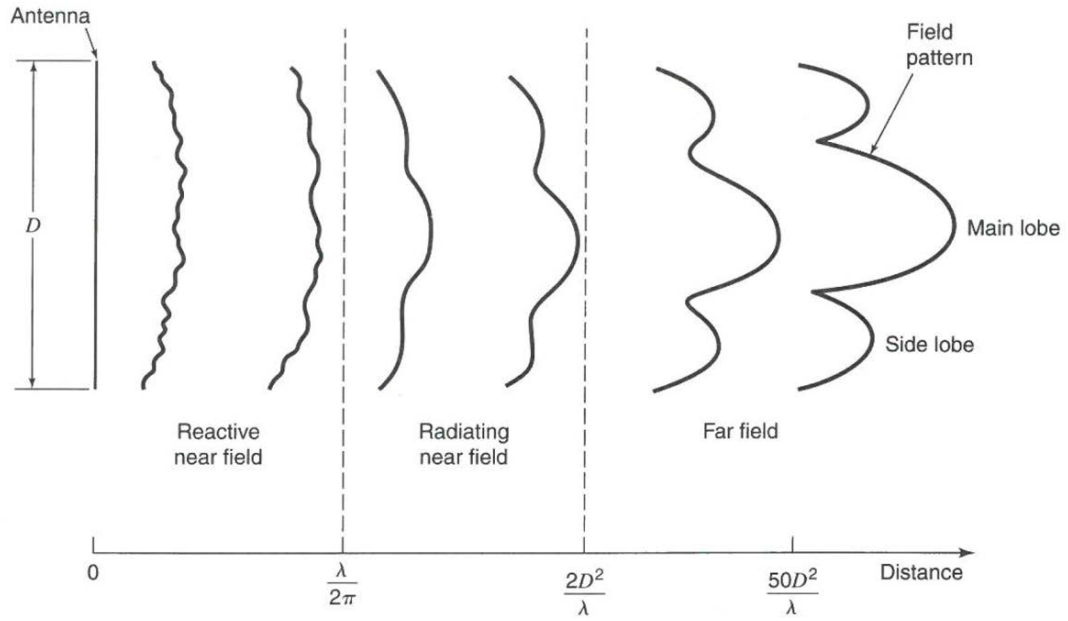


Figure 24. The image depicts the radiated regions on the antenna under test vicinity with their respective approximate boundaries [19].

These field regions/zones are functions of the distance and angle from the antenna. They are divided in two different regions: reactive and radiating. The reactive region is located very close to the antenna. Therefore, at very close distances, the antenna would have both reactive and radiating components. For long distance communication the reactive energy is insignificant because it rapidly decays as the distance from the antenna increases [81].

This first region close to the antenna, where the reactive energy strength dominates, is called reactive near-field region (or the evanescent zone). Farther than the reactive near-field region is the radiating region in which radiating fields dominate. The radiating region is subdivided into radiating near-field (or Fresnel zone) and radiating far-field (or Fraunhofer zone) regions shown on Figure 23 and Figure 24.

*Near field Region:*

$\beta R = 2\pi R/\lambda \ll 1$ to obtain:

$$H_\phi = \frac{Idl}{4\pi R^2}\sin\theta \qquad \text{Equation 55}$$

$$\mathrm{E}_R = -\frac{p}{4\pi\varepsilon_0 R^3}2\cos\theta \qquad \text{Equation 56}$$

$$\mathrm{E}_\theta = -\frac{p}{4\pi\varepsilon_0 R^3}2\sin\theta \qquad \text{Equation 57}$$

*Far field Region:*

$\beta R = 2\pi R/\lambda \gg 1$ to obtain:

$$H_\phi = j\frac{Idl}{4\pi}\left(\frac{e^{-j\beta R}}{R}\right)\beta\,\sin\theta \qquad \text{Equation 58}$$

$$\mathrm{E}_\theta = j\frac{Idl}{4\pi}\left(\frac{e^{-j\beta R}}{R}\right)\eta_0\,\beta\,\sin\theta \qquad \text{Equation 59}$$

From Figure 24 and the equations describing the near- and far-fields, we observe that as one moves away from the antenna, the radiation pattern changes and stabilizes in the far field. Furthermore, in the near field, the **E**- and **H**-fields rapidly change with distance due to the $1/R^3$ factor.

The calculated field zone boundaries around the dipole antenna underwater are illustrated in Figure 25 at operating frequency of 315 MHz. The zones are as follows: reactive near field is ~0.017 m, radiating near field or transition region is ~0.053 m and after the boundary of the transition region is the far field. As we see in Figure 3, showing the mussel bed underwater wireless sensor network and their links, we concluded that we

will be transmitting mostly in the far field region, but some transmission in the near radiating field is possible as shown in Figure 25.

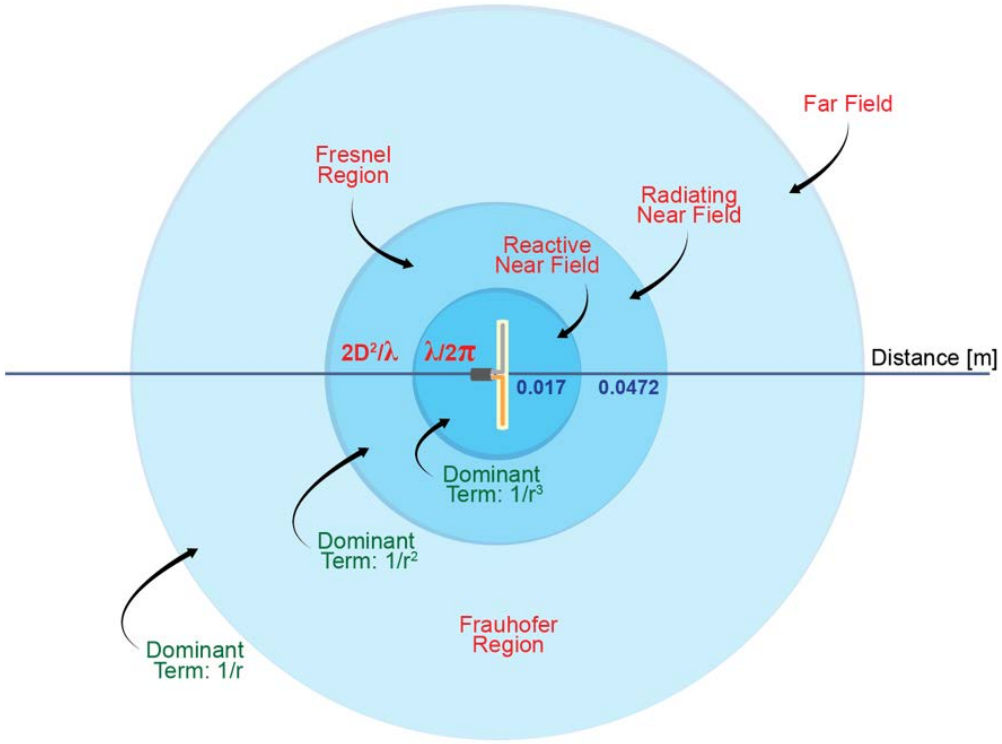


Figure 25. Half-wave dipole antenna field zones are depicted with their boundaries and dominant terms at different distances from the antenna. Taking into account freshwater medium properties, the half-wave dipole antenna length is ~5 cm.

## EM Properties of Mussel Shell, River Water, and Sand at River Bottom

### Relative Permittivity of the Freshwater Mussel Shell

There are many factors apart from the antenna geometry that we need to take into account in our research. These factors include the electrical and chemical properties of the mussel shell, river water, river sand, and so on. We have performed a number of experiments and tests to study and analyze all the materials involved in the whole system under different circumstances that are relevant to our investigation.

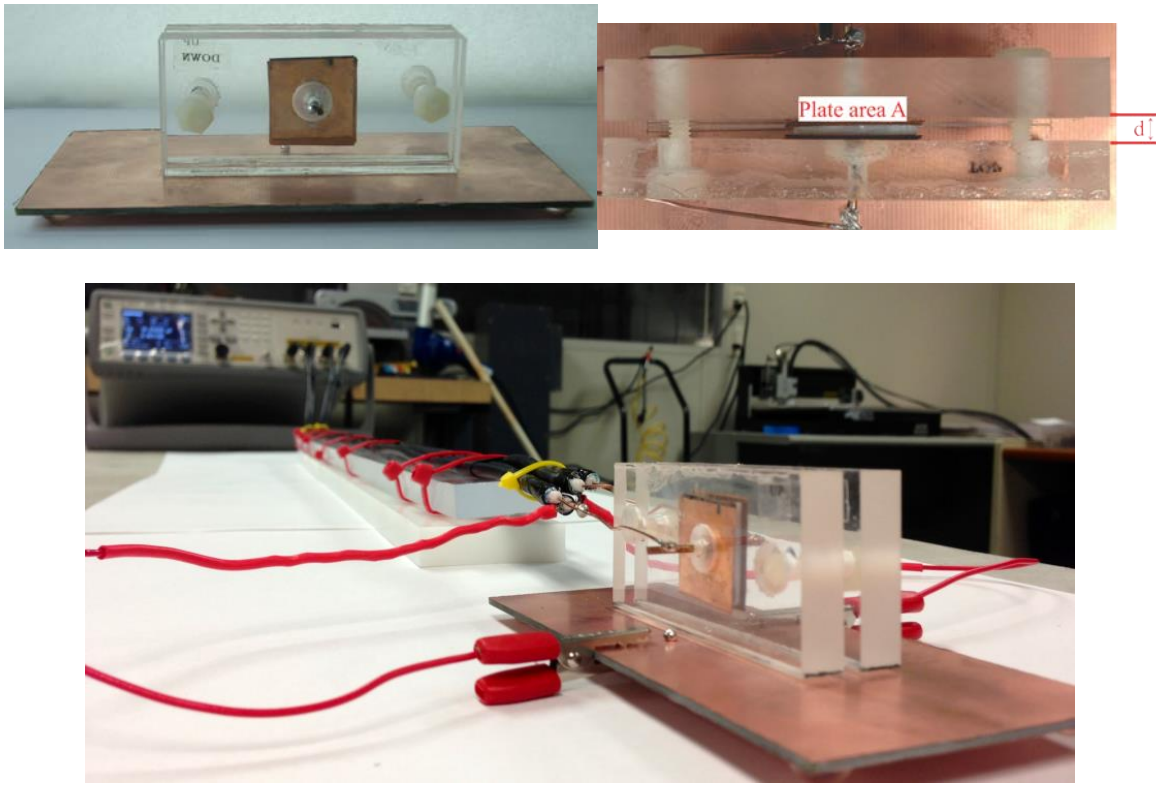


Figure 26. Mussel shell capacitor created to study the electrical properties of the material. The precision LCR is shown with our own built fur terminal sensing or Kelvin connection.

*Mussel Shell Parallel-plate Capacitor*

We constructed a capacitor using a flat square piece of a mussel shell using multiples layers of copper foil (for low frequencies) and copper tape with BNC connector (high frequencies). They are shown in Figure 26 and Figure 27. The mussel shell piece used to build the capacitor has dimensions of approximately 0.01 m per each side, and 0.002 m thick. First, for low frequencies, we used the Agilent E4980A Precision LCR meter [82] over 20 Hz to 2 MHz frequency range to measure capacitance. Then, we calculated the mussel shell relative permittivity $\varepsilon_r$ from

$$\mathrm{C} = \varepsilon_0 \varepsilon_r \frac{A}{d} \qquad \text{Equation 60}$$

where,

| | |
|---|---|
| $\mathrm{C}$ | capacitance [F], |
| $\varepsilon_0$ | vacuum permittivity, permittivity of free space (8.854 187 817 x $10^{-12}$ F/m), |
| $\varepsilon_r$ | relative permittivity of the material, |
| $A$ | $A$ is the area of overlap of the two plates [$m^2$] |
| $d$ | separation between the plates [m]. |

we obtained a relative permittivity of about 10 for the mussel shell.

The LCR meter can only measure up to 2 MHz, therefore we used the VNA to measure around the operating frequency of the antenna (Figure 28). Since we were measuring at higher frequencies, we used a copper tape and BNC connector to reduce the lead inductances. We rebuilt our mussel shell capacitor using copper tape as the plates of the capacitor as shown in Figure 27. Once the parallel plate capacitor was rebuilt, the

capacitance was measured with the VNA. Figure 29 shows a comparison of the LCR measurements versus the VNA measurements at low frequencies, 30 kHz to 2 MHz. Figure 30 shows VNA measurements results of mussel capacitor at higher frequencies.

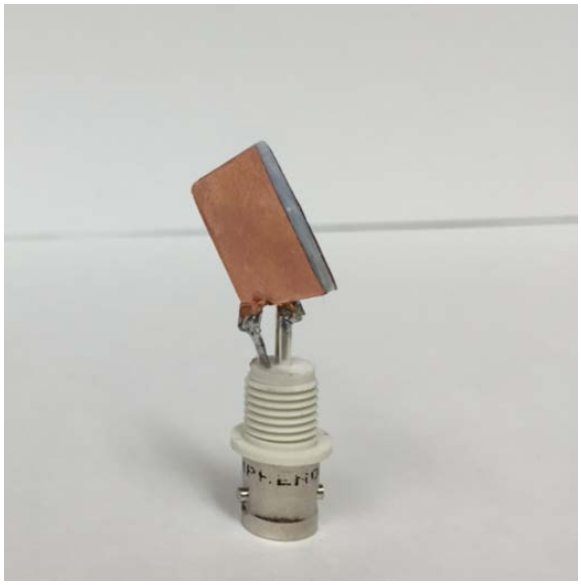

Figure 27. Mussel shell parallel plate capacitor soldered directly to BNC connector

Figure 28. VNA with mussel shell parallel plate capacitor

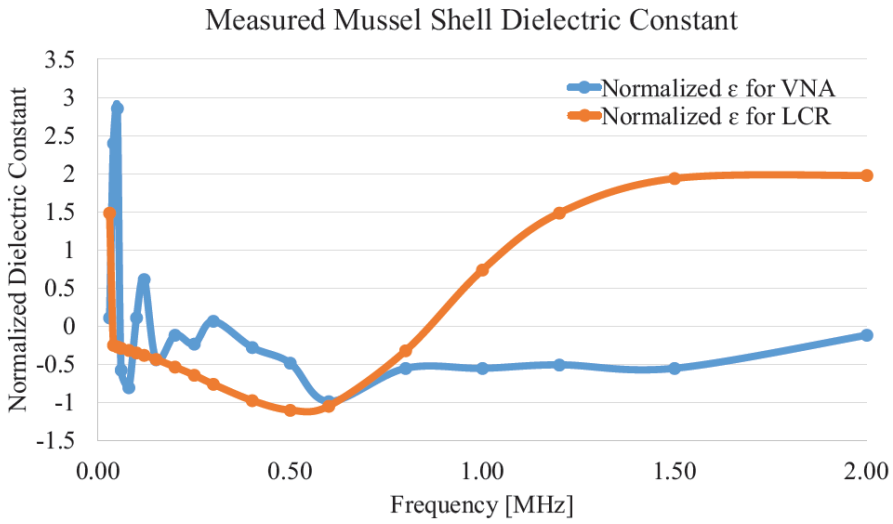


Figure 29. LCR vs VNA Measurements of Dielectric Constant from Parallel Plate Capacitor

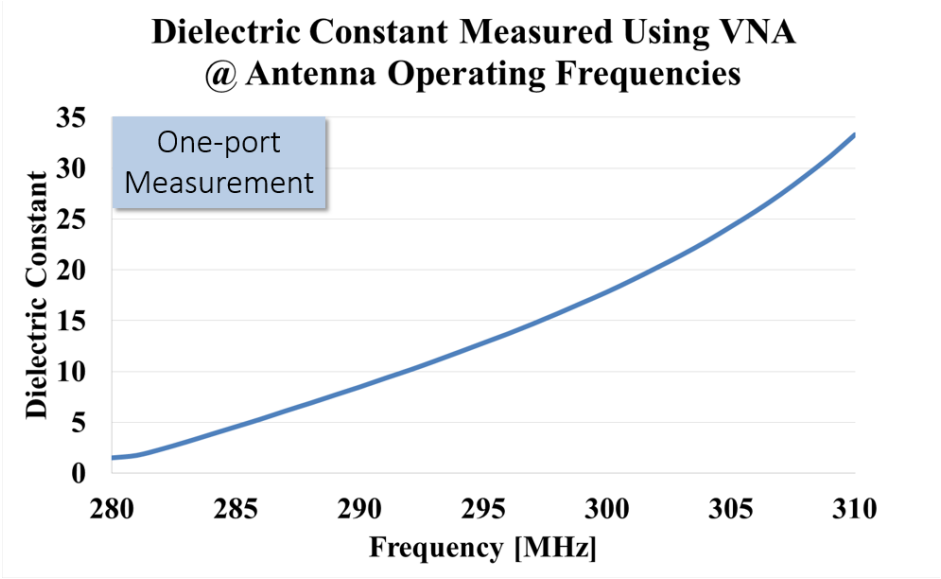


Figure 30. Measured dielectric constant of parallel plate capacitor over antenna operating frequencies

*Mussel Shell Material Coaxial Transmission Line*

A coaxial transmission line was built from a copper rod and tubing, BNC port connectors, N port connectors, Plexiglas and pulverized mussel shell, Figure 31. The

mussel shell powder served as the dielectric medium that filled the coaxial transmission line. Figure 32 shows the inner conductor, mussel shell dielectric medium and the outer conductor of the mussel shell transmission line.

Figure 31. Coaxial transmission line with pulverized mussel shell insulator

Figure 32. Inner conductor and pulverized mussel shell insulator of the coaxial Tx. line

The VNA was used to measure all S-parameters ($S_{11}$, $S_{12}$, $S_{22}$, and $S_{21}$). Then, using the following equations to solve for the mussel material dielectric constant.

$$Z_{11} = \frac{((1+S_{11})(1-S_{22})+S_{12}S_{21})}{\Delta s} Z_0 \qquad \text{Equation 61}$$

$$Z = \sqrt{\frac{L}{C}} = \frac{1}{2\pi}\sqrt{\frac{\mu}{\varepsilon}} ln\frac{D}{d} \qquad \text{Equation 62}$$

Where in Equation 61 $\Delta s$ is the determinant of the S-parameter matrix and $Z_0$ is the impedance of the system which is 50Ω. In Equation 62 we solve for $\varepsilon$ and $\mu$ can be approximated to be 1, *D* is the diameter of the outer conductor (copper tubing) and *d* is the diameter of the inner conductor (copper rod). Figure 33 shows VNA measurements results of mussel material coaxial transmission line at higher frequencies.

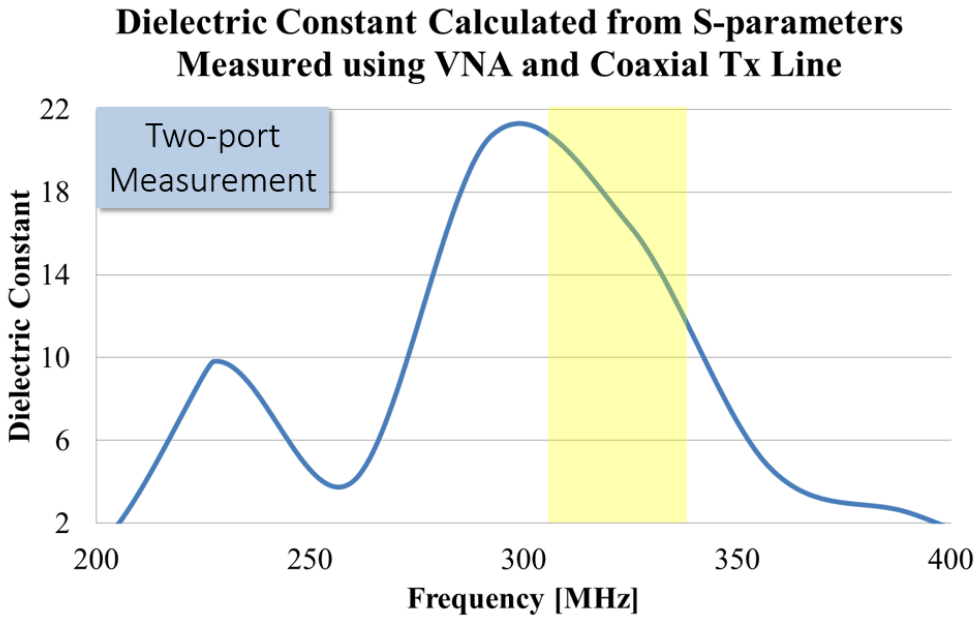


Figure 33. Dielectric constant from coaxial transmission line

*Water Conductivity*

Conductivity of water is an important property for us, since we are propagating EM waves underwater. We collected samples of Iowa City tap water, Iowa Aquatics center diving pool water, and Iowa River water.

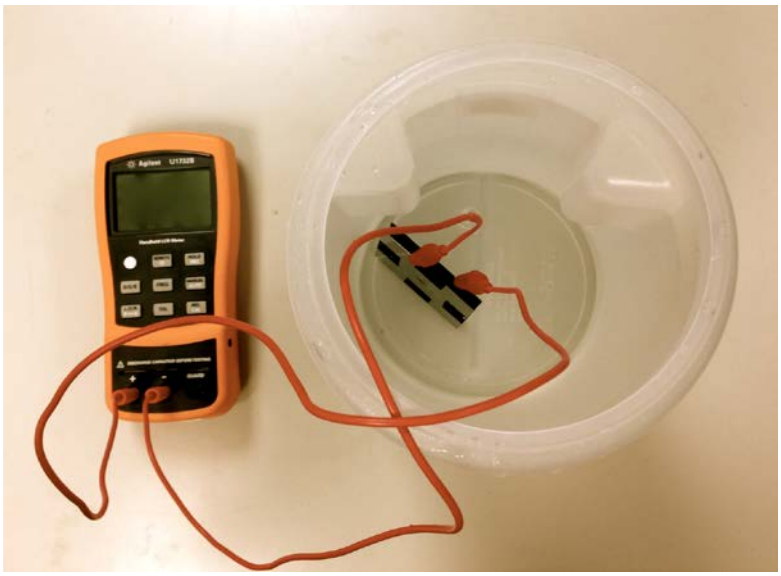

(a) Measurement setting using a portable U1732B Agilent LCR meter.

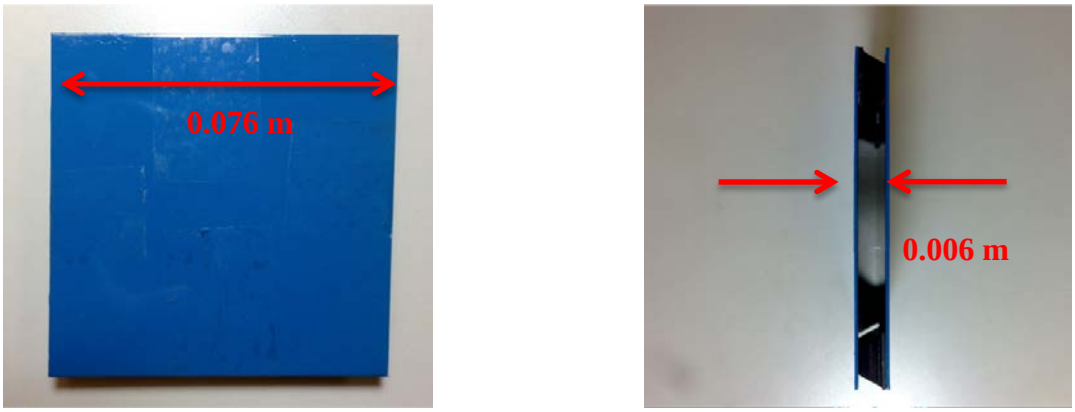


(a) Parallel metallic plates with their dimensions.

Figure 34. Water conductivity measurement experiment.

We used two separated metallic plates immersed in the water and measured the resistance using an U1732B Agilent LCR meter [82]. The plates had dimensions of $7.6 \times 7.6$ cm and the backsides were painted to insulate them from the water. We calculated the conductivity from the measured resistance and known area and separation of the plates. The results are shown in Table 1.

Table 1.Water conductivity experiment results.

| **Iowa River** | **IC tap water** | **UI Diving Pool** |
|---|---|---|
| $\sim 56$ mS/m | $\sim 27$ mS/m | $\sim 218$ mS/m |

*Shells elemental analysis:*

Mussel shell samples are shown in Figure 35 shows and Table 2 contains mussel shells dimensions. Shells were pulverized manually in our lab as shown in Figure 36. The shell fine powder was sent for elemental analysis to The University of Iowa – State Hygienic Laboratory. Results are shown on Figure 36. From the results it is noted that Ca is the most abundant metal in the shells probably forming compounds such as $CaCO_3$/$CaHPO_4$/$Ca_3(PO4)_2$ providing rigidity to the structure of the shell. Shells are made mostly of calcite, which is $CaCO_3$, calcium carbonate. It is also relevant to note the amount of iron present because it can form dielectric compounds such as ferric oxide (FeO) or Ferrous oxide ($Fe_2O_3$) with high relative permittivity. Another element with a noticeable amount in the table is Na. This element can form compounds such as sodium silicate with a high relative permittivity as well.

Table 2. Mussel shell samples dimensions

| Mussel Samples | Width [mm] | Length [mm] |
|---|---|---|
| 1 | 91.61 | 139.62 |
| 2 | 94.60 | 140.32 |
| 3 | 71.24 | 130.28 |
| 4 | 71.37 | 125.89 |
| 5 | 77.44 | 118.20 |
| 6 | 76.65 | 116.72 |
| 7 | 74.58 | 109.76 |
| 8 | 75.05 | 110.83 |
| AVG | 79.07 | 123.95 |


Figure 35. Mussel shells samples.

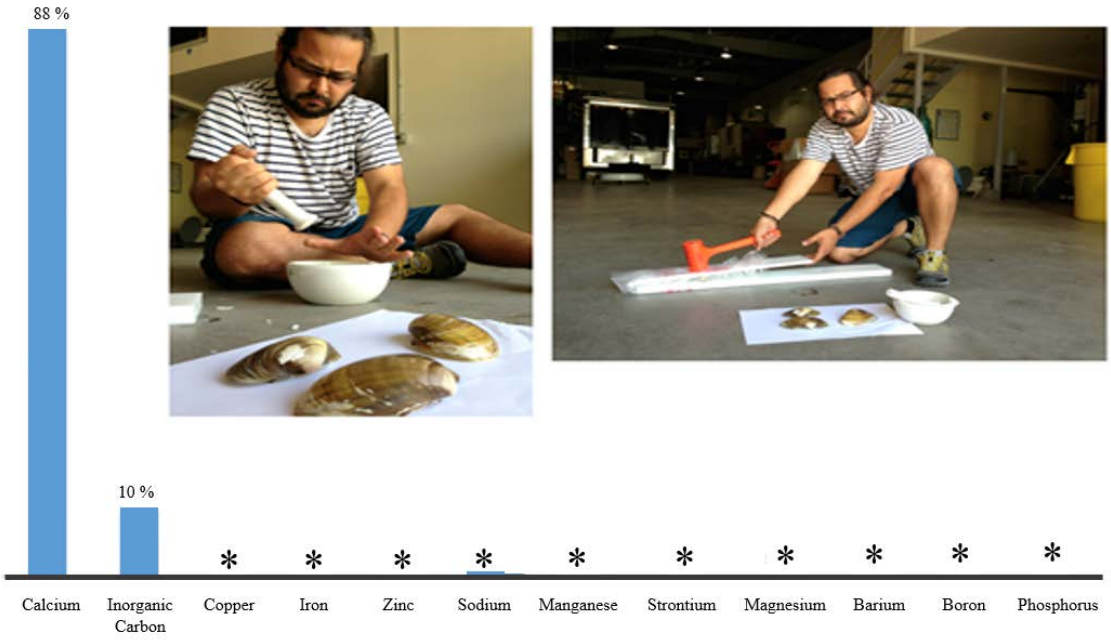


Figure 36. UI State Hygienic Laboratory shells elemental composition analysis results.

* Means that each of these elements with has less than 1% in the composition of the shell

# CHAPTER IV. EXPERIMENTAL AND SIMULATED PROTOCOLS

## Preliminaries

My thesis is to design, construct, and test an antenna on a mussel shell for an underwater biological sensor network. We selected a curved spiral antenna, because it has the required properties for our underwater application. In this section we document the measurement procedures and results on a *dipole* antenna. The reason for using dipole antenna measurements is to give us practice, experience, and confidence in making antenna measurements.

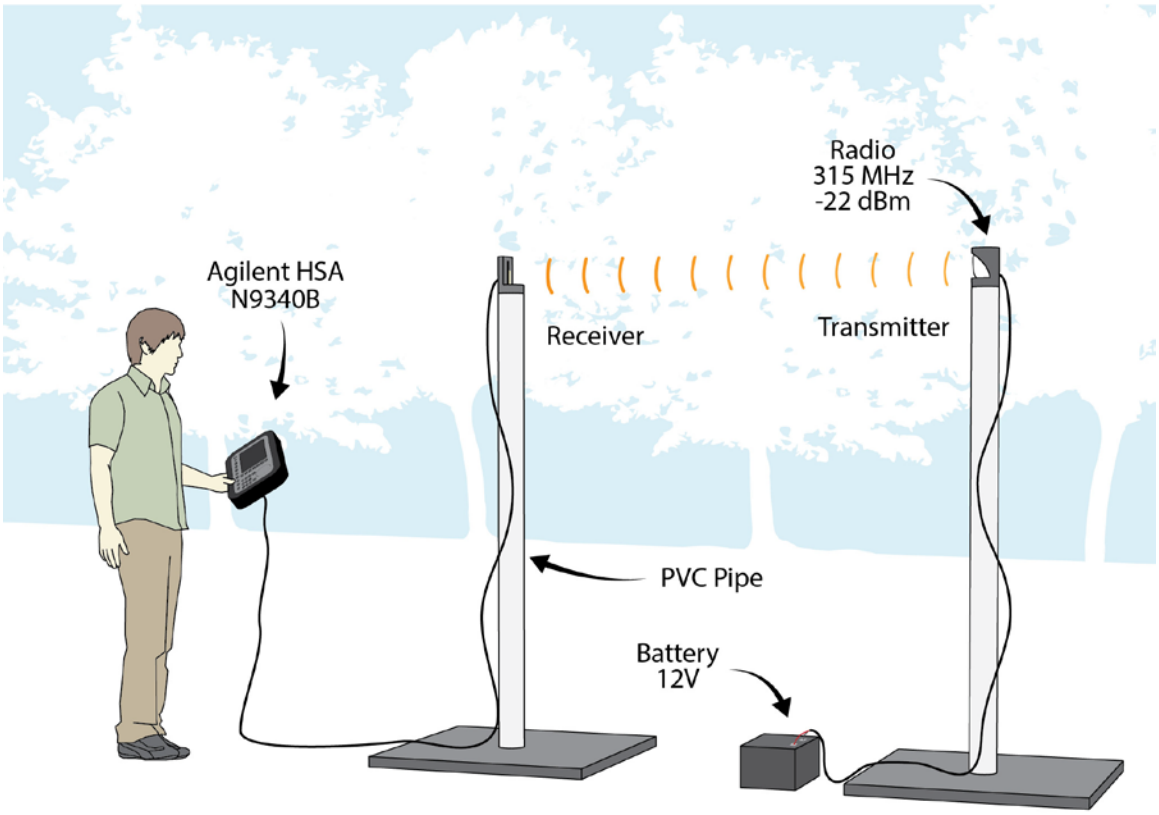


Figure 37. Experimental setup used for air measurements at Reynolds park at Iowa City, IA.

The expected results for a dipole are well-known and intuitive, so it makes sense to refine our measurement skills using a known quantity. We choose the center-fed dipole antenna because it is a fundamental and widely-used type of radiating structure, from the antenna theory standpoint [83]. It is popular mainly because it is easy to build and it has efficient performance [84]. Therefore, we built dipole antennas for the transmitter (radio) and receiver (spectrum analyzer). For the transmitting we use a half-wave dipole and for the receiving a short-dipole. The wavelength is calculated with freshwater as the medium of propagation, is approximately 0.1 m at 315 MHz. The length of the transmitting half-wave dipole antenna is then 0.05 m. The receiving dipole antenna is a short dipole. Short dipoles are of length equal to or less that 10% of the wavelength (0.01 m) and are also known as elemental dipoles. By using a short dipole antenna at the receiver, we approximate a point measurement.

We performed dipole antenna measurements in the air and water. The measurements in the air are a precursor to underwater experiments, due to the easier maneuverability of the setting and equipment in air. Taking into account that the attenuation of the signal in air and water are different, we used the same RF modules but different transmitted power configurations. We used $-10$ dBm and $-22$ dBm of transmitted power in water and air, respectively. The air testing, see in Figure 37, aids us to learn the logistics involved in these experiments. For example, we devised improvements in the experimental setting structure based upon our testing in air. We found it practical to use polymerizing vinyl chloride (PVC) hosepipes, flanges, and squared bases to build two masts for the test fixture. Each of the PVC pipe masts consist of two separable parts.

The air measurements gave us confidence in the dipole antenna model validation process, including obtaining the radiation patterns. We needed to take into account the transmitted power of the radios, power supplies, cable connections, structure connections, instrumentation equipment, location, and facilities of the experiment. We trained ourselves in the operation of the equipment, where to place the radios in the field, how to rotate the transmitter and the receiver antenna, and radio, how to transport the tools, equipment and gear, and planned safety protocols for air and underwater experiments through air testing.

## Antenna-Radio Testing System

The antenna-radio system used on the underwater and air experiments at the pool and tank is shown in Figure 38. For the spiral antennas we 3-D print the structure that houses the antennas. We then inlay 16 AWG copper wire into the grooves in the housing. Then, we use a 2 m, 50 Ω coaxial cable between the antenna and the radio box to reduce the radio box radiation that could interfere with our measurements. The radio box was insulated with an RF absorber material designed for our operating frequency range. The radio box contains a TRM-315-LT transmitter sealed in epoxy to protect the electronics. A 12 V battery powers the radio.

## Dipole Antenna Air Measurements

We constructed several versions of dipole antennas. In order to minimize connector losses, we constructed the dipole from a 50 Ω RG-58 coaxial cable. The dipole antennas were constructed in the following fashion. We took a coaxial cable and cut a connector out in one of the sides of the cable. At the open-end side, the two-wire lines behave as an open circuit transmission line. The center-fed dipole antenna can be obtained by simply folding

the two-wire lines. It should be noted that the lengths of two-wire lines are the same, 0.05 m and/or a quarter-wavelength (at 315 MHz in freshwater) for the transmitter dipole antenna.

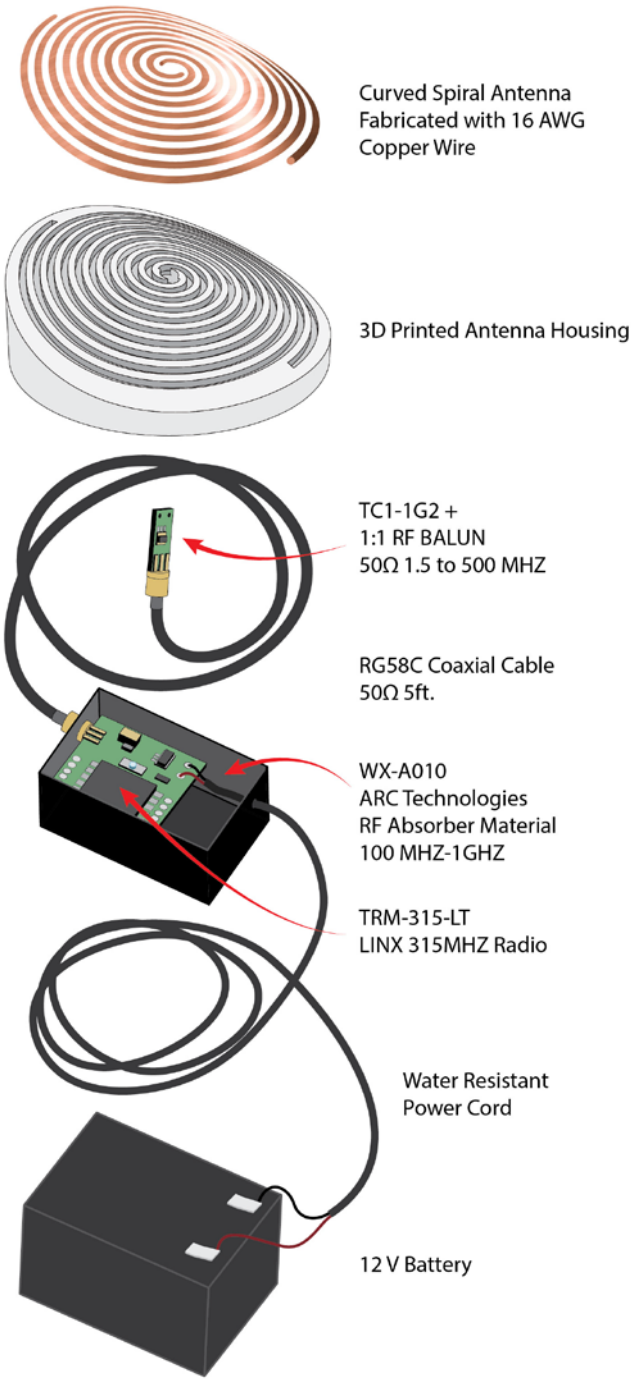


Figure 38. The antenna-radio system used in the underwater and air experiments.

The location chosen to practice the air measurements was Reynolds Park in Iowa City, IA. We decided to use this site because it has a flat, open field. This park is also located far from the high-voltage power lines and trees that may contribute to interference signals. The idea of using a location with these characteristics arose due to preliminary results obtained through air measurements collected in the parking lot of the building where our lab is located. The air results showed some anomalies. We concluded that all these undesired results were due to the reflections from the walls of the building, trees, and other obstacles.

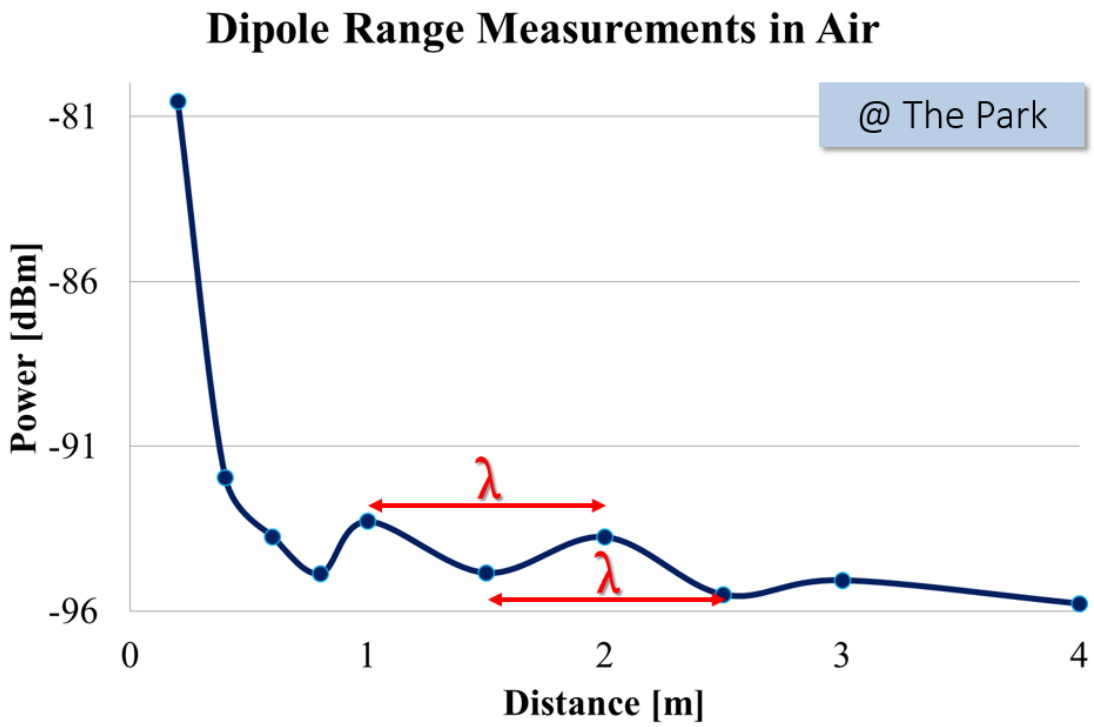


Figure 39. Dipole antennas range measurements in air using an Agilent Handled Spectrum Analyzer N9340B. The measurements were collected by increments of $\lambda_{water}/4$.

For air validation, we performed two sets of experiments. We collected data of azimuth and range measurements using different transmit powers ($-10$ dBm and

−22 dBm). The azimuth measurements were taken at a counterclockwise rotation of 22.5°. The quarter-wavelength in air at 315 MHz is approximately 0.24 m. Range measurements were in 0.24 m increments.

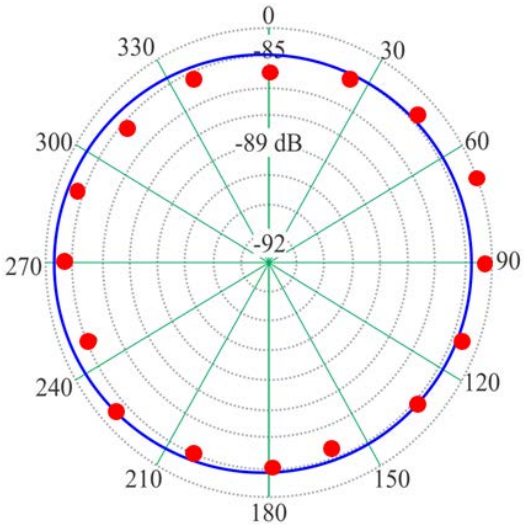


Azimuth measurement located in the far-field of the antenna.

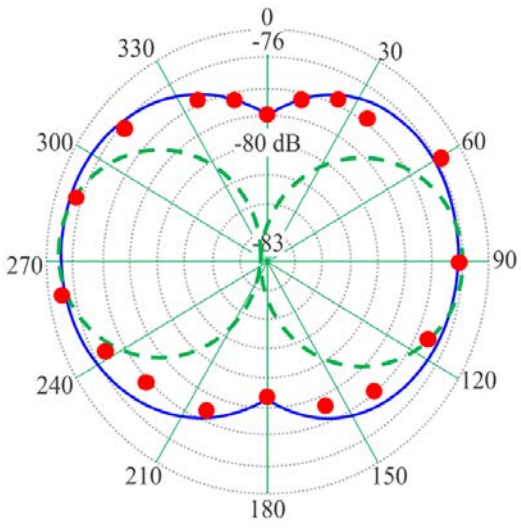


Elevation measurement located in the near field of the antenna.

Figure 40. Half-wave dipole antennas measurements in air. Azimuth measurements (red) matched well with ideal (blue). Far-field elevation measurements is difficult since this would require the measurement probe to be at least 5 m aloft of the antenna. Consequently, we performed elevation measurements in the near field.

In the initial air experiment, we positioned the transmitter dipole antenna parallel to the top of the PVC pipe and measured azimuth. When we plotted the radiation pattern of these measurements we realized that all of the patterns were shifted off the center. This was due to the angle displacement by the rotation of the PVC pipe. In the second version of the experiment, we installed a cable gland in the top of the PVC pipe to center and secure one of the ends of the dipole antenna. The subsequent sets of collected data were consistent

with dipole antennas. The plotted radiation patterns were centered and had constant values over the azimuth rotations.

## Underwater Antenna Measurements

### Underwater Experiments in Tank located in Laboratory Facilities

The experimental setup— shown in Figure 41, Figure 42, and Figure 44— consists of a large cylindrical tank of 2.6 m diameter and 2.1 m height. The tank was filled with Iowa City tap water that has a conductivity of ~34 mS/m [23] which is similar to Iowa River water and similar to mussel's habitat. PVC pipes were used for support of the antenna under test from top of the tank.

### Range Measurements

Figure 41 shows the experimental setup used to make antenna range measurements. In order to have precise measurements, we used a computer-controlled stepper motor to move the receiving antennas.

### Elevation and Azimuthal Measurements

The experimental setup used for the underwater antenna elevation and azimuth measurements is shown in Figure 42. The tank is filled with Iowa City tap water and with the position of the transmitter antenna on the figure, azimuth measurements were collected at $22.5^{o}$ rotation angle increments. The receiving antenna is fixed and the transmitting antennas rotate $360^{o}$. The elevation measurements were collected by rotating the transmitting antenna $90^{o}$, facing down to the bottom of the water, and again with $22.5^{o}$ increments.

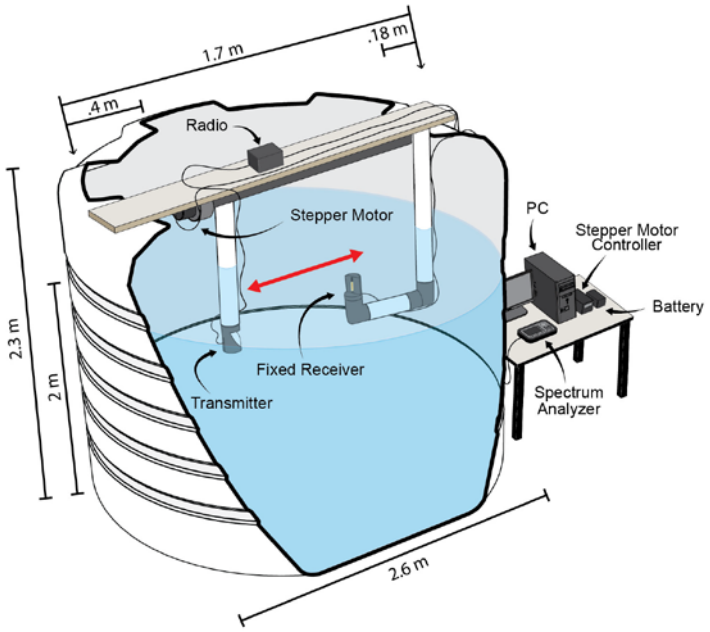


Figure 41. Experimental setup for evaluating range measurements of underwater antennas. The tank is filled with Iowa City tap water and the stepper motor precisely controls the distance between the transmitter and the receiving antennas. The stepper was computer-controlled.

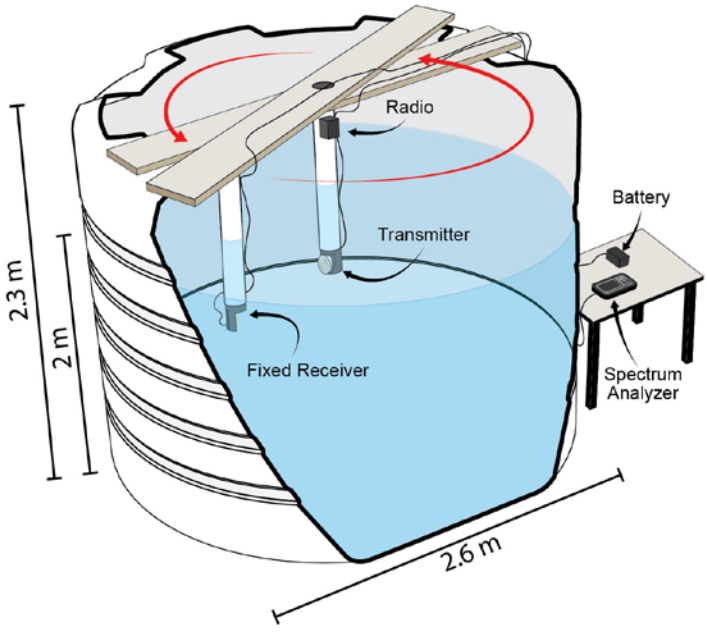


Figure 42. Experimental setup for azimuth and elevation measurements.

**Antenna Input Impedance Measurements**

We used a VNA for measuring the antenna's $S_{11}$ parameter, which is the return loss. The VNA transmits a small power signal to the antenna under test and measures the amount of power that is reflected back. $S_{11}$ is fundamentally the magnitude of the reflection coefficient [85].

The experimental setup used for the underwater antenna $S_{11}$ measurements is shown in Figure 43 and Figure 44. The tank is filled with Iowa City tap water and the antenna under test is placed in the center of the tank in different media. Measurements were obtained over a frequency range of 250 to 397 MHz.

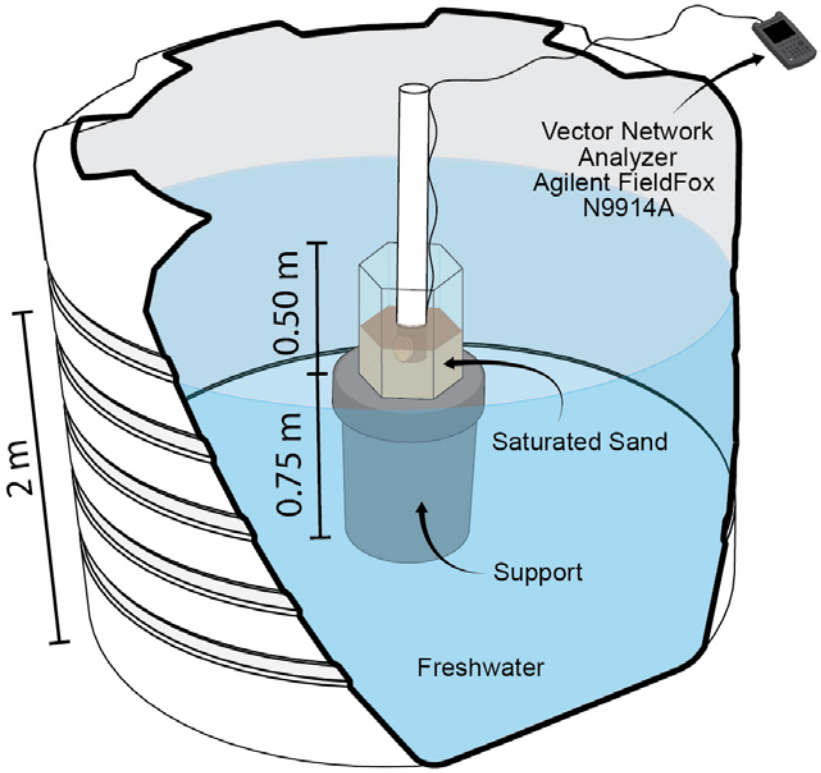


Figure 43. Experimental setup to measure antenna input reflection coefficient ($S_{11}$) in saturated sand.

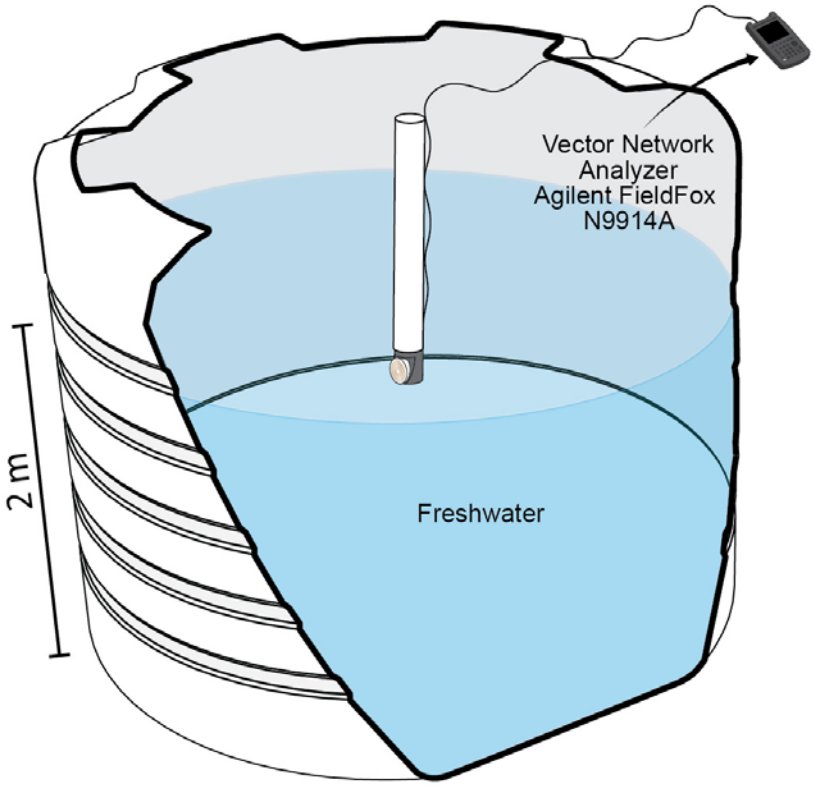


Figure 44. Experimental setup to measure antenna input reflection coefficient ($S_{11}$) in freshwater.

**Underwater Experiments in Diving Pool Located in the University of Iowa Aquatic Center**

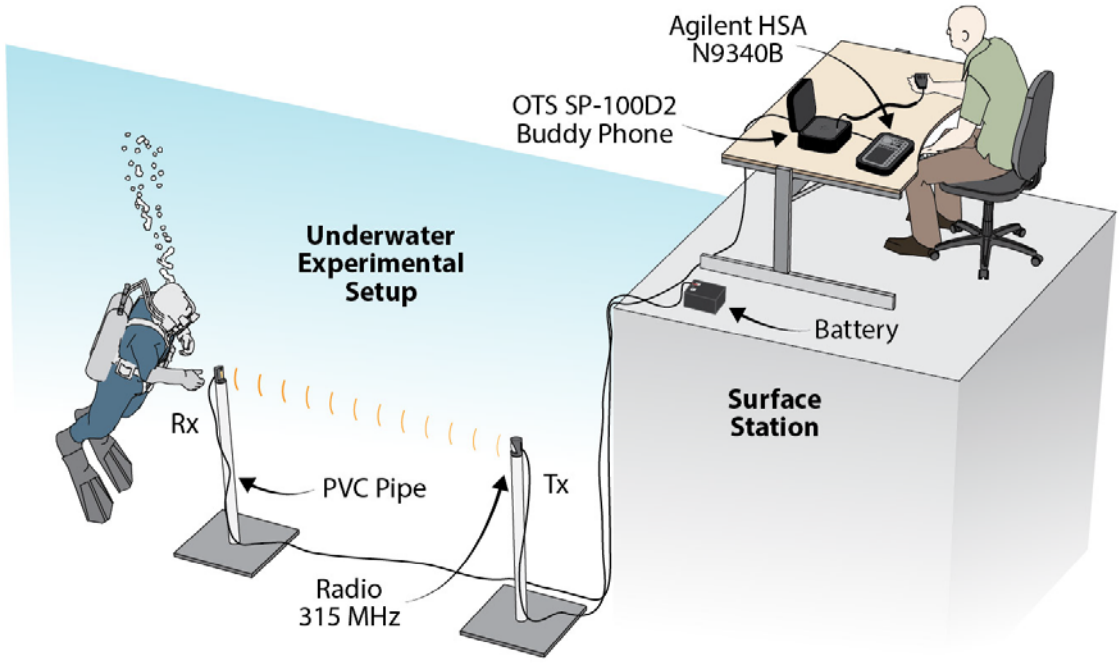


Figure 45. Illustrating the underwater experimental setup used at diving pool.

We collaborated with the University of Iowa Aquatics center in Figure 45 and Figure 46. They allowed us to use the diving pool for intervals of an hour and half twice a week. The diving pool dimensions are depth of 5.6 m, 18 m of length, 23 m of width and approximately 300,000 liters of water capacity. We hired a certified diver to make the measurements in the bottom of the dive pool. The PVC masts are 2.8 m height. We chose this height because the measured height of the water surface in the center of the dive pool is 5.6 m. Thus, the 2.8 m PVC masts place the dipole antennas in the center of the water to avoid possible interference related to reflection from the walls, and water surface. The

purpose of using the diving pool is to have a medium with minimal interference, which is approximately infinite in comparison with the propagation range of the signal underwater.

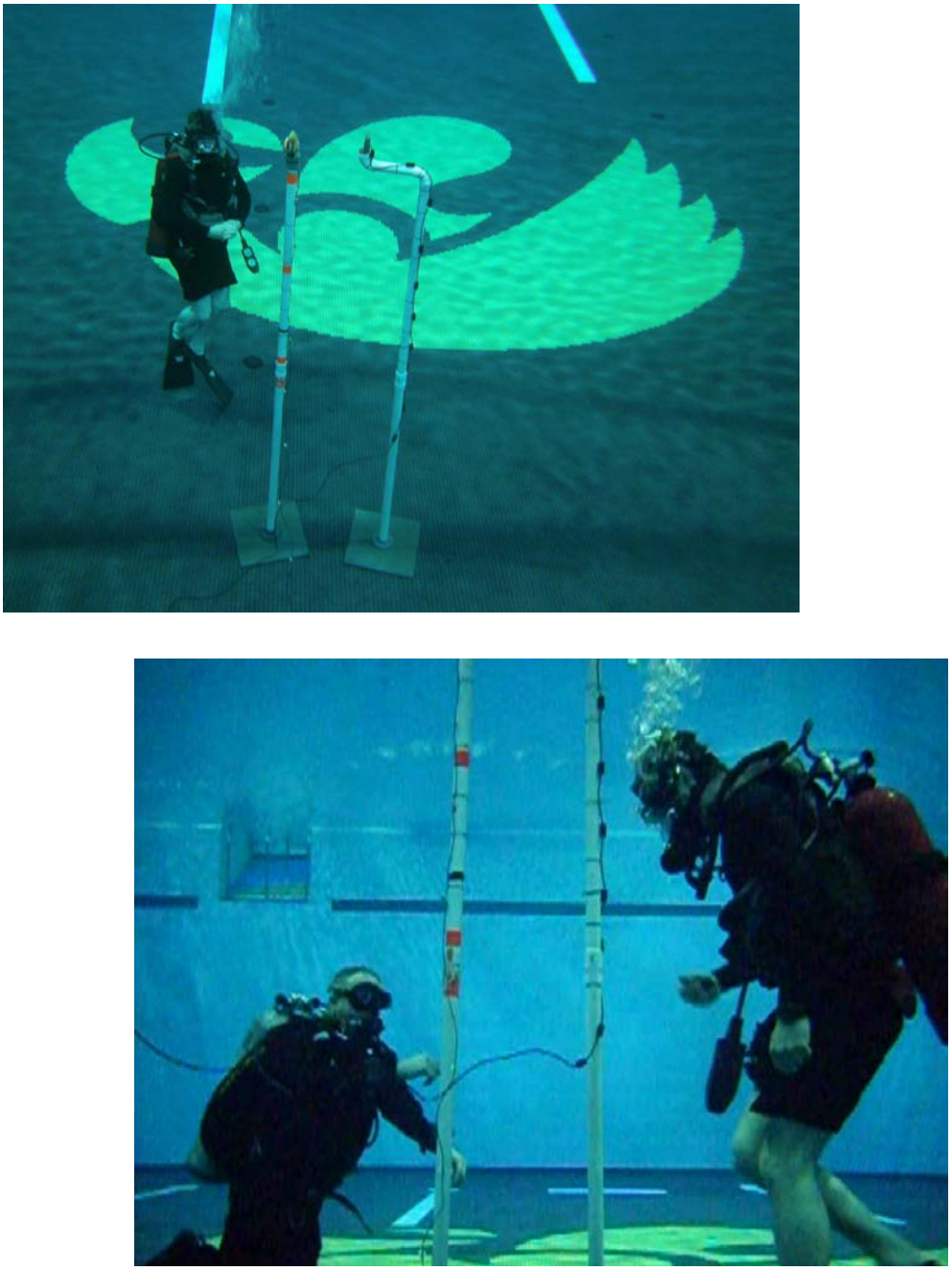

Figure 46. Inside The University of Iowa Aquatic Center – diving pool photographs showing the actual setup and the certified divers.

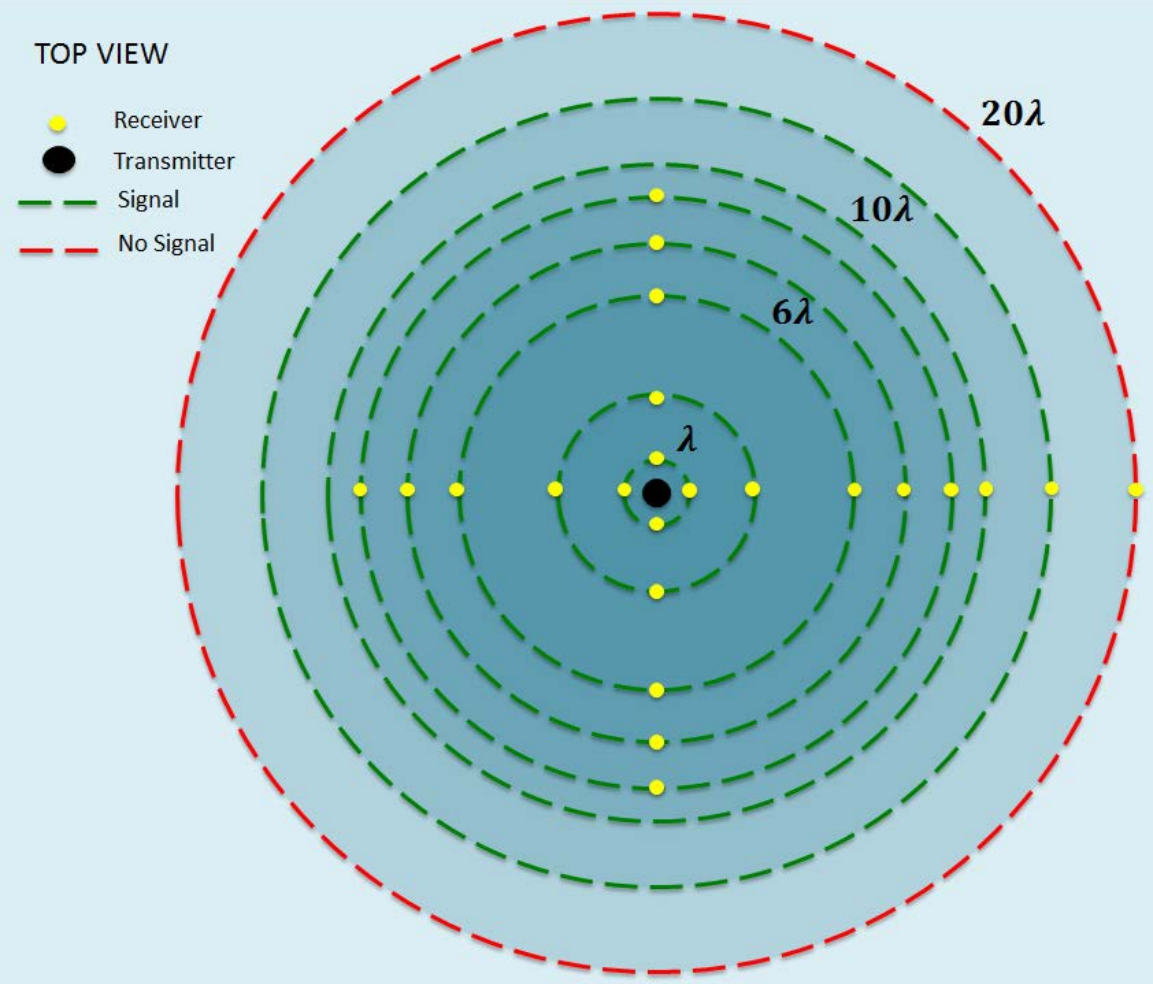


Figure 47. Exploratory plan of the location and graphical results of the signal strength of the measurements underwater with power of −10 dBm. After this initial study, we chose to limit our measurement to around ∼9$\lambda$.

Further, we designed and built a simpler board without all the sensors and other devices in the cyber-mussel in Figure 48. The new design included a radio module, a 3.3 V adjustable voltage regulator and other elements seal with epoxy to protect the RF modules when submerged, see Figure 49. The radio module's transmit power depends on the power supply voltage. This allows us convenient control of the transmit power. By adjusting the transmitter power levels such that the maximum reception range was 1 m, we mimic the case of an infinite medium to avoid multipath reflection interference.

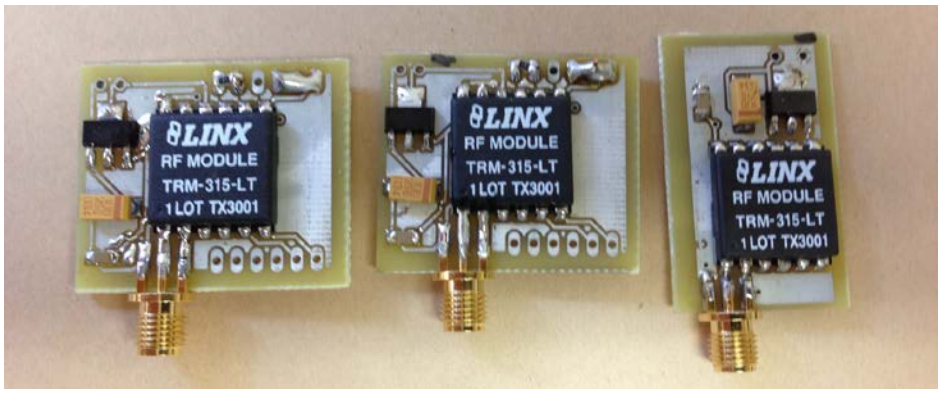


Figure 48. Board design specifically for the antenna testing without all the sensor and components that are included in the cybermussel backpack.

The underwater dipole antenna validation measurements that we carried out were elevation, azimuth and range. We used counterclockwise rotation of 22.5º increments. We did range measurements by increments of quarter-wavelength in water of 0.025 m, approximately (see Figure 50 and Figure 51).

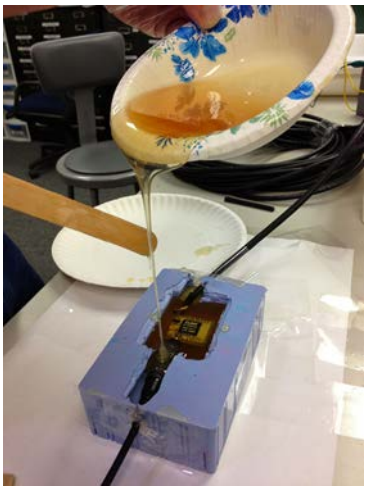

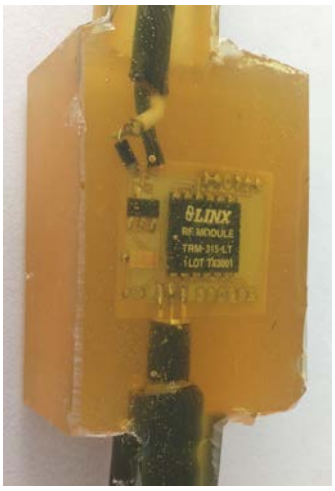

Figure 49. Any type of underwater work with electronic devices such as radios mounted in a circuit board requires significant effort to properly waterproof the equipment.

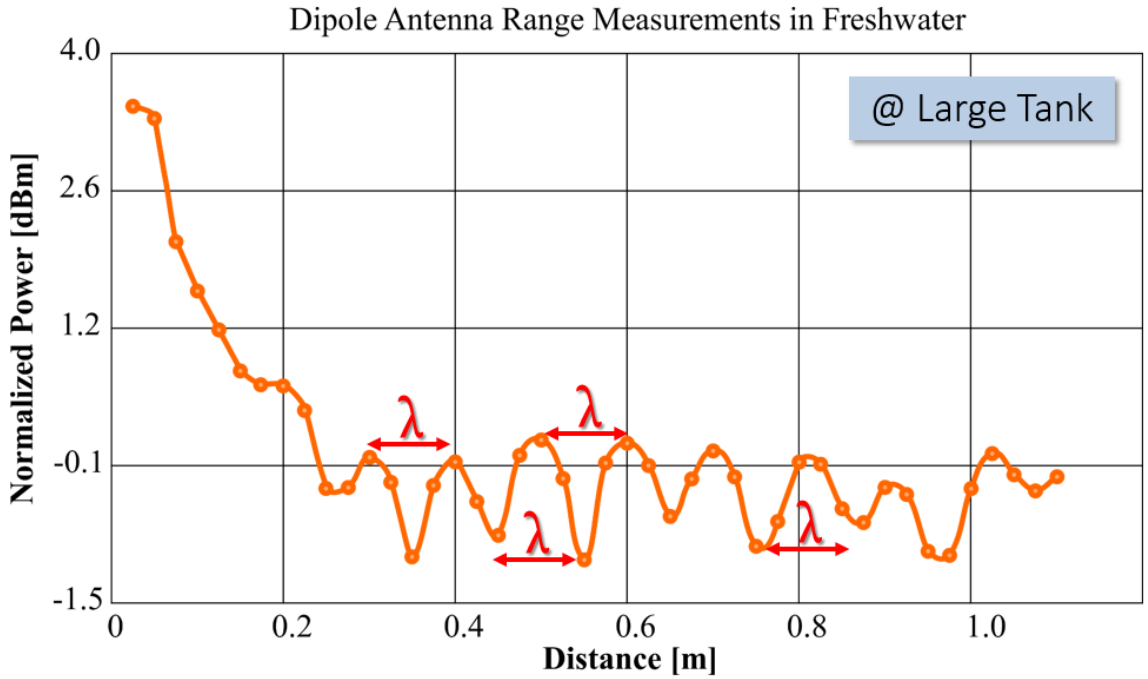


Figure 50. Underwater range dipole antennas measurements. The measurements were collected by increments of $\lambda_{water}/4$.

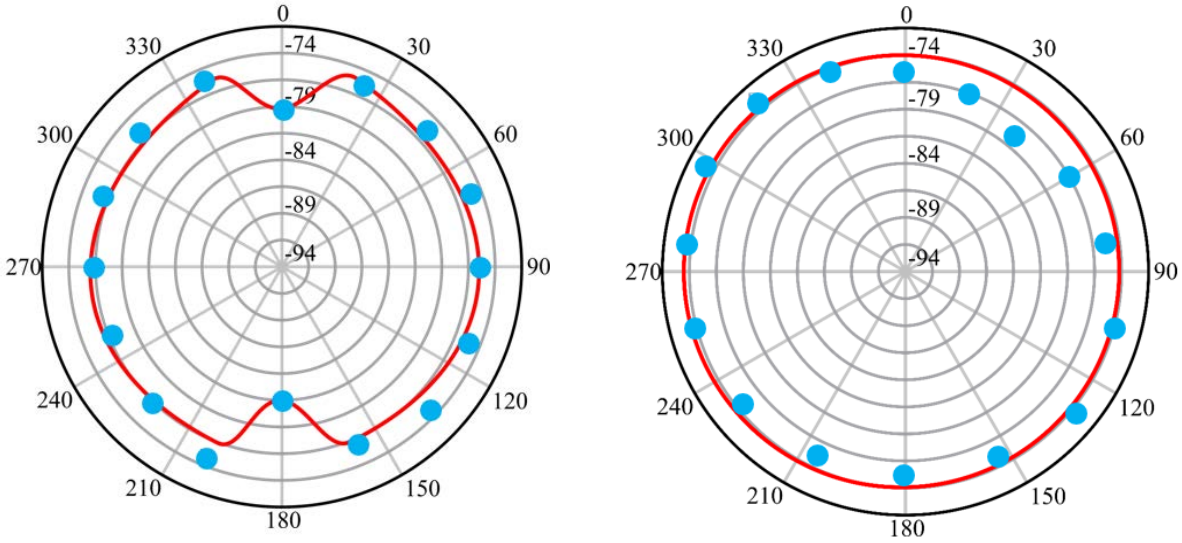


Figure 51. Dipole antenna elevation and azimuth measurements in freshwater. The measurements were collected by rotation increments of $22.5^{o}$

## Dipole Antenna Simulations

FEKO EMSS is used for the numerical analysis of the antennas in this thesis. In order to obtain solid understanding of the simulation engine and its limitations, well-known results were replicated. Therefore, Hertzian dipole were simulated and examined power vs. distance to check if one can observe reactive storage region, near field, far field, and transitions regions.

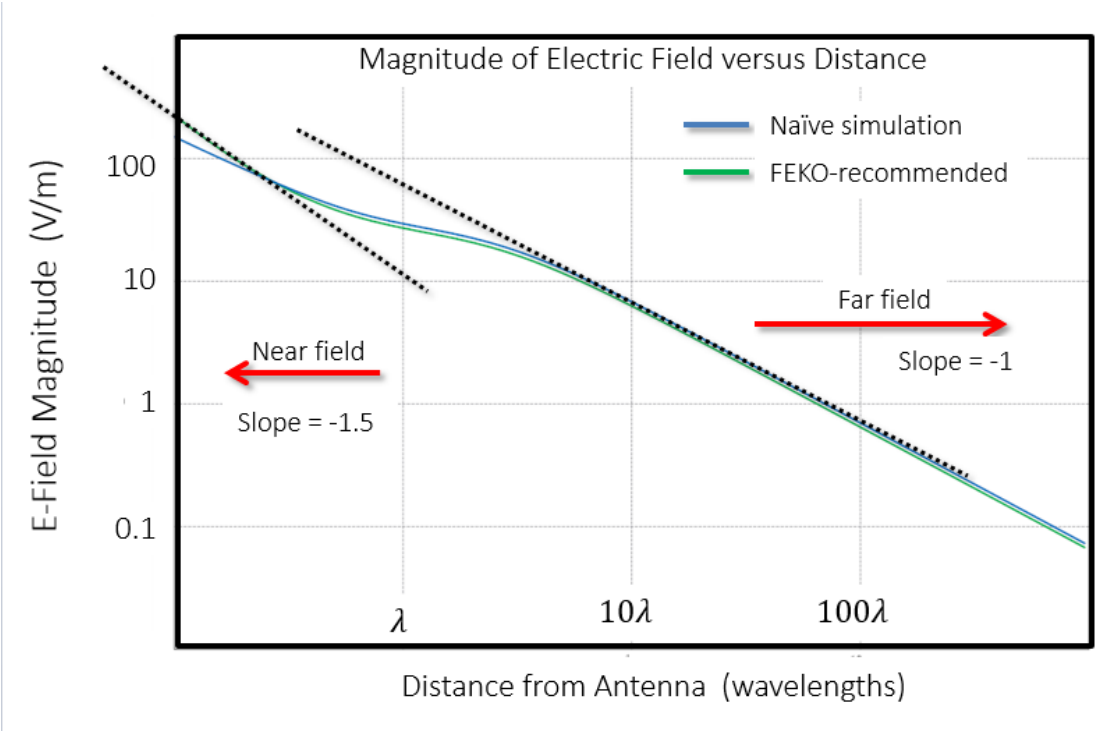


Figure 52. Dipole antenna in freshwater numerical analysis using FEKO. The range plot is shown depicting the Near and Far field regions of a naïve (simple pieces of wires) and FEKO-recommend structural design (thinner cylinder).

Dipole is the simplest antennas and should be easy to simulate in a great tool like FEKO. However, in my initial simulation I did the naïve approach. I built the dipole using a simple wire, and I was not obtaining the expected results for a well–known and –develop antenna. As is shown in Figure 52, I was not obtaining the corresponding slope for the different regions surrounding the antenna. Then, I contacted FEKO technical support and

work really close to them to learn deeply about this CEM software tool. The FEKO's support advised me to build the dipole using cylinders with small radios instead of simple wires. Cylinders for the arms of the dipoles work better since the simulation engine treats wires and a limiting case of cylinders. Using cylinders forces the simulation engine to use a finer mesh. With this approach, the slope for the far-field matches what theory predicts. The near-field slope improved as well, but did not achieve a value between -2 and -3 as theory predict. However, the trend is correct, and the remaining difference can be attributed to limited computational resources. Further, dipole simulations results for elevation and azimuth are shown in Figure 53.

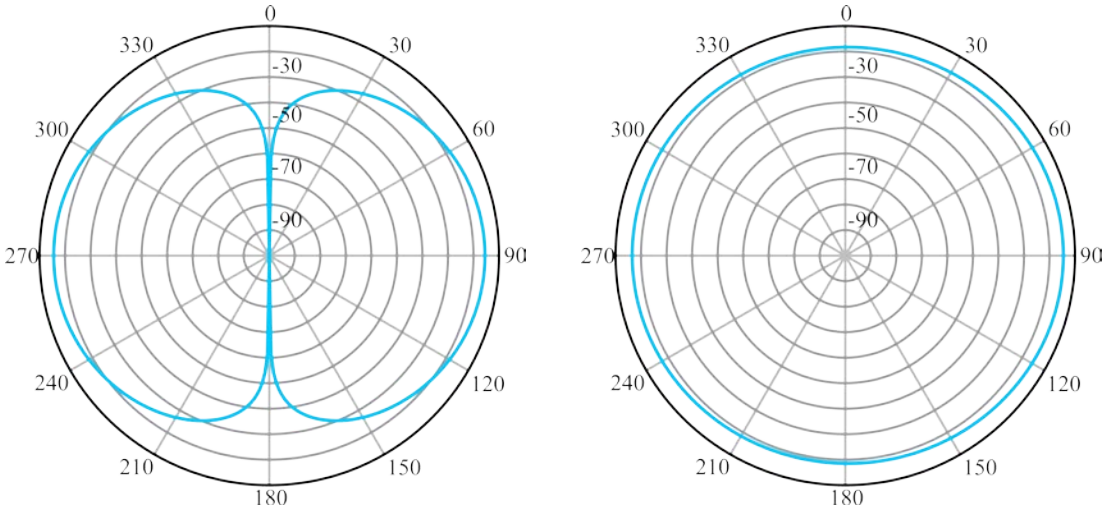


Figure 53. Dipole antenna elevation and azimuth simulations in freshwater using FEKO CEM software tool. The measurements were calculated by rotation increments of $1^{o}$.

# CHAPTER V. SPIRAL ANTENNAS

In general, spiral antennas belong to the class of frequency-independent antennas. Frequency-independent antennas having a relatively constant radiation pattern, polarization and input impedance over a wide range of frequencies [18, 86]. Spiral antennas in general are mostly self-complementary. Self-complementary means that in the case of a spiral antenna, the metal arms cover the same area as the non-metal gaps between the spiral arms. Planar spiral antennas typically have a bi-directional radiation pattern. Planar spiral antennas are often equipped with a conducting ground plane or an absorber-filled cavity in the backside to eliminate the backside radiation. One can separate flat spiral antennas into two groups, namely, those that are equiangular, and those that are Archimedean. Within these groups there many variations.

## Flat Archimedean Spiral Antennas

For us to embark on the study of planar (flat) spiral antennas, one has to review the theoretical analysis done by Dyson and Curtis in 1959 and 1960, respectively. Prior to this time spiral antennas were studied *experimentally* for almost six years. Thus, the theoretical contribution of Curtis and Dyson was of vital importance for the development of planar spiral antennas. Dyson presented the theoretical analysis of flat equiangular spiral antennas and Curtis did the same but for flat Archimedean spiral antennas. Their papers are quite detailed and comprehensive—they begin with a theoretical analysis, present designs for antenna prototypes, and compare theoretical results with measurements.

## Theoretical Analysis

Curtis [57] presented the derivation of the radiation fields of the flat Archimedean spiral antenna by approximating the spiral with a series of semicircles. The usual procedure

[78] in the analysis of radiation fields is to specify the sources and then require the fields radiated by the sources. In their analysis they used auxiliary functions, known as vector potentials, which are commonly used to simplify the derivations.

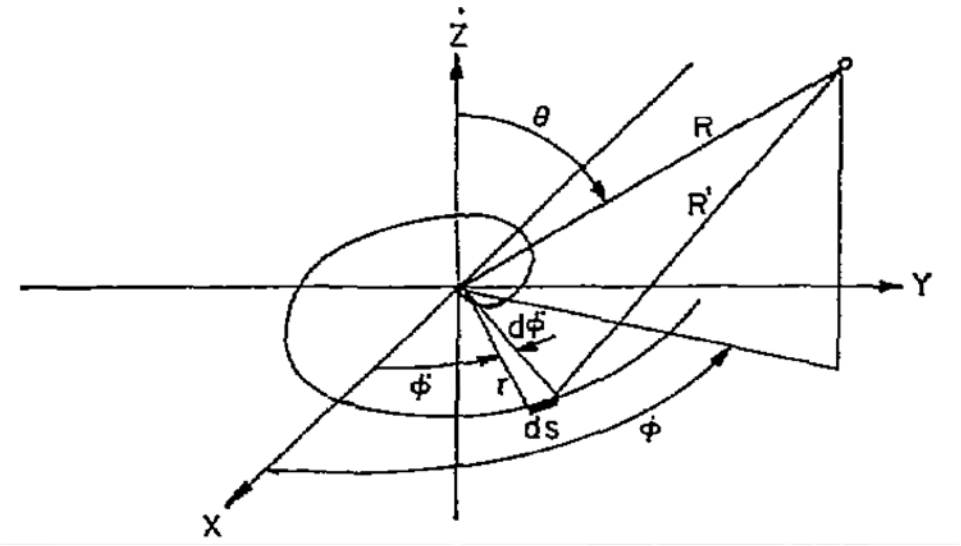


Figure 54. Coordinate system used by Curtis [57].

The coordinate system used by Curtis is shown in Figure 54, where:

| | |
|---|---|
| **A** | vector potential, |
| $\omega$ | angular frequency, |
| $\beta$ | phase constant, |
| $R'$ | distance from the current element, |
| **I** | current distribution on the spiral, |
| $s_0$ | total length out to the end of the spiral, |
| $s$ | is a unit length along the spiral, |
| $ds$ | element length on the spiral, |
| $S_\phi$ | the direction cosine between $s$ and $\phi$, |
| $S_\theta$ | the direction cosine between $s$ and $\theta$, |
| $r, \phi'$ | polar coordinates of the spiral, |
| $R, \theta, \phi$ | Spherical coordinates of the spiral. |

As a first step, one defines the vector potential generated by a source (the current element):

$$\mathbf{A} = \frac{1}{4\pi}\iiint \mathbf{I}\frac{e^{-j(\omega t-\beta R')}}{R'}dv \qquad \text{Equation 63}$$

The flat Archimedean spiral antenna is positioned symmetrically in the $x-y$ plane at $z = 0$. Considering only far-field components of the field and also the case of a line source, we obtain

$$\mathbf{A} = \frac{1}{4\pi R}\int_0^{S_0} \mathbf{I}e^{-j\beta R'}\left[S_\phi\phi - S_\theta\theta\right]ds \qquad \text{Equation 64}$$

The distance $R'$ could be approximated as follows to yield the fields in the far-field region:

$$R' = \sqrt{R^2 + r^2 - 2rR\sin\theta\cos(\phi-\phi')} \qquad \text{Equation 65}$$

$$\therefore R' \backsimeq \sqrt{R^2 - 2rR\sin\theta\cos(\phi-\phi')} \quad \text{for } R \gg r$$

Then, using a binomial expansion one can simplify $R'$ further to get

$$R' \backsimeq R\sqrt{1-\frac{2r}{R}\sin\theta\cos(\phi-\phi')} \approx R - r\,sin\,\theta\cos(\phi-\phi') \qquad \text{Equation 66}$$

$S_\phi ds$ and $S_\theta ds$, the direction cosines and element of length $ds$, in terms of polar coordinates of the flat Archimedean spiral,

$$S_\phi ds = rd\phi'\cos(\phi-\phi') - dr\sin(\phi-\phi') \qquad \text{Equation 67}$$

$$S_\theta ds = \cos\theta\,[rd\phi'\sin(\phi-\phi') + dr\cos(\phi-\phi')] \qquad \text{Equation 68}$$

As mentioned above Curtis [57] approximated the geometry of the Archimedean spiral antenna using a series of semicircles as shown in Figure 55. He first analyzed the radiation from one semicircle and then generalized it for multiple semicircles, obtained after significant algebraic manipulation.

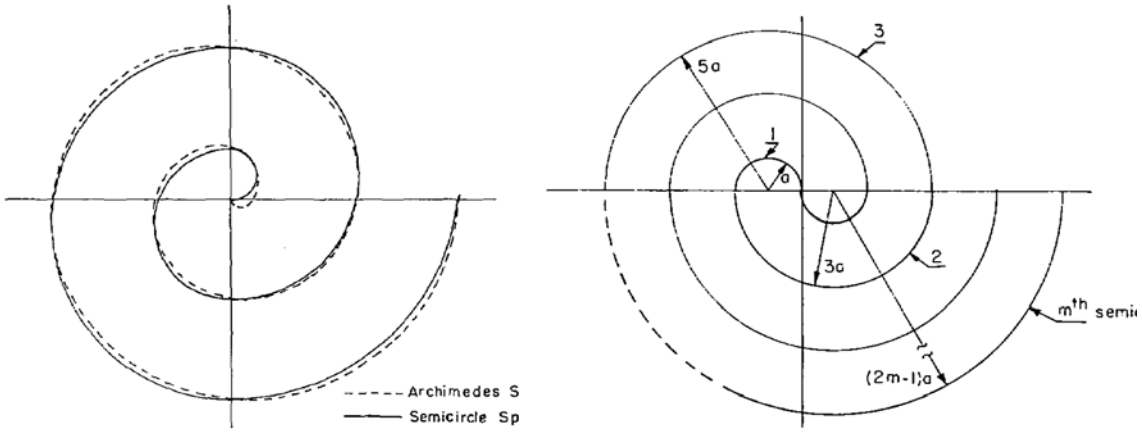


Figure 55. Left: one-arm spiral approximation using semi-circles. Right: two-arm spiral approximated using semi-circles [57].

**Description of the flat Archimedean Spiral Antenna**

The general equation for any spiral is:

$$r = f(\phi') \qquad \text{Equation 69}$$

The length along any spiral $S$ is given by,

$$S = \int_0^{\phi'} \left[ \left( \frac{dr}{d\phi'} \right)^2 + r^2 \right]^{\frac{1}{2}} d\phi' \qquad \text{Equation 70}$$

In the special case of the Archimedean spiral antenna, the spiral is expressed as

$$r = r_0 + a\phi' \qquad \text{Equation 71}$$

We could take Equation 69 and substitute it into Equation 70 and find an exact expression of the length along the spiral, which is a complicated expression as shown in [57]. Instead we can approximate $S$ with a simpler expression where the length along the spiral in function of $\phi'$,

$$S = a\phi' \quad \text{Equation 72}$$

Equation 70 is the arc of a circle, and is what Curtis [57] used to approximate the spiral. He visualized the construction of a spiral of any number of turns by using several semicircles with different radii.

**Flat Archimedean Spiral Antenna Practical Design**

The design of a sample two-arm Archimedean spiral antenna that we used in initial tests is governed by the parameters shown in

Table 3. The design equation [87] for an $N$ turn Archimedean spiral is given by

$$s = w = \frac{(r_{out} - r_{in})}{4N} \quad \text{Equation 73}$$

The lowest and highest operating frequencies of the spiral antenna determine the inner and outer radius. The inner radius is obtained when $r_{in} = \lambda/4$, and under this condition we obtained Equation 72. Similarly, the outer radius, which determines the lowest frequency, occurs when the circumference of the spiral is equal to one wavelength; $\text{Circumference} = 2\pi r_{out}$, then we obtain that $\lambda = c/2\pi r_{out}$, which leads to Equation 73. From Equation 72 and Equation 73, one could calculate the spiral parameters using the medium where the antenna will operate properties such as freshwater ($\lambda_{freswater} \approx 10\ cm$) and saturated sand ($\lambda_{saturatedsand} \approx 17\ cm$).

$$r_{in} \leq \frac{c}{(2\pi f_{high})} \leq \frac{\lambda_{low}}{2\pi}$$ Equation 74

$$r_{out} \geq \frac{c}{(2\pi f_{low})} \geq \frac{\lambda_{high}}{2\pi}$$ Equation 75

We used 250 MHz and 397 MHz as our frequency range, which has a geometric mean of 315 MHz, the nominal operating frequency to produce the antenna in Figure 56 with design parameters given in Table 3.

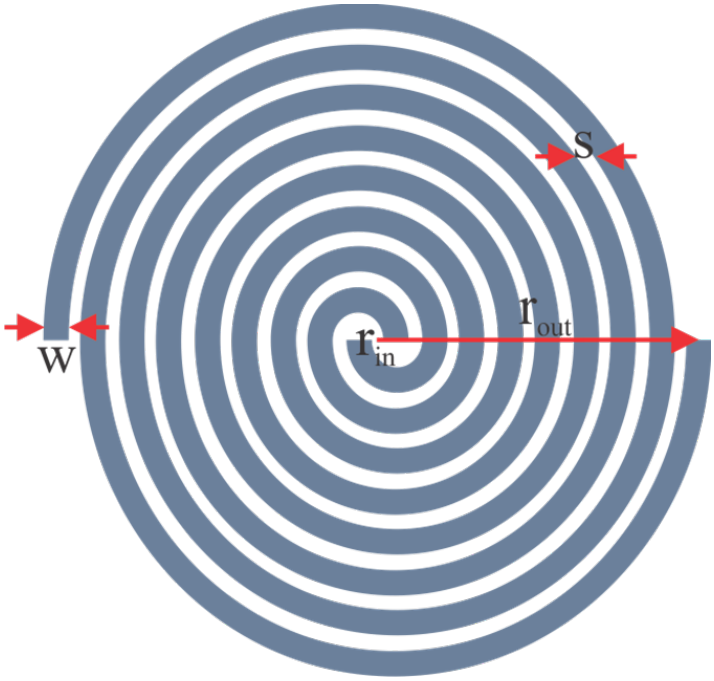


Figure 56. Flat Archimedean spiral antenna with its design parameters.

Table 3. Flat Archimedean spiral antenna specifications

| Symbol | Value | Description |
|---|---|---|
| $s$ | 1.175 mm | spacing between turns |
| $w$ | 1.175 mm | width of the arms |
| $r_{in}$ | 1.5 mm | inner radius |
| $r_{out}$ | 25 mm | outer radius |
| $N$ | 5 | number of turns |
| $\lambda_{low}$ | ~10 cm | freshwater medium |
| $\lambda_{high}$ | ~ 17 cm | saturated sand medium |
| $f_{low}$ | 250 MHz | low frequency |
| $f_{high}$ | 397 MHz | high frequency |

# CHAPTER VI. CURVED SPIRAL ANTENNAS AND CORRECTION PROCEDURE

## Curved Spiral Antennas-Brief Summary

Spiral antennas are normally flat, but some researchers have explored the possibilities of curved spirals with square and Archimedean configurations [63, 64]. In [63] the authors simulated a curved spiral antenna, printed on a dielectric cylinder. Their results show that the curved antennas exhibited greater variation of input impedance and gain with frequency than their flat spiral reference.

In [64] the authors simulated a curved spiral antenna above a conducting cylinder. They used a flat spiral antenna above a flat conductive surface as a reference. Their results show that above some threshold cylinder height, antenna input impedance and gain are essentially constant. Further, the antenna input impedance is largely independent of the cylinder radius, and the antenna gain shows a slight increase as the cylinder radius increases. The overall gain of the curved spiral antenna is lower than that of the reference flat spiral, about 2.7 dB. The radiation patterns show marked dependence on both the cylinder height and radius. The general trend is that if height or radius is increased, the radiation lobe towards the cylinder disappears.

The authors in [65] investigated employing an array of square spiral antennas on an hollow cylinder to compensate for the loss of the back lobe and create an omnidirectional radiation pattern.

## Two-Step Curved Spiral Antennas Correction Procedure

### Step One: Corrected Curved Spiral Cross-sections Elements

We now show a procedure to find the location of the corrected elements for curved spiral antenna from their cross-section elements using any arbitrary observation point. The first part is a procedure to find the corrected elements locations for curved spiral from the projected points of the flat spiral over a curved surface. In this case we are projecting over a spherical surface similar as the outline of a mussel shell.

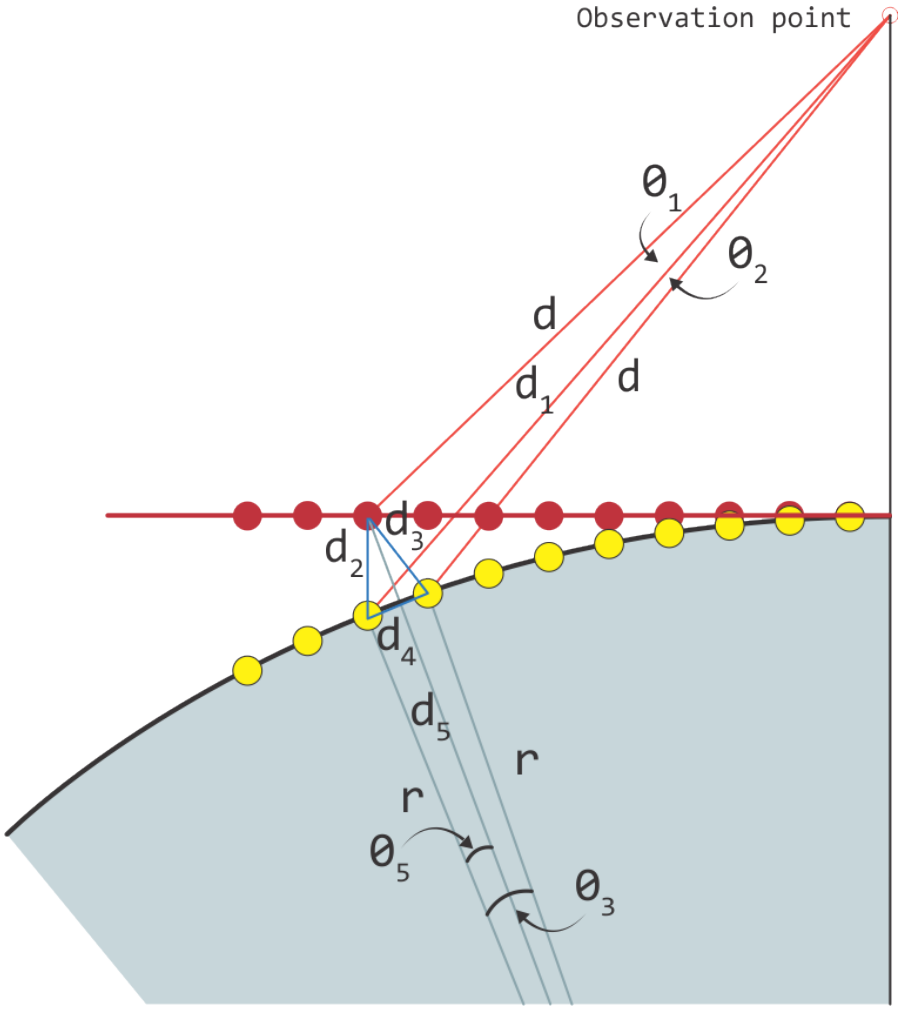


Figure 57. Cross-section cut of the flat and curved spiral showing the geometric components used in the corrected curved spiral antenna elements.

In our derivations, there are known parameters and unknown parameters. These are as follows:

- Known parameters $\{d, d_1, d_2, d_5, r, \theta_1\}$
- Unknown parameters $\{d_3, d_4, \theta_3, \theta_5\}$

From Figure 57, using the upper triangle by the Pythagorean Theorem gives

$$\sin\left(\frac{\theta_1 + \theta_2}{2}\right) = \frac{d_3}{2d} \quad \text{Equation 76}$$

$$d_3 = 2d \sin\left(\frac{\theta_1 + \theta_2}{2}\right) \quad \text{Equation 77}$$

Similarly, using the center and lower triangles in Figure 57, and using the cosine rule on the left half triangle results in

$$d_2^2 = d_5^2 + r^2 - 2d_5 r \cos\theta_5 \quad \text{Equation 78}$$

$$\theta_5 = \cos^{-1}\left(\frac{d_5^2 + r^2 - d_2^2}{2d_5 r}\right) \quad \text{Equation 79}$$

Since $\theta_3 = \theta_5 + \theta_6$,

$$\theta_6 = \theta_3 - \cos^{-1}\left(\frac{d_5^2 + r^2 - d_2^2}{2d_5 r}\right) \quad \text{Equation 80}$$

Using cosine rule on right half triangle gives

$$d_3^2 = d_5^2 + r^2 - 2d_5 r \cos\left(\theta_3 - \cos^{-1}\left(\frac{d_5^2 + r^2 - d_2^2}{2d_5 r}\right)\right) \quad \text{Equation 81}$$

Combining Equation 70 and Equation 79 leads to

$$4d^2 \sin^2\left(\frac{\theta_1+\theta_2}{2}\right) = d_5^2 + r^2 - 2d_5 r\ \cos\left(\theta_3 - \cos^{-1}\left(\frac{d_5^2+r^2-d_2^2}{2d_5 r}\right)\right) \quad \text{Equation 82}$$

In this equation, only unknown parameters are $(\theta_2, \theta_3)$. Using the lower triangle form by $d_4$ as base and $r$ on both sides, we can obtain:

$$\sin\left(\frac{\theta_3}{2}\right) = \frac{d_4}{2r} \quad \text{Equation 83}$$

$$\theta_3 = 2\sin^{-1}\left(\frac{d_4}{2r}\right) \quad \text{Equation 84}$$

Using top triangle form by $d_4$ as base and $d_1$ and $d$, then:

$$d_4^2 = d_1^2 + d^2 - dd_1\cos\theta_2 \quad \text{Equation 85}$$

$$d_4 = \sqrt{d_1^2 + d^2 - 2dd_1\cos\theta_2} \quad \text{Equation 86}$$

Combining Equation 82, Equation 84, and Equation 80 leads to:

$$4d^2 \sin^2\left(\frac{\theta_1+\theta_2}{2}\right) = d_5^2 + r^2 - 2d_5 r\ \cos\left(2\sin^{-1}\left(\frac{\sqrt{d_1^2+d^2-2dd_1\cos\theta_2}}{2r}\right) - \cos^{-1}\left(\frac{d_5^2+r^2-d_2^2}{2d_5 r}\right)\right) \quad \text{Equation 87}$$

Here, we have an equation with $\theta_2$ being the only unknown parameter. After solving for $\theta_2$, we calculate the $\Delta d$ needed to correct the curved spiral elements as follows:

$$\Delta d = r\theta_3 = 2r\sin^{-1}\left(\frac{d_4}{2r}\right) \quad \text{Equation 88}$$

$$\Delta d = 2r \sin^{-1}\left(\frac{\sqrt{d_1^2 + d^2 - 2dd_1\cos\theta_2}}{2r}\right) \qquad \text{Equation 89}$$

By substituting the known values in Equation 87 and solving for the new co-ordinates of the spiral, we obtain what is shown on Figure 58 as an example.

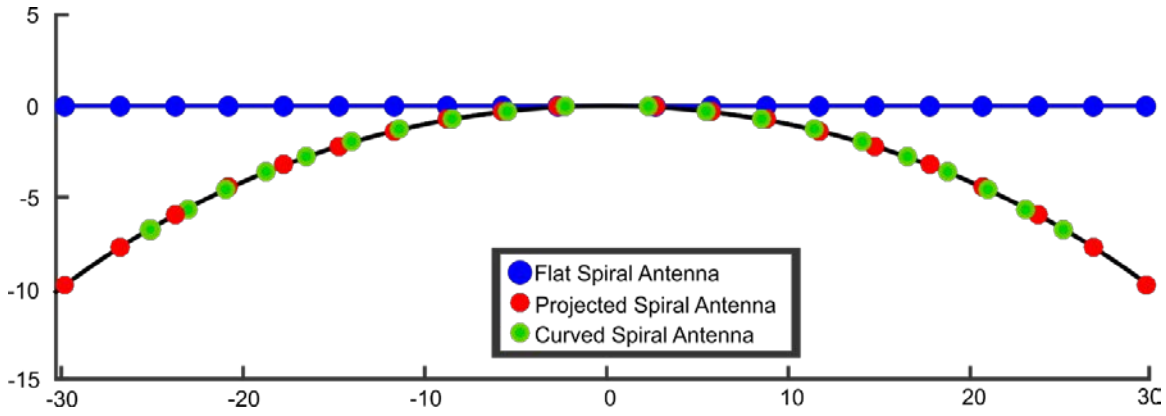


Figure 58. Cross-section calculating showing flat spiral elements, projected spiral elements and calculated corrected curved spiral elements.

**Step Two: Corrected Curved Spiral Elements**

In this section, we are going to find a set of corrected elements of the curved spiral projected over a spherical surface for the entire spiral but for a specific observation point. Here, we make an assumption that we know some parameters required for the calculations based on the locations of the flat spiral and the center and radius of the curved spiral. In the previous section, we showed how to find all the unknown parameters using the known parameters. Therefore, we found all the equations for the specific location of the curved points. We do this specific calculation procedure in order to generate all the elements of the spiral and feed then into a numerical calculation EM tool such as FEKO to calculate

the $S_{11}$ parameter. Comparison is made with the actual measurements done using the VNA in freshwater and saturated sand.

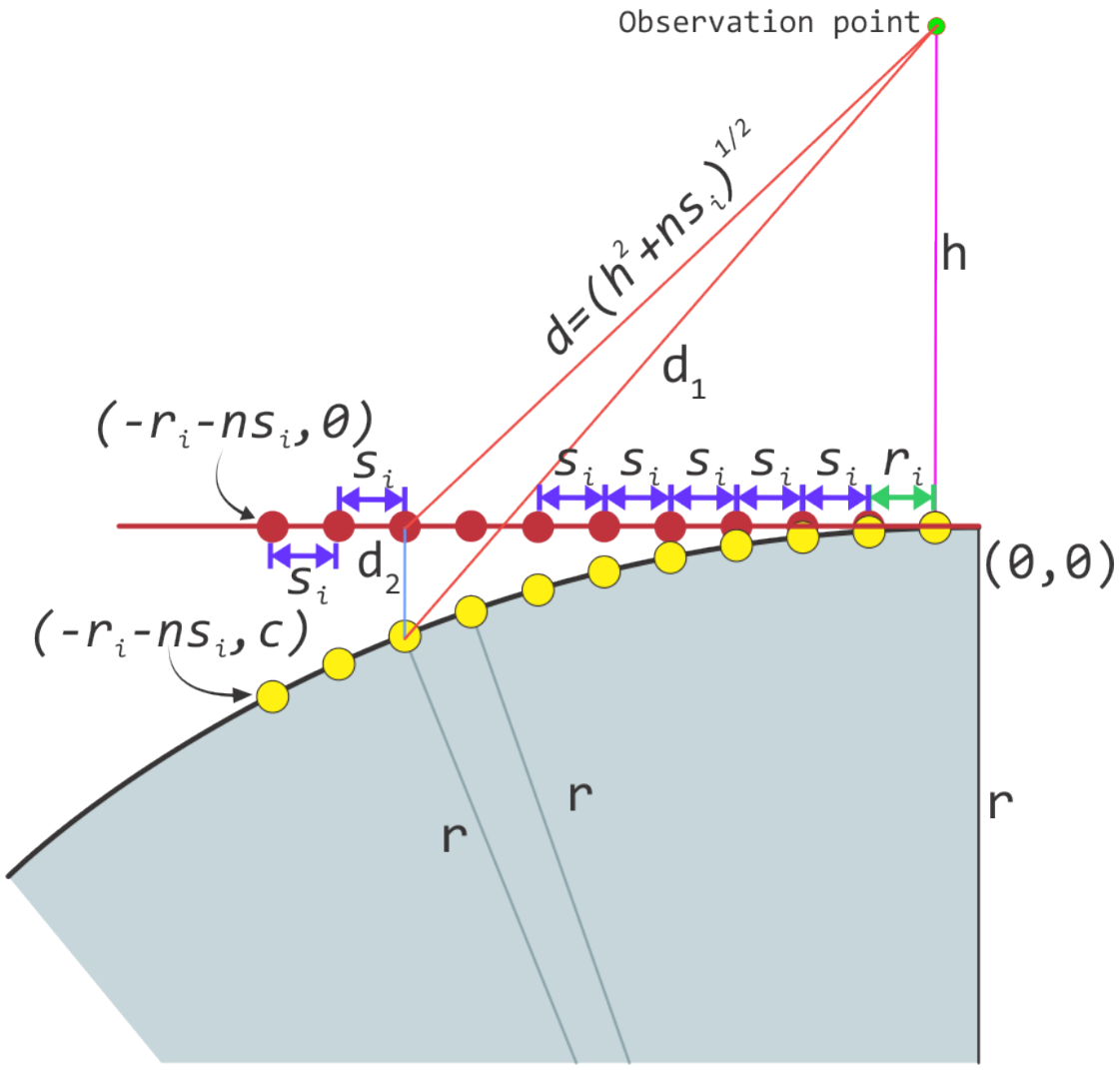


Figure 59. Illustration of parameters for finding spiral elements over the 3D contour.

We start our formulations by finding $c$, using equation of the circle

$$(x-0)^2+\left(c-(-r)\right)^2=r^2 \qquad \text{Equation 90}$$

$$x^2 + (c + r)^2 = r^2 \qquad \text{Equation 91}$$

Then, now, from the drawing we know that $x = -r_i - ns_i$ to obtain,

$$(-r_i - ns_i)^2 + (c + r)^2 = r^2 \qquad \text{Equation 92}$$

$$c^2 + 2rc + (r_i + ns_i)^2 = 0 \qquad \text{Equation 93}$$

$$c = \frac{-2r \pm \sqrt{4r^2 - 4(r_i + ns_i)^2}}{2} \qquad \text{Equation 94}$$

Simplifying we obtain the following for $c$,

$$c = r\left(-1 \pm \sqrt{1 - \left(\frac{r_i + ns_i}{r}\right)^2}\right) \qquad \text{Equation 95}$$

We note that for $c$ to be real, $r > r_i + ns_i$. Also there are two solutions. We are interested in the less negative answer, the first intersection from north to south. Therefore, we are ignoring the more negative solution of $c$ since they are located in the lower part of the circumference and we are projecting the flat spiral only in the upper part of the surface of the sphere. Thus, we obtain a unique solution for $c$ as follows:

$$c = r\left(-1 + \sqrt{1 - \left(\frac{r_i + ns_i}{r}\right)^2}\right) \qquad \text{Equation 96}$$

Then, using the distance between the two points $(-r_i - ns_i, 0)$ and $(-r_i - ns_i, c)$, we find $d_2$ to be same as $c$,

$$d_2 = \sqrt{\left((-r_i - ns_i) - (-r_i - ns_i)\right)^2 + (0 - c)^2} \qquad \text{Equation 97}$$

$$\mathrm{d}_2 = -c = r\left(1 - \sqrt{1 - \left(\frac{r_i + ns_i}{r}\right)^2}\right) \qquad \text{Equation 98}$$

By using a similar approach, we obtain $d_5$,

$$d_5 = \sqrt{r^2 + (r_i + ns_i)^2} \qquad \text{Equation 99}$$

Similarly, we obtain $d_1$,

$$\mathrm{d}_1 = \sqrt{\left((-r_i - ns_i) - (-r_i)\right)^2 + (c - h)^2} \qquad \text{Equation 100}$$

$$d_1 = \sqrt{(ns_i)^2 + (c - h)^2} \qquad \text{Equation 101}$$

These equations derived so far give us the 2D coordinates of the cross-section at to this point. The curved spiral is in 3D, we need a third coordinate to have the completed set for the cross-section over the curvature surface (in this case, spherical). A 3D spheres obeys the equation $x^2 + y^2 + z^2 = r^2$. Given that the points in 3D are on the surface of a sphere, we can generate the $z$ co-ordinates fairly straightforward because we know $r$ as well as the $x$ and $y$ co-ordinates. Now, we move on to generating all point on the spiral passing through the generated 3D points. First we will employ using successive half circles to complete the sphere, similar to the approach adopted in 2D spiral generation giving the cross-section of points. However, in this case, we generate semi-spheres instead of semi-circles. Consider two points to be considered: $(x_i, y_i, z_i)$ and $(x_f, y_f, z_f)$ with center

$(x_c, y_c, z_c)$ and $r_2 = \frac{1}{2}\left\|\begin{matrix} x_i - x_f \\ y_i - y_f \\ z_i - z_f \end{matrix}\right\|$. Then, the spirals are defined using the rotation angle parameters $\theta$ and $\psi$ as follows,

$$x - x_c = r_2 \, sin\,\theta \, cos\,\psi \qquad \text{Equation 102}$$

$$y - y_c = r_2 \, sin\,\theta \, \sin\psi \qquad \text{Equation 103}$$

$$z - z_c = r_2 \cos\theta \qquad \text{Equation 104}$$

We note that $\psi$ alternates between 0 to $\pi$ radians and $\pi$ to $2\pi$ radians for consecutive semi-spheres. However, $\theta$ is from $\theta_i = \cos^{-1}(\frac{z_i - z_c}{r_2})$ to $\theta_f = \cos^{-1}(\frac{z_f - z_c}{r_2})$.

# CHAPTER VII. SPIRAL ANTENNAS SIMULATIONS

We used the FEKO EMSS simulation software, mentioned previously, for the numerical investigation. It uses the method of moments (MoM) technique [88]. We started our study of spiral antennas by simulating the well-known flat Archimedean spiral antenna in free space to give us confidence in the simulation procedure since we were reproducing known results. Furthermore, we simulated a projected spiral. As we have already pointed out in the previous chapter, we created a curved spiral antenna using the design equations for a flat spiral antenna, then projected the flat antenna on a curved surface similar to the mussel shell, and then correcting for the curvature effects. The design of our flat two-arm Archimedean spiral antenna is governed by the parameters shown in Table 3.

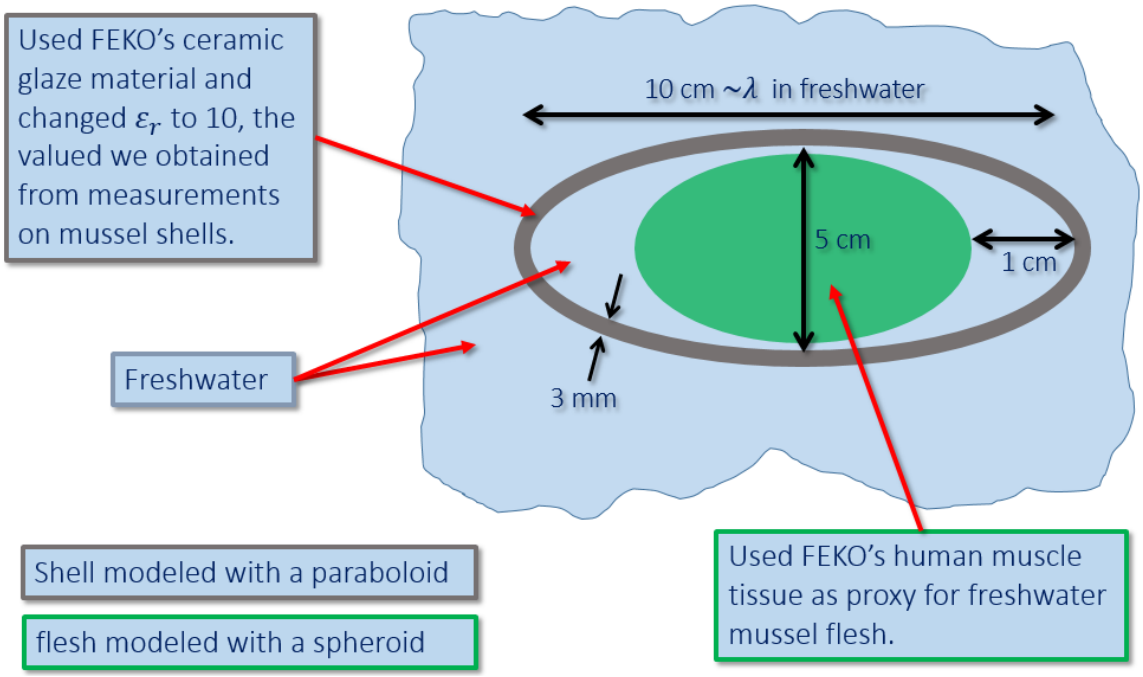


Figure 60. Mussel Model depicting materials and dimensions.

In the subsequent simulations all modeled spiral antennas have the same set of dimensions as Table 3. Further, single frequency was selected for the numerical analysis.

The voltage source magnitude is 1 V, and zero phase with a port impedance of 50 Ω. The Poynting vector calculations were done are shown in Table 4.

Table 4. Poynting vector parameters calculation in water

($\varepsilon_r = 81$ and $\sigma = 0.04$ S/m [23]).

| Parameter | Start | End | Increment | Number of field points |
|---|---|---|---|---|
| $r$ | $0^\circ$ | 6 m | 10 cm | 61 |
| $\theta$ | $0^\circ$ | $180^\circ$ | $5^\circ$ | 37 |
| $\phi$ | $0^\circ$ | $360^\circ$ | $5^\circ$ | 73 |

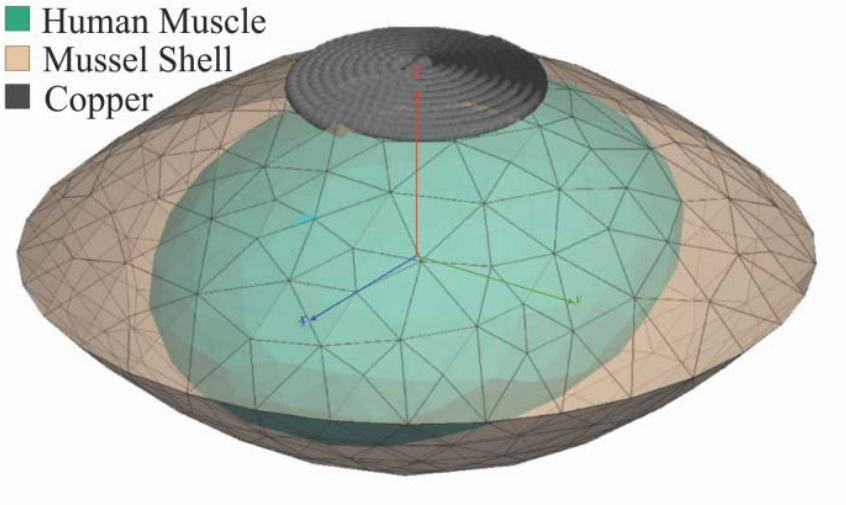


Figure 61. 3D model of the geometry and mesh for the simulation. The shells are modeled as a paraboloid with a radius of 5 cm and a focal depth of 2.5 cm. The radiation patterns were calculated in spherical coordinates in increments of radius $\boldsymbol{r}$ by 10 cm, angle $\theta$ by 5°, angle $\phi$ by 5° with a total of 83,731 field points.

**Projected Spiral Mounted in Mussel Simulation**

The simulation incorporates the antenna, the mussel shell, and the mussel tissue. We performed a chemical analysis on the mussel shell, and a typical shell consists of mostly calcium, with some inorganic carbon, manganese, and sodium. We measured (Summary

of Relevant EM Theory Related to ThesisChapter III) the relative permittivity of a shell as 10.45, and this is the value we used the simulations.

We used human muscle tissue from FEKO's built-in materials library to simulate mussel flesh. The mussel's flesh was created with spheroid of radii $x = 4$, $y = 3$, and $z = 2$ cm. We approximated the shells using a paraboloid with radius of 5 cm and focal depth of 2.5 cm. These are representative of an adult pocketbook mussel's dimensions. Mussels' shells have an average thickness of about 3 mm.

Figure 61 depicts 3-D the simulation geometry. The dielectric section is formed by the mussel's shells and flesh, and has a mesh size of 1 cm with 308 triangles. The metallic section is formed by the antenna's wires with radius of 1.12 mm and has mesh size of 1.5 mm with 512 triangles.

We simulated at a range of distances; here we report the results at a distance of 3 m from the antenna. In river water, 3 m is in the antenna far field. We compare the radiation patterns and the $S_{11}$ parameter of a flat spiral antenna with a curved spiral antenna. Figure 62 illustrates our results, which are broadly consistent with previous work [63, 64]. With respect to the radiation pattern of the flat spiral antenna, we note that the back lobe is suppressed. This is a consequence of reflection from the mussel shell and absorption through the mussel flesh.

**Discussion**

With respect to the curved antenna, its gain is slightly less (2 dB) than the gain for the flat spiral. This is similar to the results in [64] where the decrease was 2.7 dB. The

radiation pattern plot shows that the curved antenna attenuates the back lobe, here by about 2 dB. Attenuation of the back lobe is consistent with the results in [63, 64].

Both the magnitude and phase of the input impedance shows more variation as a function of frequency for the curved spiral than for the flat spiral. This variation was also observed in [64]. However, in [64] the input impedance showed a 50% change (from their Fig. 7), while for the antenna reported here, the variation in input impedance is significantly larger with 90% variation in magnitude. One reason for this increase is because our antenna has two curvatures, while the one in [64] has one. One can think of our curved antenna as "less flat" than the one in [64]. For a spiral antenna, it is the combination of its plane geometry and location of differential radiating elements in that plane that leads to its broadband characteristics. Thus, if one disturbs the location of these radiating elements, these properties are compromised.

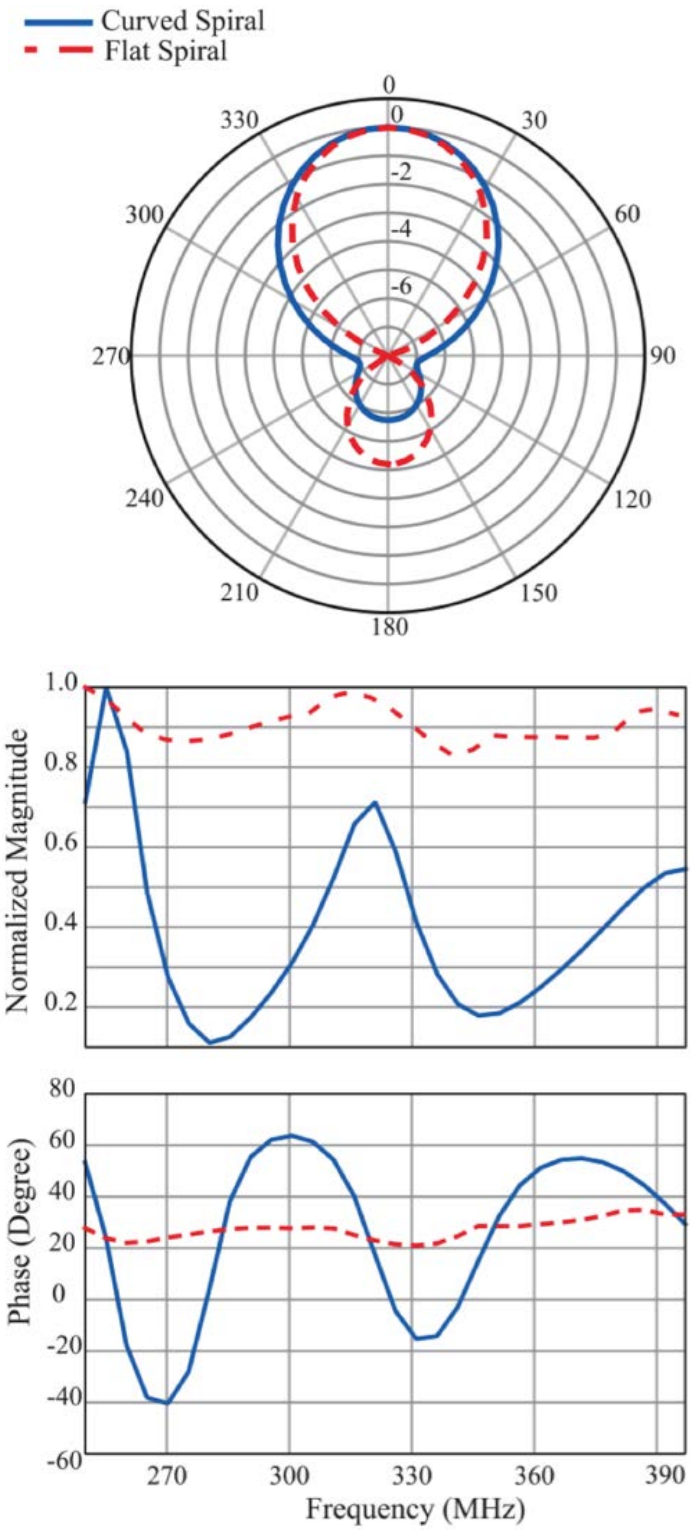


Figure 62. Normalized power and normalized $S_{11}$ simulation results for a projected spiral antenna mounted on a mussel.

# CHAPTER VIII. RESULTS AND DISCUSSION

In this section, we document the results of the antennas we investigated, namely dipole, flat spiral, and projected spiral antennas. Further, we compare experimental results with theoretical and simulated results. In Figure 41, Figure 42, Figure 43, and Figure 44, we illustrate the experimental setups used in the laboratory facilities. We used a large tank of about ~12-square-meter of water. We also made measurements in the University of Iowa Diving pool with the aid of a certified diver as shown in Figure 46. The diving pool volume is about ~410-square-meter, which is suitable to mimic an infinitive medium with the adequate radio input voltage. For each one of the antennas under study we measured range, azimuth, and elevation. Additionally, we measured the antenna's $S_{11}$ $S$-parameter with a VNA. Antennas were submerged in Iowa City tap water, and a saturated mixture of Iowa River sand and water.

## Range Measurements

Range measurements and simulated results are presented in Figure 63 and Figure 64. Figure 63 shows range measurements for a dipole-, flat-, and projected spiral antenna in freshwater. These measurements were made in a tank as described previously, and on the axis of symmetry of the antennas. As expected, for all the antennas the power decays rapidly near the antennas and after several wavelengths (around 0.6 m or 6 wavelengths here) the power decays less rapidly. The dipole antenna shows periodic variation in power with distance. Examining the plot shows that local maxima/minima are spaced 0.1 m (i.e., 1 wavelength) apart, and we conclude that these are the results of reflections from the tank walls. We don't see similar periodic variation for dipoles in the pool, since the boundaries of the pool are effectively at $d = \infty$ in that instance. As one would expect, we don't

observe periodic variations with the spiral antennas. These antennas are broadband and less susceptible to multipath effects. Figure 64 compares the simulation results with the measurement values for the flat spiral antenna and the agreement is good.

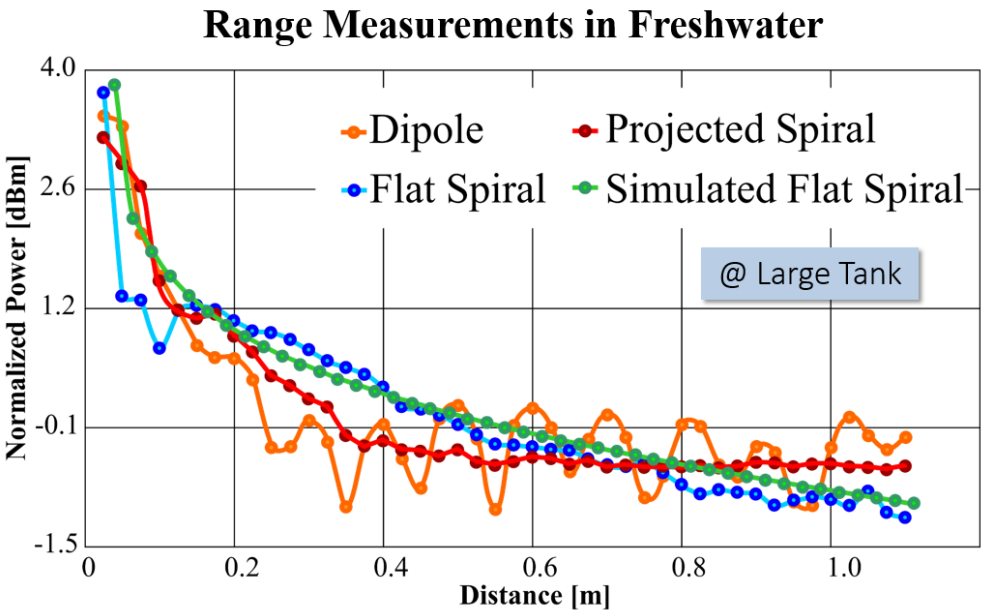


Figure 63. Range measurements in freshwater for dipole, flat spiral and projected spiral antennas.

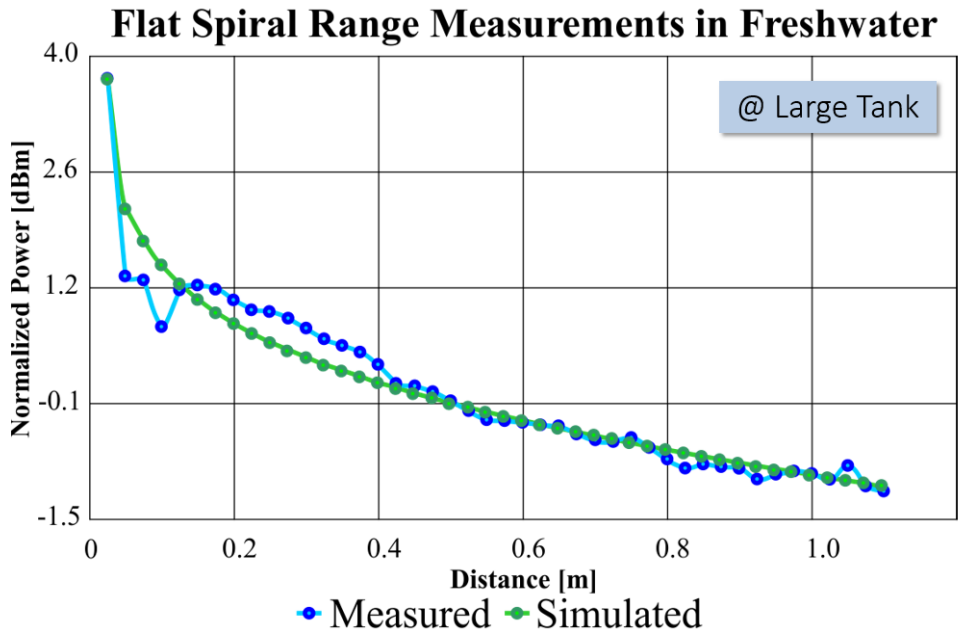


Figure 64. Simulated and measured range for a flat spiral antenna.

## Elevation and Azimuth

These measurements are tedious to obtain in the tank and the pool since we (a diver in case of the pool) manually rotate the antennas. We performed elevation measurements only in the large tank.

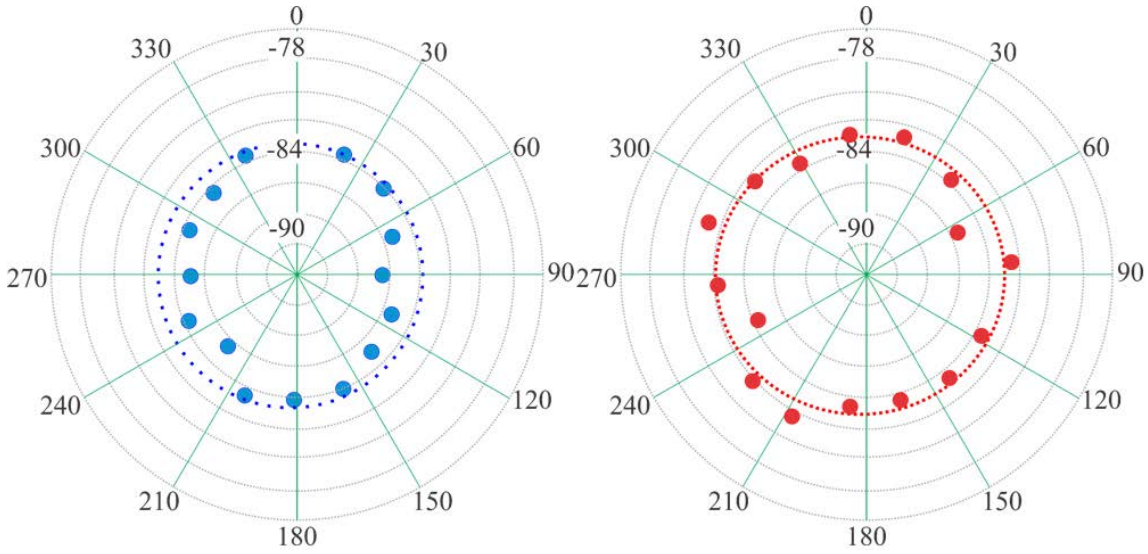


Figure 65. Elevation measurements for a flat (blue) and projected (red) spiral antennas in freshwater.

Figure 65 shows elevation measurements for the flat and projected spiral antennas measured using the tank facilities. The measured results are showing the measured points and the dotted line represents the expected results for each antenna. Measured results are consistent with the theoretical results.

Figure 66 shows azimuth measurements for the flat and projected spiral antennas measured using the tank. We can see that the flat spiral displays its bi-directional pattern. The projected spiral exhibits broader radiation pattern in the forward lobe and less in the backward lobe, which are intuitive results after bending the spiral. Both, elevation and azimuth results are congruent with simulation results discussed in previous chapter.

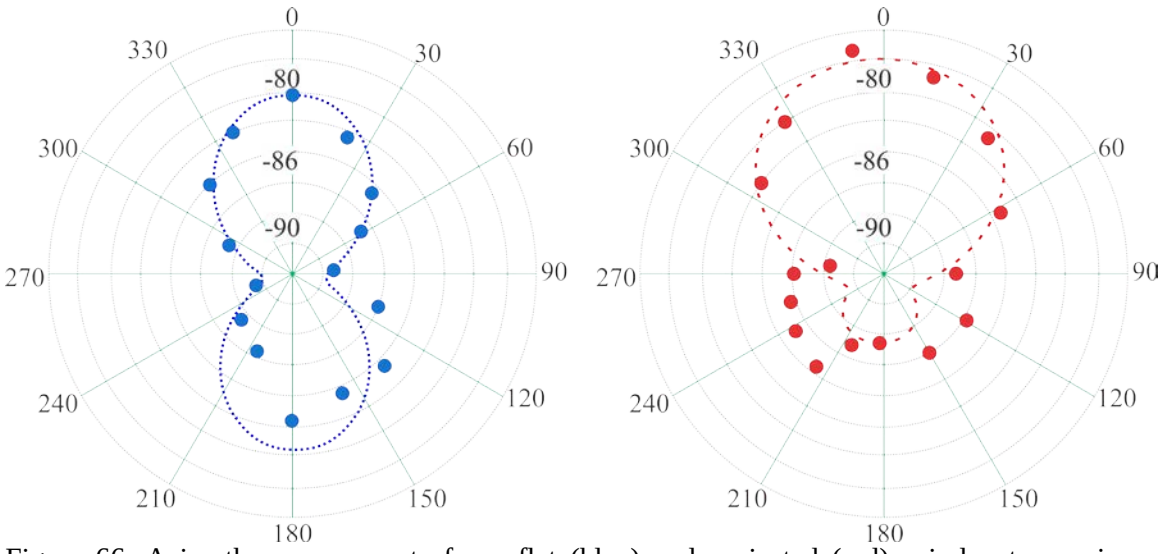


Figure 66. Azimuth measurements for a flat (blue) and projected (red) spiral antennas in freshwater. Points are measured values and lines are the theoretical values.

## $S_{11}$ Measurements

Figure 67 shows that the curved spiral antenna has less variation in $S_{11}$ over the range of frequencies than either the flat or projected spiral. This results shows that one can fabricate a curved spiral antenna to fit it on the contour of the mussel shell and obtain relatively constant reflection coefficient in freshwater and thus providing a consistent match to the radio-antenna system. Figure 69 shows consistency between measured and calculated results. The trends of the measure the calculated response are congruent.

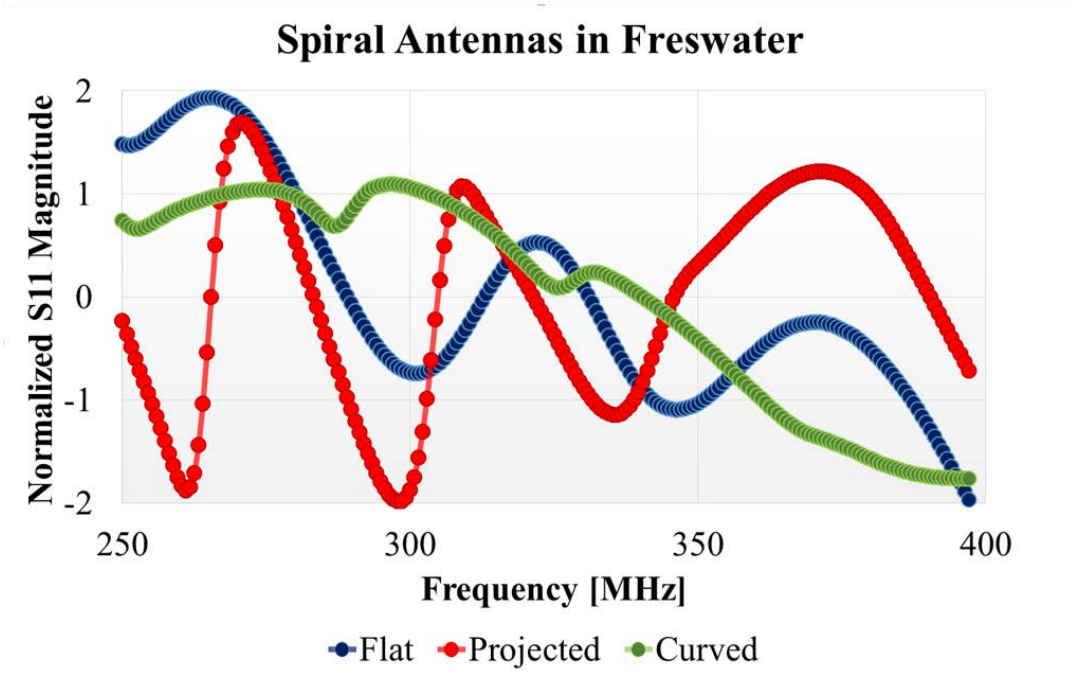


Figure 67. Normalized $S_{11}$ magnitude for a flat-, projected-, and curved spiral antenna.

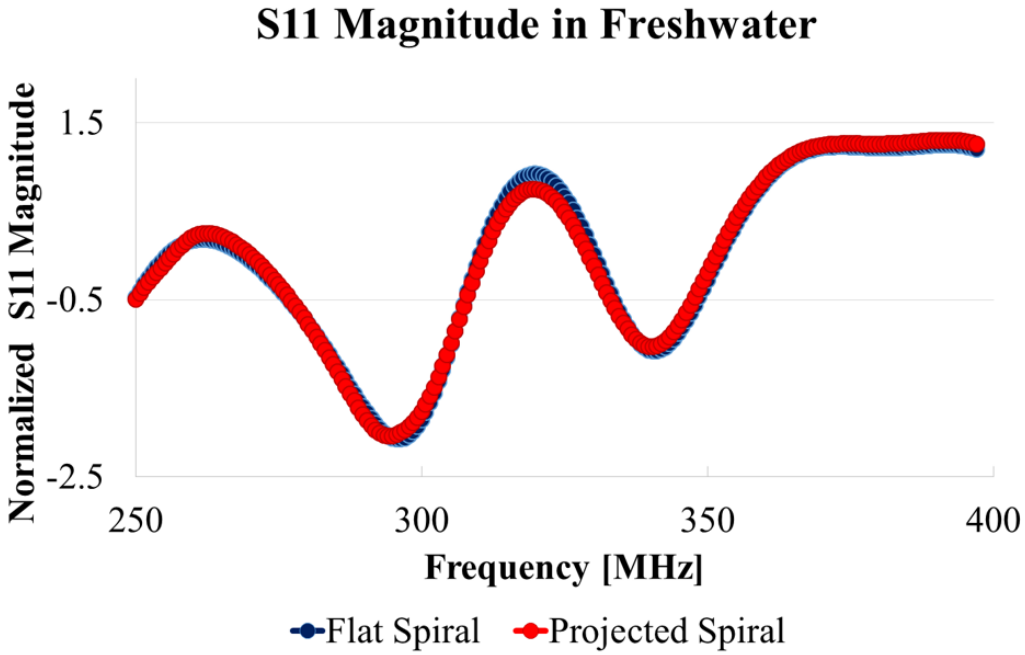


Figure 68. The projected surface in this simulation is 2.5 times than that of the surface for Figure 61. This result demonstrates that as the projected spiral antenna surface radius increases, its $S_{11}$ behavior approaches that of the flat spiral.

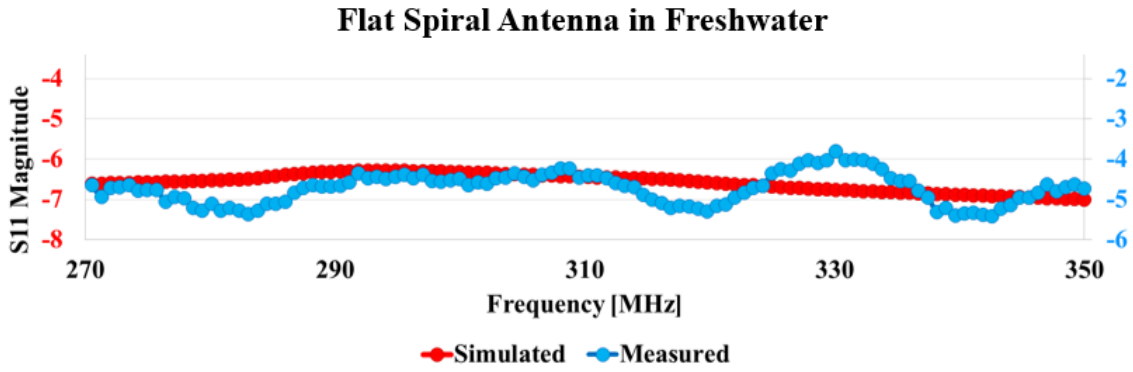


Figure 69. Normalized S11 simulated with FEKO and measured in freshwater as is illustrated in Figure 44 using a VNA. The measured and calculated results are consistent.

# CONCLUSIONS

The work presented here flowed from a larger on-going research effort of instrumenting freshwater mussels with a suite of sensors and radios to create so-called cybermussels. A cybermussel is a freshwater mussel (typically a pocketbook) with a backpack attached to it. The backpack houses electronics, sensors, a radio and an antenna. The focus of this thesis was the design, fabrication, and testing of "optimal" antennas for these cybermussels. The requirements for an ideal cybermussel antenna include the following. The antenna should be compact and form-fit the mussel shell. It should exhibit constant input impedance across the different EM environments its host (the mussel) finds itself. The antenna should also exhibit a broad radiation pattern, as the orientation of the antenna is random. Traditional (flat) spiral antennas meet most of these criteria. In this our work we investigated the effectiveness of curving the spiral (in two dimensions) to form-fit the mussel shell.

We performed a literature review covering underwater antennas, underwater-freshwater radio propagation, and spiral antennas. The literature review revealed that underwater communication has been studied for almost a century, but mostly in seawater. Underwater-seawater communication uses much lower frequencies and larger antennas than our application. Sparse research related to (fresh) underwater antenna exists, but much of this is not directly relevant to our work. Spiral antennas meet the criteria for a desirable antenna for a cybermussel. Spiral antennas have been studied for almost six decades, but to the best of our knowledge there is no previous work on spiral antennas for underwater applications. Additionally, limited research related to curved spiral antennas exist.

However, this research covers curving in one dimension and with simple antenna backing. Also, there are no published experimental results for these curved antennas.

Next, we summarized the EM theory related to this thesis. This review revealed that the wavelength in freshwater is approximately 0.1 of that in air. Therefore, the effective dimensions of the antenna are also 0.1 of that in air, and this allows us to have reasonable antenna size at our operating frequency (around 300 MHz). Additionally, freshwater at these frequencies is a lossy dielectric, which is important to our application.

Spiral antennas are fundamentally broadband. The broadband characteristic implies relatively constant input impedance. Constant input impedance is desired since mussels burrow in and out of the silt, changing the EM environment their backpack antennas operate in. This affects the antenna's $S_{11}$ parameter (related to input impedance) and can lead to impedance mismatch between radio and antenna. This reduces the radiated power, reducing the communication range, and battery life. Additionally, impedance mismatch can lead to instability in the radios.

Our overall approach was to (a) design, (b) simulate and (c) experimentally validate our antenna designs. We adjusted the protocols for each of these steps until the results were congruent. We performed extensive computer simulations investigating various aspects of the antennas. For example, we started with simple dipole antennas in air and refined our measurement- and simulation techniques and parameters to reproduce well-known results: near/far field power-range relationships, and elevation- and azimuth power relations. Next, we repeated these procedures with underwater dipole antennas in a large tank as well

as a large pool. After gaining skill and confidence in our techniques we moved onto flat-, projected-, and curved spiral antennas in freshwater.

We developed a procedure to design what we call a *projected spiral* antenna. The design procedure starts from the well-known flat spiral antenna, and then we project the antenna geometry onto a sphere with similar curvature as a mussel shell. This works reasonably well. However, projecting disturbs the intrinsic properties of the flat spiral antenna. We then developed a two-step procedure to create what we call a *curved spiral* antenna. This procedure starts with a projected spiral and then applies a geometric correction. This increases the antenna's performance with respect to constant $S_{11}$ and radiation pattern.

We performed most of the experimental validation in a tank located in our laboratory, and we performed some experiments in a large diving pool. Ideally, one would perform antenna tests in an (underwater) anechoic chamber. With proper placement of the antenna, the diving pool approximates an anechoic chamber quite well. On the other hand, the tank is efficient with respect of resources and cost, but because of its size, reflections from the tank boundary and water-air boundaries are ever present.

The tank allows for the use of a computer-controlled translation stage for more precise increments and movements during our measurements. Once set up, one could easily and quickly make multiple measurements on the antennas. Regarding the reflections in the tank, at first we considered this to be problematic. However, during the course of our work, we came to realize that we can use this to our advantage. For example, narrowband antennas such as dipoles should exhibit clear multipath interference that shows

up as ripples in antenna range measurements. The characteristics of these ripples (i.e., spatial frequency) should correspond to our intuition and simple hand-calculations. On the other hand, broad-band antennas such as the spirals we used should experience much less multipath effects and this should also be evident in range plots. Additionally, one can *simulate* the behaviors of either type of antenna and compare with measurements, whether in a tank or an anechoic (simulated with a pool). We conclude that while experimental validation is a pool is probably ideal, validation in a laboratory-based tank is a convenient and very viable alternative.

We used a commercial CEM tool to perform many simulations on the various antennas investigated in this thesis. Computer simulation allows one to perform numerical experiments, reducing the use of material, facilities, and support personnel time, thus reducing the cost of the research. However, it is mandatory that one has intimate knowledge of the simulation software's capabilities and especially its limitations. For example, in our research the cybermussel antennas would often operate in the near field, or in the transition region between near- and far fields. This is a consequence of the fact that the wavelength at the operating frequency in water is about 0.1 m and the spatial distribution of mussels in their natural environment. However, the CEM tool we used had defaults configured for air. Through several iterations with technical support from the CEM tool manufacturer, we configured the tool to work properly for our application.

While not the focus of the thesis, we developed a variety of techniques and resources related to the engineering and manufacture of curved spiral antennas. We have a CAD pipeline that works as follows. We take a live mussel and place it in a 3-D scanner. Within a few minutes we have the 3-D geometry of the mussel's shell and we place the

mussel back in a holding tank. Next, we manipulate the 3-D geometry in CAD software and create projected spiral antenna housing. The housing is then printed with a 3D printer. Next, the antenna wire is laid into the spiral grooves and the antenna is covered with a thin layer of epoxy to provide additional mechanical stability. A small annex to the spiral antenna houses the radio and backpack electronics. The completed backpack and spiral antenna are then affixed to the mussel, which can then be returned to its natural habitat. In this fashion, each mussel has a custom, tailor fit backpack.

# REFERENCES


[1] K. P. Hunt, J. J. Niemeier, and A. Kruger, "Antennas for mussel-based underwater biological sensor networks in rivers," in *Proceedings of the Fifth ACM International Workshop on UnderWater Networks*, 2010.

[2] K. P. Hunt, J. J. Niemeier, and A. Kruger, "RF communications in underwater wireless sensor networks," in *Electro/Information Technology (EIT), 2010 IEEE International Conference on*, 2010, pp. 1-6.

[3] H. E. Baidoo-Williams, J. S. Bril, M. B. Diken, J. Durst, J. McClurg, S. Dasgupta, *et al.*, "Cybermussels: a biological sensor network using freshwater mussels," presented at the Proceedings of the 11th international conference on Information Processing in Sensor Networks, Beijing, China, 2012.

[4] J. Bril, C. Just, J. Loperfido, and N. Young, "Upper Mississippi River Basin Envirohydrologic Observatory," in *ASCE Conference Proceedings*, 2009, pp. 342-323.

[5] A. Kruger, C. L. Just, R. Mudumbai, S. Dasgupta, T. J. Newton, J. Durst, *et al.*, "Freshwater Mussels as Biological Sensors and Cyclers of Aquatic Nitrogen Constituents: An Experimental Investigation," in *AGU Fall Meeting Abstracts*, 2011, p. 0527.

[6] J. S. Bril, "Assessing the effects of native freshwater mussels on aquatic nitrogen dynamics," 2012.

[7] S. Joyce, "The dead zones: oxygen- starved coastal waters," *Environmental health perspectives*, vol. 108, p. A120, 2000.

[8] E. Nedeau, "The amazing alewife," *Gulf of Maine Times*, vol. 7, 2003.

[9] C. C. Vaughn and C. C. Hakenkamp, "The functional role of burrowing bivalves in freshwater ecosystems," *Freshwater Biology*, vol. 46, pp. 1431-1446, 2001.

[10] J. R. Fischer, T. E. Neebling, and M. C. Quist, "Development and evaluation of a boat-mounted RFID antenna for monitoring freshwater mussels," *Freshwater Science*, vol. 31, pp. 148-153, 2012/03/01 2012.

[11] C. C. Vaughn, K. B. Gido, and D. E. Spooner, "Ecosystem processes performed by unionid mussels in stream mesocosms: species roles and effects of abundance," *Hydrobiologia*, vol. 527, pp. 35-47, 2004.

[12] M. Faria, L. Carrasco, S. Diez, M. C. Riva, J. M. Bayona, and C. Barata, "Multi-biomarker responses in the freshwater mussel Dreissena polymorpha exposed to polychlorobiphenyls and metals," *Comparative Biochemistry and Physiology Part C: Toxicology & Pharmacology*, vol. 149, pp. 281-288, 2009.

[13] Y. de Lafontaine, F. Gagné, C. Blaise, G. Costan, P. Gagnon, and H. Chan, "Biomarkers in zebra mussels (Dreissena polymorpha) for the assessment and monitoring of water quality of the St Lawrence River (Canada)," *Aquatic toxicology*, vol. 50, pp. 51-71, 2000.

[14] S.-J. Won, A. Novillo, N. Custodia, M. T. Rie, K. Fitzgerald, M. Osada, *et al.*, "The freshwater mussel (Elliptio complanata) as a sentinel species: vitellogenin and steroid receptors," *Integrative and comparative biology*, vol. 45, pp. 72-80, 2005.

[15] B. Sures, "Environmental parasitology: relevancy of parasites in monitoring environmental pollution," *Trends in parasitology*, vol. 20, pp. 170-177, 2004.
[16] H. D. Taylor, A. Kruger, and J. J. Niemeier, "Embedded electronics for a mussel-based biological sensor," in *Sensors Applications Symposium (SAS), 2013 IEEE*, 2013, pp. 148-151.
[17] J. Kaiser, "The Archimedean two- wire spiral antenna," *IRE Transactions on Antennas and Propagation*, vol. 8, pp. 312-323, 1960.
[18] W. L. Stutzman and G. A. Thiele, *Antenna theory and design*. New York: New York : J. Wiley, 1998.
[19] J. D. Kraus and R. J. Marhefka, *Antennas for all Applications*, 3rd ed. Boston: McGraw-Hill, 2002.
[20] "SAS-517 Log Periodic Antenna 80 MHz – 4 GHz," ed. USA: A. H. Systems Inc.
[21] "Model 0285 Log Periodic Antenna 2-18GHz Wideband Antenna," ed. Australia: Syndetic Pty Ltd.
[22] "QSPCP0.5-22SLH Circularly Polarized Spiral Antenna 0.5 to 22 GHz," ed. UK: Q-par Angus Ltd Barons Cross Laboratories.
[23] J. J. Niemeier, "Radio in hydroscience unconventional links and new sensor possibilities," PhD Dissertation, Electrical and Computer Engineering, University of Iowa, Iowa City, Iowa, 2010.
[24] A. R. Barnard, "Development of Supersonic Intensity in Reverberant Environments (SIRE) with Applications in Underwater Acoustics," The Pennsylvania State University, 2010.
[25] R. Mittra, "A look at some challenging problems in computational electromagnetics," *Antennas and Propagation Magazine, IEEE*, vol. 46, pp. 18-32, 2004.
[26] J. A. W. a. P. D. Lowell, "Development of loop aerials for submarine radio communication," *Phys. Rev.*, vol. 14, p. 193, 1919.
[27] A. Taylor, "Short Wave Reception and Transmission on Ground Wires (Subterranean and Submarine)," *Radio Engineers, Proceedings of the Institute of*, vol. 7, pp. 337-361, 1919.
[28] R. R. Batcher, "Loop antenna for submarines," *Wireless Age*, vol. 7, p. 28, 1920.
[29] R. K. Moore, "The theory of radio communications between submerged submarines," PhD, Cornell University, Ithaca, NY, 1951.
[30] J. R. Wait, "ELECTROMAGNETIC FIELDS OF CURRENT-CARRYING WIRES IN A CONDUCTING MEDIUM," *Canadian Journal of Physics*, vol. 30, pp. 512-523, 1952/09/01 1952.
[31] J. R. Wait, "The Magnetic Dipole Antenna Immersed in a Conducting Medium," *Proceedings of the IRE*, vol. 40, pp. 1244-1245, Oct. 1952 1952.
[32] J. R. Wait, "Insulated loop antenna immersed in a conducting medium," *J. Res. Nat\'l Bur. Std. D*, vol. 59D, pp. 133-137, 1957.
[33] J. R. Wait and L. L. Campbell, "The fields of an electric dipole in a semi-infinite conducting medium," *Journal of Geophysical Research*, vol. 58, pp. 21-28, 1953.
[34] W. Anderson and R. K. Moore, "Frequency spectra of transient electromagnetic pulses in a conducting medium," *Antennas and Propagation, IRE Transactions on*, vol. 8, pp. 603-607, 1960.

[35] R. K. Moore, "Effects of a surrounding conducting medium on antenna analysis," *Antennas and Propagation, IEEE Transactions on,* vol. 11, pp. 216-225, 1963.
[36] M. B. Kraichman, "Basic Experimental Studies of the Magnetic Field from Electromagnetic Sources Immersed in a Semi-Infinite Conducting Medium," *Journal of Research of the National Bureau of Standards - D. Radio Propagation,* vol. 64D, January-February 1960.
[37] J. R. Wait, "Project sanguine," *Science (New York, NY),* vol. 178, pp. 272-275, 1972.
[38] F. L. Dowling, "The sanguine communication system," *Naval Research Reviews,* vol. 27, 1974.
[39] D. L. Jones. (1985, July) Sending Signals to Submarines. *New Scientist Magazine*. 37-41.
[40] J. Merrill, "Some early historical aspects of Project Sanguine," *Communications, IEEE Transactions on,* vol. 22, pp. 359-363, 1974.
[41] B. Keiser, "Early development of the project sanguine radiating system," *Communications, IEEE Transactions on,* vol. 22, pp. 364-371, 1974.
[42] C. Fessenden and D. Cheng, "Development of a trailing-wire E-field submarine antenna for extremely low frequency (ELF) reception," *Communications, IEEE Transactions on,* vol. 22, pp. 428-437, 1974.
[43] R. W. Turner, "Submarine Communication Antenna Systems," *Proceedings of the IRE,* vol. 47, pp. 735-739, 1959.
[44] S. Durrani, "Air-to-undersea communication with electric dipoles," *Antennas and Propagation, IRE Transactions on,* vol. 10, pp. 524-528, 1962.
[45] H. A. Wheeler, "Fundamental limitaions of a small VLF antenna for submarines," *Antennas and Propagation, IRE Transactions on,* vol. 6, pp. 123-125, 1958.
[46] R. K. Moore, "Radio communication in the sea," *Spectrum, IEEE,* vol. 4, pp. 42-51, 1967.
[47] M. Siegel and R. W. P. King, "Electromagnetic propagation between antennas submerged in the ocean," *Antennas and Propagation, IEEE Transactions on,* vol. 21, pp. 507-513, 1973.
[48] G. S. Saran and G. Held, "Field strength mesurements in fresh water," *Journal of Research of the National Bureau of Standards D,* vol. 52, pp. 435-437, 1960.
[49] L. Shen, R. King, and R. Sorbello, "Measured field of a directional antenna submerged in a lake," *Antennas and Propagation, IEEE Transactions on,* vol. 24, pp. 891-894, 1976.
[50] H. M. Hafez, W. J. Chudobiak, and J. S. Wight, "The Attenuation Rate in Fresh Water at VHF Frequencies," *Instrumentation and Measurement, IEEE Transactions on,* vol. 28, pp. 71-74, 1979.
[51] G. S. Smith, "Directive properties of antennas for transmission into a material half-space," *Antennas and Propagation, IEEE Transactions on,* vol. 32, pp. 232-246, 1984.
[52] J. R. Fischer, T. E. Neebling, and M. C. Quist, "Development and evaluation of a boat-mounted RFID antenna for monitoring freshwater mussels," *Development,* vol. 31, 2012.
[53] V. Rumsey, "Frequency independent antennas," in *IRE International Convention Record*, 1957, pp. 114-118.

[54] E. M. Turner, "Spiral slot antenna," 1958.
[55] J. Dyson, "The equiangular spiral antenna," *Antennas and Propagation, IRE Transactions on*, vol. 7, pp. 181-187, 1959.
[56] J. Dyson, "The unidirectional equiangular spiral antenna," *IRE Transactions on Antennas and Propagation*, vol. 7, pp. 329-334, 1959.
[57] W. Curtis, "Spiral antennas," *Antennas and Propagation, IRE Transactions on*, vol. 8, pp. 298-306, 1960.
[58] R. Bawer and J. Wolfe, "The spiral antenna," in *IRE International Convention Record*, 1960, pp. 84-95.
[59] T. E. Morgan, "Reduced Size Spiral Antenna," in *Microwave Conference, 1979. 9th European*, 1979, pp. 181-185.
[60] V. H. Rumsey, *Frequency independent antennas*. New York: New York, Academic Press, 1966.
[61] R. DuHamel and D. Isbell, "Broadband logarithmically periodic antenna structures," in *IRE International Convention Record*, 1957, pp. 119-128.
[62] C. Tang, "A class of modified log-spiral antennas," *Antennas and Propagation, IEEE Transactions on*, vol. 11, pp. 422-427, 1963.
[63] J. Wu, S. K. Khamas, and G. G. Cook, "Analysis of a Conformal Archimedean Spiral Antenna Printed Within Layered Dielectric Cylindrical Media Using the Method of Moments," *Antennas and Propagation, IEEE Transactions on*, vol. 60, pp. 3967-3971, 2012.
[64] H. Nakano and K. Nakayama, "A curved spiral antenna above a conducting cylinder," *Antennas and Propagation, IEEE Transactions on*, vol. 47, pp. 3-8, 1999.
[65] I. Nakayama, T. Kawano, and H. Nakano, "A conformal spiral array antenna radiating an omnidirectional circularly-polarized wave," in *Antennas and Propagation Society International Symposium, 1999. IEEE*, 1999, pp. 894-897 vol.2.
[66] S. K. Khamas, "Moment Method Analysis of an Archimedean Spiral Printed on a Layered Dielectric Sphere," *Antennas and Propagation, IEEE Transactions on*, vol. 56, pp. 345-352, 2008.
[67] H. Nakano, S. Okuzawa, K. Ohishi, H. Mimaki, and J. Yamauchi, "A curl antenna," *Antennas and Propagation, IEEE Transactions on*, vol. 41, pp. 1570-1575, 1993.
[68] H. Nakano and H. Mimaki, "Axial ratio of a curl antenna," *Microwaves, Antennas and Propagation, IEE Proceedings*, vol. 144, pp. 488-490, 1997.
[69] H. Nakano, R. Satake, and J. Yamauchi, "Wideband curl antenna," in *Antenna Technology (iWAT), 2011 International Workshop on*, 2011, pp. 110-111.
[70] J. Wu, S. K. Khamas, and G. G. Cook, "Moment Method Analysis of a Conformal Curl Antenna Printed Within Layered Dielectric Cylindrical Media," *Antennas and Propagation, IEEE Transactions on*, vol. 61, pp. 3912-3917, 2013.
[71] J. D. Kraus and D. A. Fleisch, *Electromagnetics with applications*, 5th ed. Boston: McGraw-Hill, 1999.
[72] C. T. A. Johnk, *Engineering electromagnetic fields and waves*. New York: New York : Wiley, 1988.
[73] R. Bansal, *Engineering electromagnetics : applications*. Boca Raton, FL: Boca Raton, FL : CRC Taylor & Francis, 2006.

[74] K. E. Lonngren, S. V. Savov, and R. J. Jost, *Fundamentals of electromagnetics with MATLAB*. Raleigh, N.C.: Raleigh, N.C. : SciTech Pub., 2005.
[75] S. Ramo, J. R. Whinnery, and T. V. Duzer, *Fields and waves in communication electronics*. New York: New York : Wiley, 1994.
[76] T. Meissner and F. J. Wentz, "The complex dielectric constant of pure and sea water from microwave satellite observations," *Geoscience and Remote Sensing, IEEE Transactions on*, vol. 42, pp. 1836-1849, 2004.
[77] H. Blok and P. M. v. d. Berg, *Electromagnetic waves : an introductory course*. Delft [Netherlands]: Delft Netherlands : Delft University Press, 1999.
[78] C. A. Balanis, *Antenna theory : analysis and design*. Hoboken, NJ: Hoboken, NJ : John Wiley, 2005.
[79] D. K. Cheng, *Field and wave electromagnetics*. Reading, Mass.: Reading, Mass. : Addison Wesley, 1983.
[80] G. M. Djuknic, "Method of measuring a pattern of electromagnetic radiation," ed: Google Patents, 2003.
[81] R. C. Johnson and H. Jasik, *Antenna Engineering Handbook*: McGraw-Hill, 1993.
[82] "Agilent U1731B/U1732B Dual Display Handheld LCR Meter User's and Service Guide," 3rd ed. Santa Clara, CA: Agilent Technologies, 2012.
[83] L. V. Blake and M. W. Long, *Antennas : fundamentals, design, measurement*. Raleigh, NC: Raleigh, NC : SciTech Pub., 2009.
[84] R. D. Straw, *The ARRL antenna book* vol. 18: The League, 1997.
[85] A. S. Khan, *Microwave Engineering: Concepts and Fundamentals*. Boca Raton: CRC Press Taylor & Francis Group, 2014.
[86] S. Gao, Q. Luo, and F. Zhu, *Circularly polarized antennas*, 2014.
[87] E. D. Caswell, "Design and Analysis of Star Spiral with Application to Wideband Arrays with Variable Element Sizes," PhD Dissertation, Virginia Polytechnic Institute and State University, Blacksburg, VA, 2001.
[88] "FEKO User's Manual," in *Suite 6.3*, ed. Stellenbosch, South Africa: EM Software and Systems, 2013.